Rita Paula Paiva Craveiro

Mestre em Química

Engineering Bio-based Polymers using Alternative Solvents and Processes

Dissertação para obtenção do Grau de Doutor em
Química Sustentável

Orientador: Doutor Alexandre Babo de Almeida Paiva,
Universidade Nova de Lisboa
Co-orientador: Doutora Ana Rita Cruz Duarte,Investigadora
Auxiliar ICVS/3B's
Co-orientador: Professora Doutora Susana Filipe Barreiros,
Professora Associada, Universidade Nova de
Lisboa

FACULDADE DE
CIÊNCIAS E TECNOLOGIA
UNIVERSIDADE NOVA DE LISBOA

Junho de 2015

Universidade Nova de Lisboa

Rita Paula Paiva Craveiro

Mestre em Química

Engineering Bio-based Polymers using Alternative Solvents and Processes

Dissertação para obtenção do Grau de Doutor em
Química Sustentável

Orientador: Doutor Alexandre Babo de Almeida Paiva,
Universidade Nova de Lisboa
Co-orientador: Doutora Ana Rita Cruz Duarte,Investigadora
Auxiliar ICVS/3B's
Co-orientador: Professora Doutora Susana Filipe Barreiros,
Professora Associada, Universidade Nova de
Lisboa

FACULDADE DE
CIÊNCIAS E TECNOLOGIA
UNIVERSIDADE NOVA DE LISBOA

Junho de 2015

Engineering Bio-based Polymers using Alternative Solvents and Processes

"It agitates me to pain that the skyline over there is ever our limit. I long sometimes for a power of vision that would overpass it. If I could behold all I imagine."

Jane Eyre- Charlotte Brontë

"You change all the lead sleeping in my head to gold
As the day grows dim, I hear you sing a golden hymn
It's the song I've been trying to sing…"

Arcade Fire- Neighborhood #1 (Tunnels)

Acknowledgments

Não foi fácil chegar aqui e o caminho não esteve sempre claro, condensar quatro anos em tão menos de metade custou! Mas estou certa de que sem a ajuda de várias pessoas, isso teria sido impossível, e chegada a altura dos agradecimentos, não poderia deixar de referir a sua contribuição para que esta tese pudesse tomar forma e ser concluída.

Começo por agradecer ao meu orientador e quasi-conterrâneo Doutor Alexandre Paiva. Obrigada por me teres incluido no ENiGMA, sem dúvida o início desta grande aventura. Esta tese resulta de uma sucessão de acasos felizes, que no fim ganharam força e forma...e acabei por ser tua aluna de Doutoramento! E ainda bem! Obrigada, por todas as sugestões, discussões de resultados, pelos brilhantes momentos de brainstorming e parvoíce, pela iniciação no mundo dos supercríticos, pela amizade e pelo apoio naqueles momentos em que a confiança falha. Obrigada pelo interesse, dedicação, por todos os conhecimentos transmitidos e pela tua grande disponibilidade. Foi um prazer trabalhar durante estes anos contigo e sob tua orientação, qual mestre Jedi e young padawan!

Agradeço também à Doutora Ana Rita Duarte, que é com toda a certeza um grande exemplo a seguir! Obrigada por toda a disponibilidade e conhecimentos partilhados. A verdade é que me sinto muito priveligiada por ter trabalhado neste projecto sob tua orientação! Obrigada por todas as oportunidades que me foram dando! Tenho a certeza de que o sucesso vai sempre acompanhar-te, e o mundo está aqui a um passo!

À Professora Susana Barreiros, obrigada por me ter acolhido no laboratório, por ser um grande exemplo como pessoa e cientista e por ter sempre a atenção e tempo para me aconselhar! Aprendi muito, e só tenho a agradecer-lhe por todos estes anos em que trabalhei consigo, desde o sol-gel até aos DES!

Agradeço também à Professora Madalena Dionísio que me mostrou todo este novo mundo de DSC e de DRS, e sem a qual o trabalho desta tese seria infinitamente mais pobre! Obrigada pela sua disponibilidade para discutir resultados e, na verdade, para me ensinar tanto sobre tanta coisa nova! Obrigada pela ajuda, calma e atenção!

Um grande, enorme, obrigada à minha outra metade no ENiGMA, a minha colega Marta Martins e o meu colega Ivo Aroso, sem os quais muito deste trabalho não teria sido realizado. Obrigada por toda a ajuda e generosidade. É bom trabalhar com pessoas que são também elas boas, em todos os sentidos!
Obrigada à Doutora Maria Viciosa pelas experiências de POM e à Doutora Natália Correia pela ajuda na interpretação do DSC e DRS. Um grande obrigada à minha querida Tânia, e à Verónica e Gonçalo pela ajuda nas medidas de DSC e DRS.

Gostaria ainda de agradecer ao Professor Manuel Nunes da Ponte. Obrigada por ter "acreditado" em mim e de que eu era capaz, e por me ter aceite no programa Doutoral em Química Sustentável. Oportunidades destas não surgem muitas vezes na vida, e se acabo esta tese e este doutoramento, na verdade é a si que tenho de agradecer esta chance. Obrigada!

Agradeço a todos os colegas do 427, que desde o primeiro dia (num longínquo 2011) me receberam com um sorriso na cara e que foram sempre prestáveis e disponíveis.

Resumo

O trabalho apresentado nesta tese explora novas vias para o processamento de polímeros de base biológica, desenvolvendo uma abordagem sustantável baseada no uso de solventes alternativos tais como dióxido de carbono supercrítico (scCO$_2$), líquidos iónicos (ILs) e solventes eutéticos (DES). A viabilidade da produção de polímeros porosos através do processo de expansão ("foaming") supercrítico, combinado com estes solventes, foi avaliada de modo a poder substituir as técnicas convencionais de "foaming" que usam solventes tóxicos e nocivos.

Uma nova metodologia para o processamento de polímeros é apresentada, baseada na técnica de "foaming" supercrítico, utilizando scCO$_2$ como agente de "foaming". Diferentes misturas poliméricas de base de amido foram processadas através da técnica de "foaming" supercrítico, nomeadamente amido/ácido poliláctico (SPLA) e amido/policaprolactona (SPCL). O processo de "foaming" baseia-se no facto de as moléculas de CO$_2$ conseguirem dissolver-se no polímero, alterando as suas propriedades mecânicas, e após uma despressurização adequada formarem um material poroso. Nas misturas poliméricas referidas, o CO$_2$ apresenta uma solubilidade limitada e de modo a aumentar o efeito do "foaming", dois líquidos iónicos possuíndo o catião imidazólio foram utilizados, juntamente com este processo, dopando a mistura polimérica. O uso de líquidos iónicos revelou-se útil, aumentando o efeito de "foaming".

Através de espectroscopia de infravermelho com transformada de Fourier no modo de reflectância total atenuada (FTIR-ATR), provou-se a existência de interacções entre a mistura polimérica SPLA e líquido iónico, que por sua vez diminuem as forças que sustentam a estrutura polimérica. Esta observação está directamente relacionada com a capacidade que os líquidos iónicos têm de dissolver maiores quantidades de CO$_2$. Este resultado é também claro a partir dos resultados de experiências de absorção de CO$_2$, onde os coeficientes aparentes de absorção obtidos na presença de líquido iónico são superiores quando comparados com os da mistura polimérica SPLA sem líquido iónico.

A dopagem do SPCL com líquidos iónicos também foi realizada. O "foaming" desta mistura foi bem sucedido e resultou na formação de materiais porosos com valores de condutividade próximos dos líquidos iónicos puros. Isto pode ser uma oportunidade para o desenvolvimento destes materiais, para aplicações como materiais condutores suportados.

Um outro tipo de solventes foi também utilizado no método de processamento previamente apresentado. No caso de se pretenderem diferentes aplicações para os polímeros de base biológica, a substituição dos líquidos iónicos deve ser considerada, principalmente tendo em conta que alguns destes são solventes pouco sustentáveis e de o seu perfil de toxicidade ainda não ser totalmente conhecido.

Neste trabalho os solventes eutéticos naturais – NADES – foram os escolhidos. Estes solventes apresentam algumas vantagens relativamente aos líquidos iónicos, sendo facilmente produzidos, mais baratos, biodegradáveis e muitas vezes biocompatíveis, uma vez que são compostos por metabolitos primários, tais como açúcares, ácidos carboxílcos e aminoácidos. Os NADES foram preparados e as suas propriedades físico-químicas foram avaliadas, nomeadamente o seu comportamento térmico, condutividade, densidade, viscosidade e polaridade. Com este estudo, tornou-se claro que todas estas propriedades podem variar

consoante a composição do NADES, bem como com o seu conteúdo inicial de água e temperatura.

A utilização de NADES no "foaming" do SPCL, actuando como agente de "foaming", foi também levada a cabo e bem sucedida. A estrutura de SPCL obtida após o "foaming" supercrítico apresenta melhores características (tais como a porosidade), quando comparadas com as estruturas obtidas com o uso de líquidos iónicos como agentes de "foaming".

Solventes eutéticos constituídos por compostos terapêuticos (THEDES) foram também preparados. A combinação de cloreto de colina-ácido mandélico e de mentol-ibuprofeno, resultou em THEDES com um comportamento térmico muito distinto dos seus componentes individuais. O "foaming" de SPCL com THEDES foi realizado, e a impregnação destes THEDES em matrizes de SPCL realizada através do processo de "foaming" supercrítico também foi bem sucedida, e um sistema de libertação controlada para o caso do THEDES constituído por mentol-ibuprofeno foi obtido.

Palavras chave: Química sustentável, polímeros de base biológica, solventes alternativos, líquidos iónicos, solventes eutéticos, CO_2 supercrítico, "foaming", processamento de polímeros.

Abstract

The work presented in this thesis explores novel routes for the processing of bio-based polymers, developing a sustainable approach based on the use of alternative solvents such as supercritical carbon dioxide (scCO$_2$), ionic liquids (ILs) and deep eutectic solvents (DES). The feasibility to produce polymeric foams via supercritical fluid (SCF) foaming, combined with these solvents was assessed, in order to replace conventional foaming techniques that use toxic and harmful solvents.

A polymer processing methodology is presented, based on SCF foaming and using scCO$_2$ as a foaming agent. The SCF foaming of different starch based polymeric blends was performed, namely starch/poly(lactic acid) (SPLA) and starch/poly(ε-caprolactone) (SPCL). The foaming process is based on the fact that CO$_2$ molecules can dissolve in the polymer, changing their mechanical properties and after suitable depressurization, are able to create a foamed (porous) material. In these polymer blends, CO$_2$ presents limited solubility and in order to enhance the foaming effect, two different imidazolium based ILs (IBILs) were combined with this process, by doping the blends with IL. The use of ILs proved useful and improved the foaming effect in these starch-based polymer blends.

Infrared spectroscopy (FTIR-ATR) proved the existence of interactions between the polymer blend SPLA and ILs, which in turn diminish the forces that hold the polymeric structure. This is directly related with the ability of ILs to dissolve more CO$_2$. This is also clear from the sorption experiments results, where the obtained apparent sorption coefficients in presence of IL are higher compared to the ones of the blend SPLA without IL.

The doping of SPCL with ILs was also performed. The foaming of the blend was achieved and resulted in porous materials with conductivity values close to the ones of pure ILs. This can open doors to applications as self-supported conductive materials.

A different type of solvents were also used in the previously presented processing method. If different applications of the bio-based polymers are envisaged, replacing ILs must be considered, especially due to the poor sustainability of some ILs and the fact that there is not a well-established toxicity profile.

In this work natural DES – NADES – were the solvents of choice. They present some advantages relatively to ILs since they are easy to produce, cheaper, biodegradable and often biocompatible, mainly due to the fact that they are composed of primary metabolites such as sugars, carboxylic acids and amino-acids. NADES were prepared and their physicochemical properties were assessed, namely the thermal behavior, conductivity, density, viscosity and polarity. With this study, it became clear that these properties can vary with the composition of NADES, as well as with their initial water content.

The use of NADES in the SCF foaming of SPCL, acting as foaming agent, was also performed and proved successful. The SPCL structure obtained after SCF foaming presented enhanced characteristics (such as porosity) when compared with the ones obtained using ILs as foaming enhancers.

DES constituted by therapeutic compounds (THEDES) were also prepared. The combination of choline chloride-mandelic acid, and menthol-ibuprofen, resulted in THEDES with thermal behavior very distinct from the one of their components. The foaming of SPCL with THEDES was

successful, and the impregnation of THEDES in SPCL matrices via SCF foaming was successful, and a controlled release system was obtained in the case of menthol-ibuprofen THEDES.

List of Publications

A. Paiva, **R. Craveiro**, I. Aroso, M. Martins, R.L. Reis, A.R.C. Duarte, "Natural Deep Eutectic Solvents – Solvents for the 21 st Century", *ACS Sustainable Chem. Eng.* 2(5) (2014) 1063-1071.

M. Martins, **R. Craveiro**, A. Paiva, A.R.C. Duarte, R.L. Reis, "Supercritical fluid processing of natural based polymers doped with ionic liquids", *Chem. Eng. J.* 241 (2014) 122-130.

R. Craveiro, M. Martins, G.B. Santos, N. Correia, M. Dionísio, S. Barreiros, A.R.C. Duarte, R.L. Reis, A. Paiva, "Starch-based polymer-IL composites formed by compression moulding and supercritical fluid foaming for self-supported conductive material", *RSC Adv.* 24(33) (2014), 17161-17170.33

R. Craveiro, I. Aroso, V. Flammia, T. Carvalho, M. T. Viciosa, M. Dionísio, S. Barreiros, R. L. Reis, A. R. C. Duarte, A. Paiva, "Properties and Thermal Behavior of Natural Deep Eutectic Solvents", *(Submitted to J. Mol. Liquids).*

M. Martins, R.L. Reis, A.R.C. Duarte, **R. Craveiro**, A. Paiva, "Enhanced Performance of Supercritical Fluid Foaming of Natural-Based Polymers by Deep Eutectic Solvents" *AICHE J.* 60 (2014), 3701-370

Table of Contents

List of Figures

List of Tables

Abbreviations, acronyms and symbols

%	percent
ΔH_m	melting enthalpy
ΔH_m^0	standard melting enthalpy
$\dot{\gamma}$	shear rate
M_{t_0}	cumulative amount of drug released at time t_0
$M'(\omega)$	real part of the dielectric modulus function
$M''(\omega)$	imaginary part of the complex modulus function
$M^*(\omega)$	complex dielectric modulus function
M_0	mass of diffusing substance at equilibrium
M_∞	absolute cumulative amount of drug released at infinite time
X_c	crystallinity degree
$\delta C / \delta t$	concentration gradient
$\delta P / \delta t$	depressurization rate
$\varepsilon'(\omega)$	real pat of the complex dielectric function
$\varepsilon''(\omega)$	imaginary part of the complex dielectric function
$\varepsilon^*(\omega)$	complex dielectric function
ε_0	dielectric permittivity in the vacuum
η_0	zero shear viscosity
λ_{max}	maximum wavelength
$\sigma'(f)$	real conductivity
$\sigma'(\omega)$	real part of the complex conductivity function
$\sigma''(\omega)$	imaginary part of the complex conductivity function
$\sigma^*(\omega)$	complex conductivity function
σ_0	yield stress
σ_∞	high temperature limit of conductivity
[BMIM]$^+$	1-butyl-3-methylimidazolium cation
[BMIM]Ac	1-butyl-3-methylimidazolium acetate
[BMIM]BF$_4$	1-butyl-3-methylimidazolium tetrafluoroborate
[BMIM]Cl	1-butyl-3-methylimidazolium chloride
ΔP	pressure drop
Δt	time interval
μA	microampere
μL	microliter
μm	micrometre
2D	two dimensional
3D	three dimensional
Ac$^-$	acetate anion
ATR	attenuated total reflectance
B	empirical parameter of Vogel-Fulcher-Tammann equation
ca.	*circa*; approximately
CFA	chemical foaming agent
-CH$_3$	methyl

ChCl	choline chloride
Cl$^-$	chloride anion
cm	centimetre
CO$_2$	carbon dioxide
-COOH	carboxyl
DES	deep eutectic solvent
DRS	dielectric relaxation spectroscopy
DSC	differential scanning calorimetry
E	Young's modulus
e.g.	*exempli gratia*; for example
E$_{NR}$	normalized scale for solvent polarity relative to nile red
et al.	*et alli*; and others
F	foamed
FDA	Food and Drug Administration
FTIR	Fourier transformed infrared
g	gram
GRAS	generally recognized as safe
H$_2$O	water
HBD	hydrogen bond donor
Hz	Hertz
i.e.	*id est*; in other words
I$_2$	iodine
IBILs	imidazolium based ionic liquids
ICVs/3B's	Life and Health Sciences Research Institute (ICVS), University of Minho, 3B's Research Group - Biomaterials, Biodegradables and Biomimetics
IL	ionic liquid
K	degree Kelvin
keV	kiloelectronvolt
KF	Karl- Fischer
kg	kilogram
KHz	kilohertz
kN	kilonewton
L	span
LCA	life cycle assessment
MHz	megahertz
micro-CT	micro-computed tomography
min	minute
mm	millimetre
mM	millimolar
mm/min	millimetre per minute
mol/kg	mole per kilogram
MPa	megapascal
NADES	natural deep eutectic solvent
NF	non-foamed

nm	nanometre
NSAID	non-steroidal anti-inflammatory drug
$^{\circ}C$	degree Celsius
$^{\circ}C/min$	degree Celsius per minute
P	pressure
Pa/s	Pascal per second
PBS	phosphate buffer saline
P_c	critical pressure
PC	polycarbonate
PCL	poly(ε-caprolactone)
PE	polyethylene
PEG	polyethylene glycol
PET	poly(ethylene terephtalate)
pH	hydrogen power
PHA	polyhydroxyalkanoate
PHB	poly(β-hydroxybutyrate)
PLA	poly(lactic acid)
PMMA	poly(methyl methacrylate)
POM	polarized optical microscopy
PP	polypropylene
ppm	parts per million
PS	polystyrene
PVC	polyvinyl chloride
R^2	coefficient of determination
RTIL	room temperature ionic liquid
s	second
$scCO_2$	supercritical carbon dioxide
SCF	supercritical fluid
SEM	scanning electron microscopy
SO_2	sulphur dioxide
SPCL	starch poly(ε-caprolactone)
SPLA	starch poly(lactic acid)
SPLA50	starch poly(lactic acid) 50:50
SPLA70	starch poly(lactic acid) 30:70
T	temperature
t	time
T_0	Vogel temperature
T_c	crystallization temperature
Tc	critical temperature
T_d	degradation temperature
T_g	glass transition temperature
THEDES	therapeutic deep eutectic solvents
TIPS	thermally induced phase separation
T_m	melting temperature
TPS	thermoplastic starch

UV/Vis	Ultraviolet/Visible
VFT	Vogel-Fulcher-Tammann
VOC	volatile organic compound
wt%	weight percentage
σ_{DC}	direct conductivity
C	concentration
D	diffusion coefficient
J	flux
K	constant
$M(t)$	mass of diffusing substance at time t
f	frequency of the electric field
i	imaginary number
l	length
n	release exponent
t	time
x	x axis
η	viscosity
π	Pi
σ	shear stress
ω	angular frequency

Chapter 1
Introduction

1.1. Bio-based polymers

A significant part of the world that surrounds us is based on polymers or polymeric materials, either because they are present in most products that we use daily or because they are present in nature.

Although polymers have long been used, their origin was not fully understood until the beginning of the 20th century. Most of the polymers used until then were from natural sources, and it was not until the early 1900's that synthetic polymers were prepared, such as Baekaland's Bakelite resins obtained from phenol and formaldehyde [1–3]. Still, scientists were not fully informed about the nature of these materials, thinking they consisted of colloids. It was not until the 1920's that Hermann Staudinger demonstrated that polymers are macromolecules. In the following decades, the synthetic polymers field fully bloomed [1].

Polymers have many applications, and synthetic polymers are those most used in industry. However, natural polymers are present in animals, in the form of hydrocarbons, proteins, nucleic acids, as well as in plants, playing the role of energy source, and also as important constituents of other organisms.

Polymers can have different forms, such as rubber and plastics that differ mostly in their mechanical and thermal properties [1]. Of special interest are thermoplastic materials, which are polymers that can be heated, shaped and moulded above a certain temperature, but return to their initial state when cooled.

The plastics sector represents one of the major applications for polymers in modern society. The production of plastics has been growing worldwide since the 1950's, reaching a production of 288 million tons in 2012 [4]. In Europe, the main manufacturer of plastic materials is Germany, with an overall production of 19.5 million tons in 2012, which resulted in a 25.1 billion euros revenue [4]. The most used plastics are made from petroleum derived polymers, namely polyethylene (PE), polypropylene (PP), polyvinylchloride (PVC), polystyrene (PS) and poly(ethyleneterephtalate) (PET), which have a wide range of applications, mainly in packaging and in construction (Figure 1.1) [4].

It is interesting to note that approximately 7% of the total amount of petroleum produced is used in the production of plastics. This means that this growing and profitable industry is mostly dependent on a limited resource, which raises concerns about the long debated energy crisis. Recycling alone cannot solve the petroleum dependence, since it is known that petroleum-based plastic materials are not easy to transform or to degrade in the environment [5]. Also, almost 50 % of the plastic waste that is produced in Europe is still landfilled and not recycled [6].

One of the ways to decrease this petroleum dependence is to change the raw materials the plastics industry is based on, from petroleum derived polymers to bio-based polymers. This can have a true effect in modern societies, offering economic, ecological and social benefits [4,5].

Bio-based polymers can be defined as polymeric materials produced from renewable resources [7]. Bio-based plastics in particular offer great advantages over common petroleum-based plastics, related with the fact that they are readily available, renewable, have a low cost and are in most cases biodegradable. Nevertheless, they only represent ca. 1% of the total polymers market today [7]. This can be related with the high prices of some polymer feedstocks,

a low production capacity, and a not fully developed processing technology for this kind of materials.
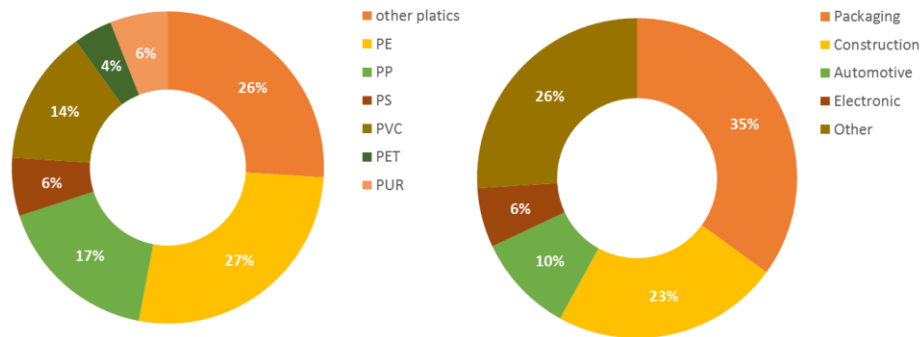
Figure 1.1- Main polymers used in the plastics sector, and their main applications (data for Germany, in 2012, adapted from [4]).

The concepts of bio-based polymers and biodegradable polymers are often assumed to be the same. However there are major differences between them. A biodegradable polymer is a material whose physical and chemical properties undergo deterioration and which completely degrades when exposed to microorganisms, carbon dioxide (aerobic process), methane (anaerobic process) and water (aerobic and anaerobic process).

In this sense, bio-based polymers can be biodegradable, as in the case of poly(lactic acid) (PLA), starch or polyhydroxyalkanoates (PHAs), or non-degradable, as in the case of biopolyethylene. Nevertheless, polymers can be derived from non-renewable resources, and still be biodegradable such as poly(ε-caprolactone) (PCL) [7].

The first bio-based polymers that were used were derived from agricultural feedstocks, but nowadays they are the result of biotechnology findings, since they can be produced by bacterial fermentation of renewable resources [7]. The class of natural bio-based polymers also comprises naturally occurring polymers, such as proteins and polysaccharides (starch, cellulose, chitin, collagen, and others).

The main ways to produce bio-based polymers using renewable feedstocks are:

1) using natural bio-based polymers with partial modifications to meet requirements (e.g. starch);
2) producing bio-based monomers by fermentation or conventional chemistry, and then proceed with the polymerization (e.g. PLA);
3) producing bio-based polymers directly from bacteria (e.g. PHA)

This is summarized in Figure 1.2 [7].
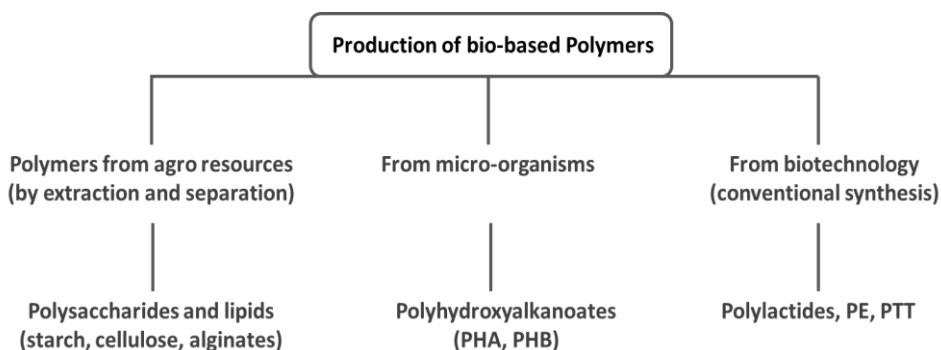
Figure 1.2- Bio-based polymer categories and production processes (adapted from [7]).

Bio-based polymers have found many applications. Bio-based plastics were first introduced in the market in the 1980's, mainly for packaging and agricultural applications.

In the following decade, the development of biodegradable products with improved properties took place, but the fact that some of these materials were petroleum derived materials meant that the main problem was not being addressed. It was not until the late 1990's that the bio-based plastic community showed interest in renewable materials [4].

Today bio-based and biodegradable materials are attracting a lot of attention. An example of such materials is starch and various aliphatic polyesters. They can be classified according to the constituent monomers, as PHAs with the general structural formula HO-R-COOH, or poly(alkylene dicarboxylate)s, and are subdivided in α-, β- and ω-hydroxy acids, according to the position of the hydroxyl (–OH) group relative to the carboxylic (–COOH) end group.

Aliphatic polyesters have been used in this work, together with starch. A brief review of the properties and applications of these polymers is given in the next sections.

1.1.2. Starch and starch-based polymers

As it was referred earlier, one of the strategies that can be used to substitute petroleum derived polymers is to use bio-based (and if possible biodegradable) polymers.

Starch is a biodegradable polymer that fulfills these requirements, mainly because it is easy to obtain from natural sources, is one of the most abundant biopolymers worldwide and is very cheap [8]. Approximately 7 million tons/year of starch are produced in Europe [9]. It is present in many plants and tubers, such as corn, wheat, rice, barley and potato.

Starch is produced by green plants for energy storage, in highly organized structures known as starch granules, located in plant cells. Starch is mainly composed by two types of molecules, namely linear and helical amylose and branched amylopectin. Amylose is an α-D-(1→6)-glucan, and amylopectin is a highly branched α-D-(1→4)-glucan with α-D-(1→6) linkages in the branch points [10]. Figure 1.3 represents the organization of the starch granules, as well as amylose and amylopectin structures.
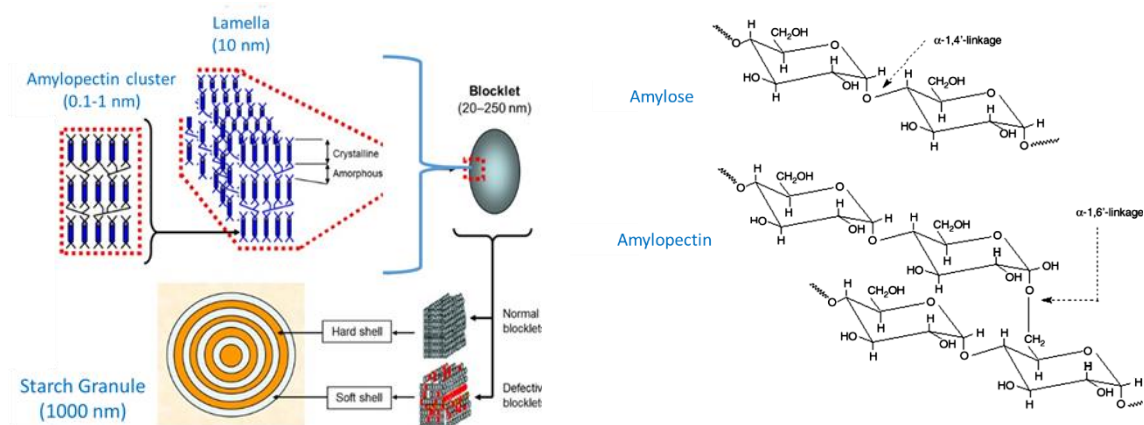
Figure 1.3- Internal organization of starch granules and molecular structure of the main components of starch - amylose and amylopectin (adapted from [8,11]).

Usually starch contains ca. 20-25% of amylose and 75-80% of amylopectin, but this is very dependent on the plant source. Starch is very hydrophilic, although its water content is highly dependent on the starch source, and also on the relative humidity at storage conditions [10].

Irrespective of its origin, starch is insoluble in cold water, but when heated, starch granules swell, and amylose and amylopectin leach out until the granules break down into a mixture of polymers in solution, which is known as the process of gelatinization [10]. The ratio between amylose and amylopectin present in starch will ultimately dictate most of its physical properties.

One of the problems of using starch is that it has limited processability, since it is very difficult to mold and transform. This is due to the fact that starch is semi-crystalline and there is also the possibility of the occurrence of retrogradation. This phenomenon consists in a natural increase of crystallinity over time, which leads to the increased brittleness of starch [7]. Also, and similar to other natural-based polymers, starch has high melting temperatures, often higher than the degradation temperature [12]. Because of this, native starch is not used directly [8].

One way to increase starch processability is to produce thermoplastic starch (TPS). TPS is obtained by casting aqueous dispersions containing starch, water and soluble plasticizers. On an industrial scale TPS is mainly produced via extrusion. The plasticizer (which can be for example glycerol, sucrose, urea or stearic acid) destroys the starch granules by breaking the inter- and intramolecular hydrogen bonds that hold the chemical structure of starch, achieving depolymerization [10]. The plasticization also helps to overcome the brittleness of starch through the softening of the structure via increased mobility of the macromolecular chains, allowing the polymer to be processed at lower temperatures.

When starch (or any semi crystalline polymer) undergoes thermal treatment, several thermophysical events can occur, such as glass transition, gelatinization, crystallization, melting and degradation. One of the critical thermophysical transitions for starch and other polymers is the glass transition, since it sets its processability limits. A plasticizer is known to increase the volume between polymer chains, lowering the glass transition temperature (T_g) [10].

1.1.3. Starch-based polymer blends

Another method to ease the processability and performance of starch is to modify its structure, either by blending, derivation, or graft copolymerization.

The blending of starch with biodegradable polymers, such as aliphatic polyesters, is common. Some of the most used polyesters for this purpose are PLA and PCL. In this work, two different starch-based materials were used, namely starch/poly(lactic acid) (SPLA) and starch/poly(ε-caprolactone) (SPCL), that will be discussed in the following sections.

1.1.3.1. Poly(lactic acid) (PLA)

An example of a poly(α-hydroxy acid) is PLA. Its basic unit is the monomer lactic acid. It can be obtained via bacterial fermentation from corn starch or sugars from renewable resources [7]. PLA can be synthesized from lactic acid (L- or D- enantiomer) by a polycondensation reaction, or by ring-opening polymerization of the lactide monomer (Figure 1.4).
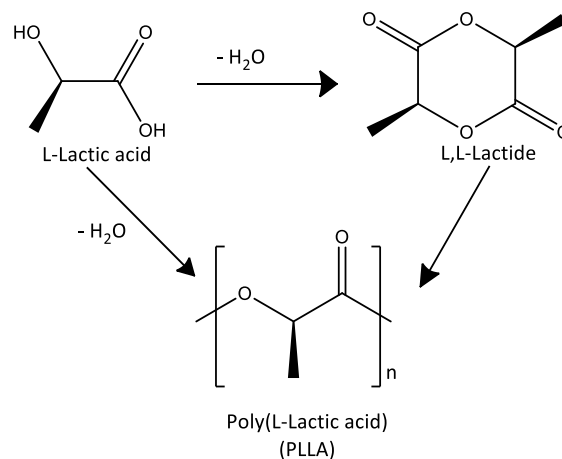
Figure 1.4- Synthesis of L,L-lactide and poly(L-lactic acid) (PLLA).

PLA has good transparency, a glossy appearance, high rigidity and the ability to tolerate various types of processing conditions. This makes PLA a good candidate to replace synthetic polymers such as PET, PS or polycarbonate (PC). The main drawbacks with its use are related to a relatively high cost, and to a glass transition temperature (T_g) of 60°C, which limits processability (poor modifiability and poor mechanical ductility) [13]. The glass transition is a second order phase transition that occurs over a temperature range within which T_g is defined. Bellow T_g, the polymer is hard and brittle, and above T_g it is moldable and soft.

There are several methods to overcome these processing limitations, such as the physical modification of PLA by blending and plasticization. Polymer blending has proved to be an effective and simple method to obtain new materials without having to synthesize new polymers [7,13]. There are examples of biodegradable polymers that have been blended with PLA, such as polyethylene glycol (PEG), poly(β-hydroxybutyrate) (PHB), poly-ε-caprolactone (PCL),

chitosan or starch. These blends resulted in materials with improved processability without sacrificing the biodegradability of PLA. Plasticization is another way to modify PLA, and is achieved by adding components (plasticizers) to the polymer so as to lower the T_g of the polymer, increasing its ductility and "softness". PEG, glycerol ad other organic based components have been used as plasticizers for PLA, resulting in PLA with improved processability.

PLA is a polymer that finds numerous applications in food packaging, membranes for the automotive industry, and even in textiles. Because PLA is a Food and Drug Administration (FDA) approved polymer, it is also applied in the biomedical field, for sutures, drug delivery devices, vascular grafts, artificial skin and orthopedic implants [9,14,15].

1.1.3.2. Poly(ε-caprolactone) (PCL)

PCL is an aliphatic polyester belonging to the poly(ω-hydroxy acid) family, and can be prepared by the ring-opening polymerization of ε-caprolactone using various catalysts (Figure 1.5), or via free radical ring-opening polymerization with 2-methylene-1-3-dioxepane.

PCL is a hydrophobic, semi-crystalline polymer with a low melting temperature (T_m= 59-60 °C), which makes it a polymer that can be easily moulded and shaped [16]. It is biodegradable (although at low rates), soluble in some organic solvents, such as chloroform and dichloromethane, and insoluble in ethanol, petroleum ether and diethyl ether [16]. Its exceptional biocompatibility together with the fact that it is also an FDA approved material, have led to applications in the biomedical field with very good results [16]. The fact that this polymer exhibits high permeability to many drugs and that it is excreted from the body once bioresorbed, makes it excellent for use in drug delivery systems, although its slow biodegradation rate makes it more suitable for long-term drug delivery purposes [16]. Also, PCL has found applications in dentistry, as a good material for surgical sutures, wound dressings and fixation devices, as well as for scaffolds [16].
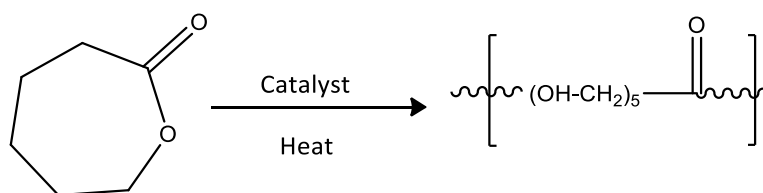
Figure 1.5- General synthesis of poly-ε-caprolactone (PCL) via ring opening polymerization.

1.2. Alternative solvents

In the processing or transforming of materials and polymers, whether they are petroleum-based or bio-based, the presence of a solvent is normally required, since the process is usually carried out in solution.

Until the last decades, aqueous or nonaqueous solvents such as organic solvents were used. When the scaling-up of a process is considered, the solvent choice plays a very important role, since it represents close to 85% of the mass utilization in a manufacturing process [17]. If the solvents to be used are organic, the emission of VOCs must be taken into account due to environmental and safety issues.

Since the birth of what is termed Green Chemistry, considerable efforts have been made to replace harmful solvents to the environment and general human health with "greener solvents" or in an ideal scenario, to implement solvent-free processes.

This is the basis of one of the 12 principles of green chemistry. These principles, first presented by Anastas and Warner in 1998 [18], should be applied to the design of chemical processes, so as to minimize environmental hazards:

"1) Prevention - it is better to prevent waste than to treat or clean up after it has been created.
2) Atom economy – synthetic methods should be designed to maximize the incorporation of all materials used in the process into the final product.
3) Less hazardous chemical synthesis – wherever practicable, synthetic methods should be designed to use and generate substances that possess little or no toxicity to human health or environment.
4) Designing safer chemicals – chemical products should be designed to affect their desired function while minimizing their toxicity.
5) Safer solvent and auxiliaries – the use of auxiliary substances (e.g., solvents, separation agents, etc.) should be made unnecessary whenever possible and innocuous when used.
6) Design for energy efficiency – energy requirements of chemical processes should be recognized for environmental and economic impacts and should be minimized. If possible, synthetic methods should be conducted at ambient temperature and pressure.
7) Use of renewable feedstocks – a raw material or feedstock should be renewable rather than depleting whenever technically and economically practicable.
8) Reduced derivatives- unnecessary derivatization (use of blocking groups, protection/deprotection, temporary modification of physical/chemical processes) should be minimized or avoided if possible, because such steps require additional reagents and can generate waste.
9) Catalysis – catalytic reagents (as selective as possible) are superior to stoichiometric reagents.
10) Design for degradation – chemical products should be designed so that at the end of their function they break down into innocuous degradation products and do not persist in the environment.
11) Real-time analysis for pollution prevention – analytical methodologies need to be further developed to allow real-time, in-process monitoring and control prior to the formation of hazardous substances.

12) Inherently safer chemistry for accident prevention – substances and the form of a substance used in a chemical process should be chosen to minimize the potential for chemical accident, including releases, explosions and fires " [18].

Green chemistry is also ruled by metrics that try to improve chemical process sustainability, such as the atom economy [19], the E-factor [20] or the mass efficiency and mass productivity [21]. The life cycle assessment (LCA) [22] together with the 12 principles is a good tool to evaluate a process or product sustainability.

Following the new paradigm of Green Chemistry, solvents such as ionic liquids (ILs), deep eutectic solvents (DES) and supercritical fluids started to gain attention in several areas of chemistry. The processing of materials and bio-based polymers was no exception.

1.2.1. Ionic liquids

Ionic liquids (ILs) are regarded as a major breakthrough in the area of recyclable solvents. They can simply be defined as ionic compounds that possess a melting temperature below 100 ^{o}C [23], or even close to room temperature (room temperature ionic liquids, RTILs). ILs are salts composed of ions, one or both of which are large, the cation having a low degree of symmetry, which reduces the lattice energy of the crystalline salt, leading to a lower melting point [24].

The field of ILs began with the discovery of ethylammonium nitrate, $[EtNH_3][NO_3]$ by Paul Walden in 1914 [23], but it was not until the 1970-1980s that major advances emerged. The potential of ILs arises from their physico-chemical properties, such as low vapor pressure, high electro-conductivity, high thermal stability and large liquid range [25].

Because ILs are composed of discrete cations and anions, there are numerous possibilities of combinations that can be engineered according to the final application. This is why ILs are also designated "tailor-made" solvents.

The most common ILs are based on imidazolium, ammonium, phosphonium, sulfonium pyridinium and pyrrolidinium cations. In the case of the anions, they can be fluorinated, such as hexafluorophosphate ($[PF_6]^-$), tetrafluoroborate ($[BF_4]^-$), trifluoroacetate ($[CF_3CO_2]^-$) or bis(trifluoromethylsulfonyl)imide ($[NTf_2]^-$), or non-fluorinated, such as tetrachloroaluminate ($[AlCl_4]^-$), nitrate ($[NO_3]^-$), acetate ($[CH_3CO_2]^-$), chloride ($[Cl]^-$) or bromide ($[Br]^-$). Some of these cations and anions are represented in Figure 1.6.

Although there is extensive research concerning many different IL families, the ones based on the imidazolium cation are the most studied [26].

ILs have found many applications, as solvents and reaction media [24], as catalysts [27–29], in batteries and solar/fuel cells [30,31], for the capture of CO_2 [30,32], among others.

ILs have also been applied in polymer sciences, playing multiple roles, in particular as solvents [33–35]. Several authors reported the ability of ILs to solubilize and modify natural polysaccharides, such as cellulose, lignocelluslosic materials, starch, chitin and chitosan [33–37]. The interactions within these polymers are similar to the interactions that are established between the polymeric chains and the IL ions, especially through the hydroxyl groups (-OH) that exist in the natural polymer structures. E.g. some authors have studied the interactions established between the ionic pair of the IL and the carboxylic (-COOH) groups of polysaccharides [38].

The term "green solvent" has been closely associated with ILs, mainly because of their negligible vapor pressure and non-flammability, which are clear advantages comparing to traditional VOCs. But it is clear that the "greenness" of ILs cannot be generalized, and they should not be called "green solvents" just because they are ILs [39,40]. One of the aspects that challenges the "greenness" of ILs is their environmental impact or, applying one of the green metrics, their E-factor. The syntheses of ILs implies extensive synthetic steps, the use of various reagents, and formation of by-products and/or waste [41]. Another very important aspect that is starting to be challenged is the eco and cytotoxicity, and biodegradability of ILs[42].

Many authors consider three generations of ILs. The first generation ILs started to be studied in the 1960's and comprised ILs with cations such as dialkylimkdazolium and alkylpyridinium, and anions such as chloroaluminate and other metal halides. They were characterized as air- and water-sensitive. To overcome these drawbacks, a second generation of ILs emerged in the 1990's, where the ILs were formed by weakly coordinating anions, such as $[BF_4]^-$ and $[PF_6]^-$ [39]. These ILs were extensively studied and characterized, and envisaged to be successful alternatives in many processes, but the high cost of their synthesis hampered industrial applications. More recently, a third generation of ILs appeared, with ions that are more biodegradable and readily available, such as natural bases, amino-acids and natural occurring carboxylic acids [39].
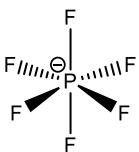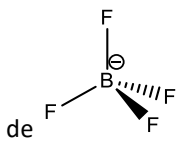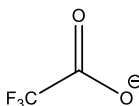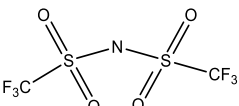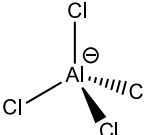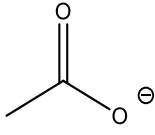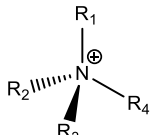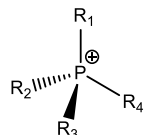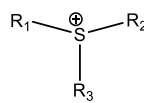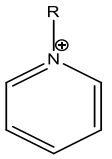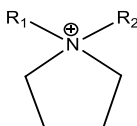
Figure 1.6- Chemical structures of the most common anions and cations that constitute ILs.

1.2.2. Deep eutectic solvents

Deep eutectic solvents (DES) appeared alongside with the third generation of ILs. DES have been termed by Abbot *et al.* in 2003 [43], and can be generally described as mixtures of hydrogen bond donors (HBDs) and simple halide salts, with a melting point lower than that of each individual component, i.e. with a eutectic point [44]. This happens due to the complexation of the salt with the HBD, and charge delocalization.

Figure 1.7 represents the behavior of a binary eutectic. In order to form a eutectic system, the two components must be miscible in the liquid state, but completely immiscible in the solid state. In the binary system presented in Figure 1.7, the *liquidus* lines represent the temperatures at which homogeneous mixtures of A+B begin to crystallize, and above those lines the mixtures are completely liquid. The *solidus* line represents the temperatures at which mixtures of A+B start to melt, and below it the mixtures are completely solid. The enclosed areas represent liquid mixtures of A+B plus solid A, or liquid mixtures of A+B plus solid B. The point where the *liquidus* and *solidus* lines meet is called the eutectic point, corresponding to the eutectic composition. A liquid of this composition is the only one which, when cooled, does not yield pure A or pure B, but rather a solid mixture of A and B [45]. The melting point depression is directly related with the strength of the interactions between the system components.
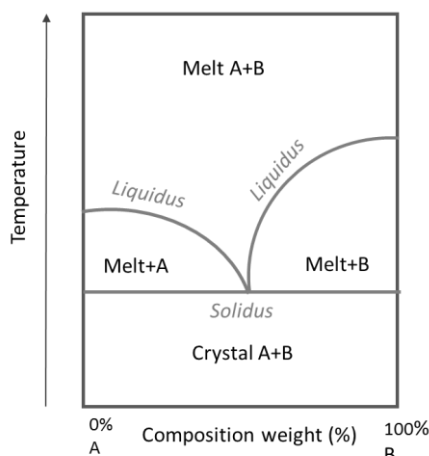
Figure 1.7- Schematic binary phase diagram of a eutectic system with two components. The point where the two *liquidus* and *solidus* boundaries meet is called the eutectic point.

One of the most common components of DES is choline chloride (ChCl), which is a cheap, biodegradable, non-toxic (derivative of vitamin B), quaternary ammonium salt. It can form DES with a variety of HBDs such as urea, oxalic acid, citric acid, succinic acid, amino-acids, among other renewable compounds. This clearly exemplifies some advantages that DES have over ILs: DES can be prepared in a simple way, without extensive synthesis steps, are biodegradable (and some even biocompatible) and non-toxic, in addition to being inexpensive, on account of being derived from renewable, abundant, resources. As such, the use of DES becomes more feasible for large scale applications, filling the gap left by second generation ILs [39].

DES share many characteristics with ILs, such as very low vapor pressure [46], although they are not true ILs because either one of their components is nonionic or they comprise two nonionic species [44].

DES have been successfully employed for extraction due to enhanced solubility of certain compounds when compared with traditional solvents. Such is the example of bioactive molecules including benzoic acid, griseofluvin, danazol or itraconazole, which are drugs with poor solubility in water, but show much higher solubility in ChCl:urea and ChCl:malonic acid DES [47]. DES have also been reported to be good extraction solvents for natural products [48] [49], and even for the extraction/dissolution of polysaccharides [50]. Pioneering work concerning the use of DES in biocatalysis was published in 1994 [51–53]. Lipases are one class of enzymes that are now known to have improved catalytic activity in DES [54]. DES have been reported also as useful solvents for separation technologies [55], nanotechnology and even DNA assembling [56]. DES also have applications in the electrochemistry area [57,58], with special emphasis on metal electrodeposition, as reported by Haerens *et al.* [59].

One of the areas that can benefit with the use of DES is the biomedical field, mostly due to the versatile, non-toxic, and biodegradable character of DES. They have already been reported to dissolve model drugs and at the same time increase their transdermal permeation and absorption, as in the case of a DES composed of menthol and camphor with dissolved ibuprofen [60]. Stott *et al.* have also reported DES ability for uses in drug delivery, with various compositions of ibuprofen combined with several terpenes [45].

As indicated, DES have improved properties compared to traditional solvents, and although they share many of IL characteristics, they are easier and cheaper to produce and in most cases non-toxic. Following a "green" chemistry philosophy, the development of even more sustainable and non-toxic DES followed, with the emergence of natural deep eutectic solvents (NADES) made from natural compounds. A small historical perspective of the DES field is given in Figure 1.8.
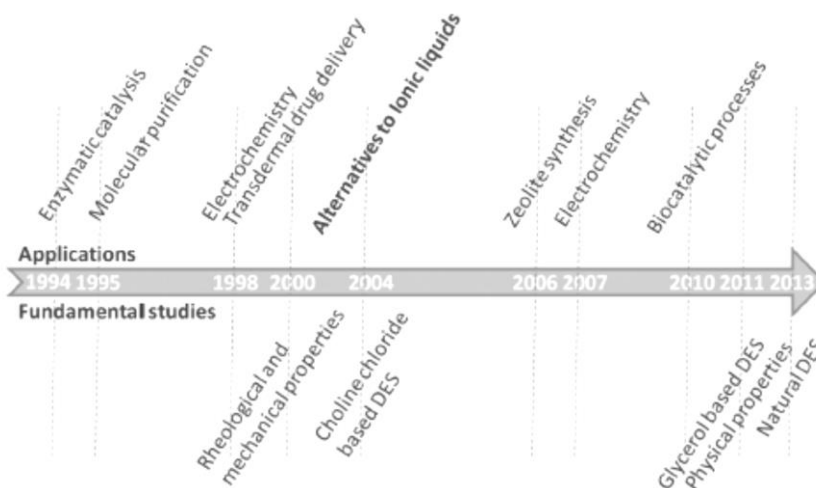
Figure 1.8 - Historical perspective of the developments in the DES field, together with some applications of DES (adapted from [61]).

1.2.2.1 Natural deep eutectic solvents

NADES are based on natural products (e.g. organic acids, amino-acids, choline chloride, sugars), which are abundant raw materials, biodegradable and have acceptable toxicity profiles [62]. NADES were termed by Choi *et al.*, following the discoveries that hypothesize that in living organisms there is an alternative medium between aqueous and lipidic media. The existence of this alternative medium can explain a great number of biological processes, such as the biosynthesis of poorly water soluble metabolites and macromolecules in the aqueous environment of cells [63]. According to the authors, these alternative media are composed of natural metabolites like organic acids, amino-acids and sugars [63]. Dai *et al.* later reported on a set of natural compounds that were able to form NADES, and some of the physico-chemical properties and applications of the latter, which broadened the concept of NADES [62].

Examples of NADES that are found in nature are the flowers' nectar, which was found to be a mixture of sugars (fructose-glucose-sucrose) and honey (a mixture of glucose and fructose) [62].

Several authors have recently been developing the concept of NADES, and detailed studies on the characterization and applications of NADES are now appearing in the literature [44,64].

As with DES, one of the applications envisaged for NADES is the extraction of natural compounds. Dai *et al.* [65] have performed the extraction of phenolic compounds of different polarities, obtaining satisfactory results. Also, Paiva *et al.* have performed the extraction of phenolic compounds from green coffee beans using a series of different NADES [61]. Extraction of phenolic compounds with known anti-oxidant activity is of the utmost importance for the pharmaceutical industry, and a growing and profitable business, but it is often difficult to carry out in conventional solvents and even in ILs, due to their poor solubility, possible contaminations with trace amounts of solvent and the poor sustainability of the process. On the other hand, NADES present good properties for the extraction of bioactive compounds, NADES have tunable polarity and viscosity, which can be adjusted as a function of the extract under study.

NADES and DES are now seen as safer and more sustainable alternatives for a great number of chemical processes and applications. Their advantages have been highlighted, and are expected to boost and create tools that allow the practice of the 12 green chemistry principles.

1.3. Supercritical fluid technology

Supercritical fluid technology has also been used in the course of this work, in order to establish a new processing methodology for bio-based polymers.

A substance or compound in nature has four known physical states: solid, liquid, gas and plasma. Figure 1.9 illustrates the solid, liquid and gaseous domains, all of them well defined by phase boundaries. When a substance or compound is above its critical temperature (T_c) and pressure (P_c) - critical point - it becomes a supercritical fluid (SCF). At the supercritical region the fluid shares properties common to liquids, namely density, and common to gases, such as

viscosity, compressibility and mass diffusion coefficient [66]. SCFs possess densities that enable the solvation of solutes, and viscosities that facilitate mass transfer phenomena [66].

Table 1.1 gives T_c and P_c values for some common substances.
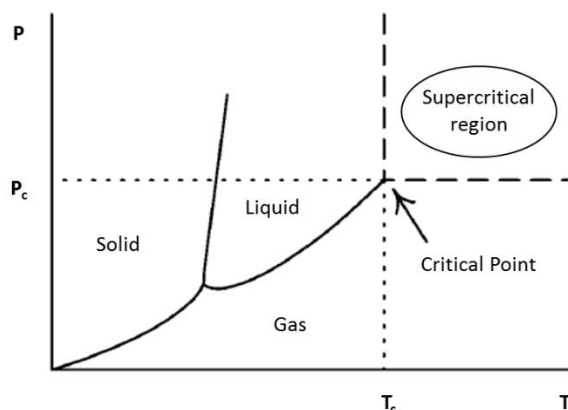
Figure 1.9- Phase diagram of a pure substance (adapted from [66]).

Table 1.1- Critical temperature and pressure of common SCFs (adapted from [66]).

Fluid	T_c (ºC)	P_c (bar)
carbon dioxide	31.1	73.8
water	374.1	221
ethane	32.5	49.1
propane	96.8	42.6
cyclohexane	279.9	40.3
methanol	240.0	79.5
ethanol	243.1	63.9
acetone	235.0	47.6

The most commonly used SCF is scCO$_2$, since it has critical parameters that are easily attained, especially a relatively low critical temperature that makes it possible to work with sensitive compounds, such as pharmaceuticals or bioactive molecules. Also, CO$_2$ is considered to be nontoxic, nonmutagenic, nonflammable and thermodynamically stable, having also a GRAS status (generally recognized as safe solvent) [66,67]. Because CO$_2$ elimination is easy (by depressurization or pressure drop), its use is more widespread. Supercritical CO$_2$ leaves no residues, contrary to the use of VOCs. Upon completion of an application, CO$_2$ can be recovered and reused, with no contributions to the greenhouse effect, and thus scCO$_2$ is also regarded as a "green" solvent. There are other substances with convenient values of critical pressure and temperature, such as ethane, but their flammability normally raises safety concerns.

1.3.1. Applications of supercritical fluid technology

One of the most common applications of $scCO_2$ is as an extraction solvent. There is extensive work on the extraction of compounds from natural sources, for example oil extraction, extraction of high added value compounds such as nutraceuticals or compounds from plants (important for cosmetic and pharmaceutical industries), among others [68]. The extraction of caffeine from coffee beans and tea is one of the examples where $scCO_2$ technology has proved to be highly efficient [69,70]. The main advantage of using $scCO_2$ as an extraction solvent is related with its mild conditions, flexibility and the possibility of modulation of the solvent power and selectivity. Its use yields a pure extract, eliminating the use of polluting organic solvents and extensive and expensive downstream processing of the extracts [68]. Also, the favorable transport properties that supercritical fluids exhibit allow deeper penetration into solid matrices, as is the case of plant cells, making the extraction process much faster and more efficient [71].

Supercritical CO_2 has also found applications in dry cleaning, wood treatment and food processing. These applications are well implemented and have been developed by established companies, such as Natex, FeyeCon, and Separex. This shows that $scCO_2$-based processes can successfully compete with more "traditional" ones that employ a large quantity of organic solvents as well as a high energy input.

It should be noted that the implementation of a supercritical fluid process, using $scCO_2$ for example, has the drawback of needing a high starting investment, but the final products purity and quality, as well as the very low environmental impact of this technology, hold major potential.

1.3.2. Polymer processing

The polymer industry is faced with the task of improving existing processes to transform and produce polymers, or to design new processes, in order to obtain materials with the desired characteristics (mechanical, optical, electrical and others).

There are several conventional polymer processing techniques, especially relevant in the plastics industry: extrusion, post die processing (that includes fibre spinning, film blowing and sheet forming), forming (including blow moulding, thermoforming and compression moulding) and injection moulding [2].

Extrusion is the most common processing technique for polymers, and refers to a continuous process where the molten polymer is pumped through a die with the desired cross-section. The polymer is then solidified by cooling after exiting from the die. It is widely used for mass production of thermoplastics and elastomers, yielding products such as tubing, pipes, and films, among others.

Another common processing technique is injection moulding, where a specific mould or cavity is injected with the fluid material (polymer), followed by the solidification of the product. The mould will determine the final shape of the processed material. It is very used for thermoplastics and rubbers.

Compression moulding techniques are more commonly used for the processing of thermosetting polymers (solid or viscous polymers that change shape irreversibly upon curing).

Although there is extensive literature on the types and characteristics of processing techniques, this will not be discussed in detail here, with the exception of foaming, a technique explored in the current work.

1.3.2.1. Conventional polymer foaming

The production of polymeric foams assumes great importance due to a continuous increase in the demand of such light-weight products. Polymeric foams have applications that range from insulator materials, shock and sound absorbents, packaging, in the automotive industry, as supports for catalysts, membranes for chemical separations, and especially in the biomedical materials' field, as scaffolds for tissue engineering, protein encapsulation and controlled release devices [67,72]. These polymeric foams have high impact strength and light weight, which ensures a higher mechanical strength-to-weight ratio, compared to other materials [67].

Whether they are synthetic or natural, polymers usually have high viscosity that makes processing difficult. Foaming is one way to overcome this drawback.

There are several conventional methods for the production of polymeric foams. In thermally induced phase separation (TIPS), a foaming or blowing agent, which is usually a low boiling organic liquid such as pentane, or a hydrochlorofluorocarbon, is dissolved in the polymer and induces a phase separation upon heating, followed by nucleation and cell growth.

According to classical nucleation theory based on the Gibbs free energy to create a void in a liquid [73], a supersaturated polymer-gas solution tends to form small bubbles (cells) in order to restore a low-energy stable state. The formation of these nuclei and consequent growth in a viscous liquid (e.g. heated polymer) is a very complex mechanism, influenced by temperature, pressure, viscosity, among others [73,74].

The TIPS method is a two-step method, in which the first step consists in exposing the polymer pellets to a foaming agent followed by transferring the partially foamed pellets to a mould and again exposing them to the foaming agent. When expansion of the polymer pellets occurs, they stick together and remain with the shape of the mould. This method has the advantage that large blocks of foamed polymer can be easily obtained, whose density can be controlled by controlling the amount of partially foamed pellets added to the mould [72].

A variation of the TIPS method to obtain polymer foams is to dissolve the polymer in a solvent at high temperatures, and then by quenching the temperature, there is a phase separation, upon which solvent removal results in a polymeric foam [72].

Another method of foaming is to use a chemical foaming agent (CFA), such as aliphatic hydrocarbons or halogenated hydrocarbons (e.g. trichloromethane, dichlorofluoromethane), which are thermally unstable components that upon heating decompose into gaseous components, causing foaming.

The casting and leaching method is also a valid alternative to produce polymer foams, where the polymer is dissolved in a volatile solvent and then cast into a mould that contains a solid porogen (usually a water soluble salt, such as NaCl or KCl). Later, the porogen is washed out and the solvent is evaporated, and a highly porous polymer is obtained. In this method, the control of size and morphology is possible, by carefully choosing the porogen.

The major problem with these conventional foaming methods is that they can lead to unwanted contaminations, and to foams that have residual organic solvents that can be harmful. Another unwanted drawback is that the incorporation of compounds is very difficult using the conventional methods. In biocompatible foams used, for example, for drug delivery, the incorporation of bioactive compounds assumes great importance, and the foaming method should not cause the loss of activity of these compounds, which is difficult when using volatile organic compounds (VOCs).

An alternative to the TIPS, casting and leaching methods is to use gases as blowing agents, and also supercritical fluids, which are "greener" and potentially non-toxic.

There has been extensive research on using gases as foaming agents, especially nitrogen and carbon dioxide, although the current work is more focused in the use of supercritical carbon dioxide ($scCO_2$), because it offers additional benefits in the processing of biopolymers.

1.3.2.2. Supercritical fluid foaming

One other interesting application of $scCO_2$, and the one concerning the work here presented, is that it is possible to process and foam bio-based polymers using $scCO_2$.

The $scCO_2$ foaming process (or SCF foaming process) can be simply represented by two steps, one where the polymer is saturated with $scCO_2$, and an expansion, second step, where CO_2 leaves the sample. The sorption of $scCO_2$ into polymers causes their swelling and also changes their mechanical and physical properties, the most important of which being the plasticization accompanied by the decrease in T_g. But this plasticization induced by $scCO_2$ also results in a reduction of the viscosity of the polymer, as well as enhanced diffusion of additives in the polymer matrix (allowing impregnation or extraction) [75]. Figure 1.10 shows some of the effects of $scCO_2$ in polymers.
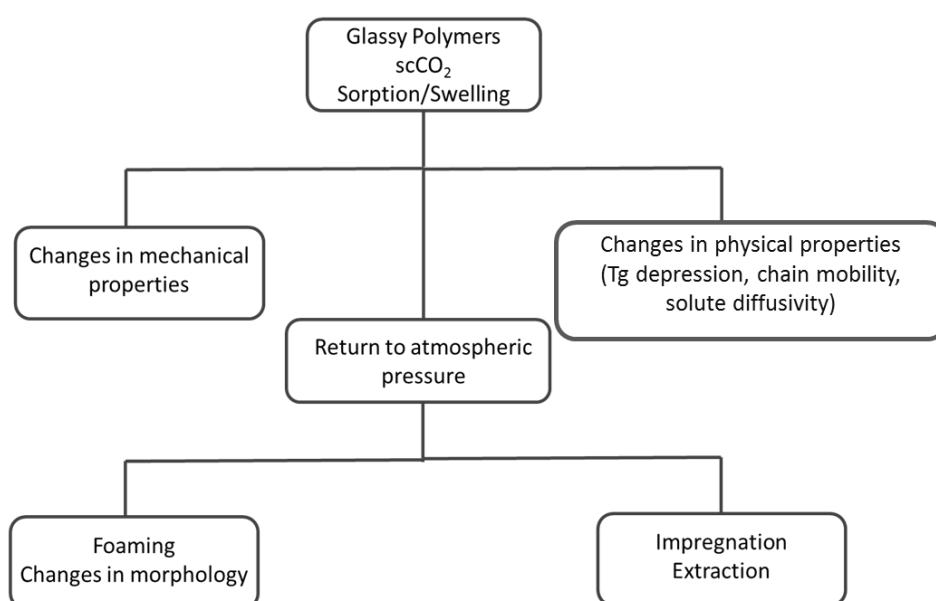
Figure 1.10- General scheme of the effects of $scCO_2$ foaming in polymers (adapted from [75]).

The plasticization effect caused by CO_2 is due to the ability of CO_2 molecules to interact with polymer molecules, reducing chain-chain interactions and increasing the polymeric chains' distance. This plasticizing effect of CO_2 is also thought to result from the ability of CO_2 molecules to interact with the basic sites in polymer molecules [75], as for example the interaction between CO_2 and carbonyl groups of poly(methyl methacrylate) (PMMA). as reported by Kazarian *et al.*, which was suggested to be a Lewis acid-base interaction [76].

Figure 1.11 represents a basic scheme of the events that occur in $scCO_2$ foaming. In the saturation step, the polymer is subjected to $scCO_2$ for a certain length of time. The T_g of the polymer decreases, and the polymer is plasticized. The polymer swells and its viscosity decreases, allowing the processing of the polymer-CO_2 mixture at comparatively lower temperatures. When the polymer is saturated, a rapid decrease in the pressure (depressurization) or an increase in temperature will shift the thermodynamic equilibrium, and CO_2 will try to escape from the polymer, causing antiplasticization [72,75].
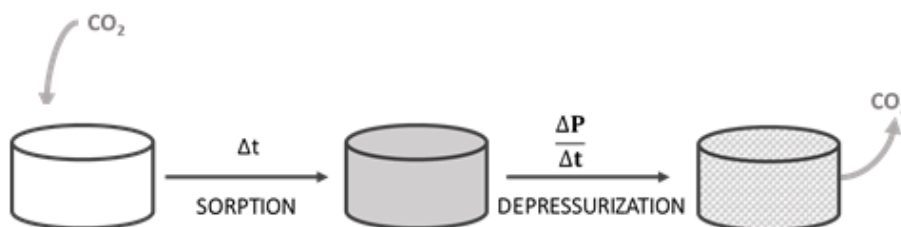
Figure 1.11- Schematic representation of the $scCO_2$ foaming of a polymeric material.

Lowering the pressure at constant temperature causes a decrease in the amount of CO_2 absorbed in the polymer. The T_g begins to rise, and the sudden reduction in pressure leads to the generation of nuclei (due to supersaturation). These nuclei grow to form a cellular (porous) structure until vitrification of the polymer occurs [77], and the foamed structure is "frozen".

Operational parameters such as the saturation pressure, the saturation temperature, depressurization rate and pressure drop, are very important for the foamed polymeric structure [77]. The combination of all these parameters will ultimately define the porosity and pore size of the final structure, but it is important to notice that they are all interdependent.

If the foaming is carried out at a constant pressure, but high temperatures, this will reduce the viscosity of the polymer and increase the CO_2 diffusivity, favoring cell growth. Higher temperatures also decrease CO_2 solubility in the polymer, meaning that there will be less CO_2 available for nucleation and growth of the pores. Higher foaming temperatures will then result in a polymer with bigger but less pores [77].

On the other hand, if the temperature is constant but the pressure is high, more CO_2 will be dissolved in the polymer. This will create a larger number of nucleation sites that will grow and form the pores, but with smaller size (more pores, but with smaller dimensions) [77].

The depressurization rate or the rate of gas release ($\Delta P/\Delta t$) from the polymer also has a crucial effect. If the release of CO_2 is very fast, the amount of pores will be high but with smaller

dimensions, due to the time allowed for cell growth. If the gas release is slower, the formation of pores is enhanced [77].

Foaming using $scCO_2$ is also intimately dependent on the solubility of this gas in the polymer. If the solubility of $scCO_2$ is low, the foaming process is compromised. However, there is the possibility to use plasticizers, as referred in a previous section, which will reduce T_g of the polymer. Organic species have been previously used as plasticizers, such as glycerol, but ionic liquids and deep eutectic solvents are also reported to act in the same manner [12,78].

The use of these solvents has the additional advantage that they are regarded as more sustainable solvents, when compared to common organic solvents.

1.4. Aims and structure of the thesis

This work focuses on green, sustainable methods for bio-based polymers processing, using different "alternative solvents", namely supercritical fluids (SCF), ionic liquids (ILs) and deep eutectic solvents (DES).

An alternative methodology for the processing of starch-based polymers is presented, accomplished via supercritical fluid foaming. The use of solvents such as ILs and DES was also assayed, in an attempt to improve the process.

Since DES and natural DES (NADES) are a new and challenging field, part of the work is also devoted to the preparation of these solvents. Their physico-chemical characterization and some applications are also described.

The thesis is divided in 7 different chapters that intend to provide a multidisciplinary approach to the field of biopolymers processing. The first two chapters introduce all the themes dealt with throughout the work, as well as the techniques and experimental methods used.

In chapter 3, a green processing methodology is presented for the starch-poly(lactic acid) (SPLA) polymer blend , where the combination of SCF technology and ILs is put forward as an alternative processing method, particularly in what concerns SCF foaming. The well-known relationship between supercritical carbon dioxide ($scCO_2$) and ILs is explored, and proven to be valuable in the foaming enhancement of this polymer blend, since the amount of CO_2 present in the polymer is higher when the polymer is doped with IL. To better understand and quantify the extent of this effect, a mathematical analysis that allowed the determination of CO_2 sorption and desorption coefficients in SPLA was also carried out, based on sorption experiments.

Chapter 4 reports work carried out in order to better understand the specific effects of IL doping in a polymer blend, starch-poly(ε caprolactone) (SPCL), and its subsequent processing via SCF foaming. Here, a starch-based polymer blend was also used, and the effects of doping with two different imidazolium-based ILs were studied. Thermal and dielectric characterizations were carried out, as well as mechanical testing, providing clues to the effects of the IL-polymer interaction and the effect of SCF foaming.

Given the fact that one of the goals of this work is to develop sustainable polymer processing methods, and that the use of ILs as "safe" solvents can sometimes be challenged, the use of IL-related solvents was suggested. Thus in chapter 5 deep eutectic solvents (DES) and their natural derivatives (NADES) are introduced. Because there is still scarce literature on the thermophysical properties of these solvents, several techniques are used to characterize them.

The application of NADES as SCF foaming enhancers is assayed in chapter 6. The work is performed in order to study the ability of NADES to behave in a similar manner to ILs, when combined with $scCO_2$ in the foaming process. Also, the preparation of DES with potential therapeutic applications, and their impregnation in the SPCL polymer blend is assessed.

The final chapter presents the global conclusions of the work carried out within the thesis, as well as some considerations on possible future work.

All the work presented in this thesis was carried out having in mind green chemistry principles, through the combination of different areas in an attempt to devise a truly sustainable route for polymer processing.

Chapter 2

Methods and Experimental

2.1. Materials and Methods

2.1.1. Materials

2.1.1.1. Polymers

In this work, different polymer blends were used. One of them is composed by corn starch and poly(lactic acid) (SPLA) with different weight percentages (wt%) of poly(lactic acid), 50%-SPLA50 and 70%- SPLA70, obtained from Novamont. The other polymer blend used along the presented work is composed of starch and poly-ε-caprolactone 70% (SPCL) and was obtained from Biocycle.

2.1.1.2. Ionic liquids

The ILs used in chapter 3 and 4, used for the purpose of supercritical fluid foaming enhancement of SPLA and SPCL, were 1-butyl-3-methylimidazolium, [BMIM]Cl and 1-butyl-3-methylimidazolium acetate [BMIM]Ac, both from Sigma-Aldrich.

2.1.1.3. Deep eutectic solvents

All the components used in the preparation of DES reported in chapters 5 and 6 were choline chloride, D-(+)-xylose, D-(+)-glucose, citric acid monohydrate (Sigma-Aldrich), D-(+)-sucrose (Fluka), L-(+)-tartaric acid (Fischer scientific) (*r*)-(-)-mandelic acid (Alfa Aesar) and (*r,s*)-(±)-menthol (Aldrich).

Ibuprofen, was obtained from ibuprofen sodium salt (Fluka). A solution of 50 mg/mL in distilled water is prepared, and the pH adjusted by adding small amounts of a solution of hydrochloric acid (1M). The ibuprofen sodium salt is reacted with the hydrochloric acid yielding ibuprofen in its acid form and sodium chloride salt. The ibuprofen is then extracted with dichloromethane (Merck) that is subsequently dried and evaporated, until a final fine white powder is obtained. The purity of the obtained ibuprofen was proved by means of FTIR spectroscopy, comparing with literature data. "The reagents were obtained with the maximum purity commercially available.

2.1.2. Methods

Different experimental techniques were used during the work presented in this thesis, in order to fully characterize the processed polymeric materials, and also to give more information on the prepared DES. A brief description on the fundamentals of each technique and the experimental conditions are presented in the following sections.

2.2.2.1. Chapters 3, 4 and 6

a) Compression moulding

The polymer samples, doped and undoped with ILs and DES, used along the work here reported were obtained by compression moulding. SPLA or SPCL were mixed with IL or DES in different weight percentage to yield homogeneous mixtures. Care was taken to ensure that no phase separation occurred. The mixture was poured into stainless steel rings (12x2 mm) and then compression molded using a Moore Hydraulic Press (UK) at 80 ^{o}C, 6 MPa, for 15 min. Heating was required to facilitate molding. This process yields a homogeneous sample.

b) Supercritical fluid foaming

As it was referred in the introduction, supercritical fluid foaming- SCF foaming, allows the creation of porous polymers, using more biocompatible and "green" technology. The CO_2-assisted foaming of biocompatible and/or biodegradable polymers, represents a new methodology and the opportunity to develop materials with interesting applications [75]. It also combines the advantages of using a supercritical fluid as a foaming agent; it is environmentally friendly, has tunable solvent power and viscosity, has a plasticization effect in glassy polymers, has an enhanced diffusion rate and can be easily and completely separated from the polymer [79]. The carbon dioxide used in the foaming and sorption experiments conducted along the work here presented (99.998 %) was supplied from Air Liquide.

The foaming process can simply be divided in three steps:
1) mixing and formation of a homogeneous solution of foaming agent (in this case $scCO_2$) and polymer melt;
2) cell nucleation, normally induced by a temperature increase of a pressure decrease;
3) cell growth and coalescence, resulting from a combination of mass transfer and fluid dynamics processes [80].
In this work, the foaming process reported in chapters 3, 4 and 6 was carried out in a batch system. The samples were placed in a high pressure vessel and then pressurized and saturated with $scCO_2$ (the experimental details are all well described in the experimental section of each chapter). After a certain time the vessel was slowly depressurized until ambient pressure (Figure 2.1).
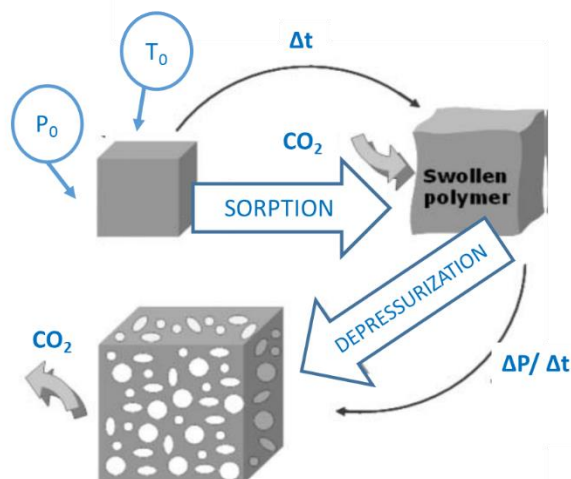
Figure 2.1- Schematic representation of the SCF foaming process of a polymer (adapted from [81]).

The nucleation and cell growth that will result in the foamed polymer, are controlled by the pressure release rate and by the foaming temperature [80]. In fact, the temperature of the foaming, the pressure drop rate and the CO_2 concentration on the polymer (solubility) are essential factors to take into account in the SCF foaming process [80].

A homogeneous nucleation process is directly related to a process of activation that leads to the formation of an initial unstable disperse phase (nucleus); the resulting nuclei grow and form the final cells (pores) or they can collapse on itself. If the nuclei reach a critical dimension, they grow until physically and thermodynamically possible [79]. In this supercritical fluid (SCF) foaming process, the formation of the nuclei is related to the thermodynamic instability that occurs in the depressurization step (and consequently to the depressurization rate).

As it was previously referred, the foaming temperature is of critical importance in this foaming process; an increase in temperature increases CO_2 diffusivity inside the polymer reducing its viscosity, and the pores are formed more easily. Also, an increase in temperature decreases solubility of CO_2 in the polymer, meaning that there are less gas molecules and less nucleation sites, leaving more space for the cells to grow. This means that, higher the temperature, larger (but fewer) the pores [79].

Pressure is also of paramount importance for the SCF foaming process. Increasing the pressure increases the solubility of CO_2 within the polymer (more CO_2 dissolved in the polymer); this leads to an increase in the supersaturation of the polymer during depressurization, and more cells are nucleated within the sample volume. With higher pressures, more cells are obtained, but also smaller cells due to decreased diffusivity of $scCO_2$ inside the polymer.

Another important parameter in the SCF foaming process is the solubility of $scCO_2$ in the polymer, which will later determine the extent of the plasticizing effect of CO_2. This has been one of the drawbacks when SCF foaming of natural-based polymers was considered, the low solubility of $scCO_2$. However, there is the possibility to use plasticizers (as it was referred in the previous chapter), which will reduce the glass transition temperature (T_g) of the polymer.

Following previous work, that presented the use of an ionic liquid (IL) as a plasticizer for the SCF foaming of the polymer blend SPCL, the same approach was adopted in this work

(chapters 3 and 4). ILs have been reported as plasticizers of natural polymers, and the synergy they establish with scCO$_2$ is advantageous for this purpose, since they are able to dissolve certain amounts of CO$_2$, but are not soluble in the scCO$_2$ phase. In the work reported by Duarte *et al.* [82], the influence of the foaming pressure, temperature, soaking time and presence of IL in the foaming of SPCL were studied. It was observed that the presence of IL does in fact enhance the SCF foaming ability, and that higher pressures (20.0 MPa) result in foams of higher porosity, and that temperatures close to 40 °C also result in foams of maximum porosity. Also, it was observed that a maximum of one hour of soaking time (time of contact between polymer and scCO$_2$) resulted in maximum porosity.

The experimental conditions for the foaming experiments reported in this thesis were then similar to the ones reported previously. Even in the case of chapter 6, where different deep eutectic solvents are studied as possible foaming enhancers for the polymer blend SPCL; they are expected to behave similarly to ILs, with the advantage of being more biodegradable and biocompatible, which can envisage different applications.

A study on the sorption ability of the polymer blend SPLA, undoped and doped with IL was also performed in chapter 3. Since it was already observed that starch-based polymer blends doped with IL were able to exhibit enhanced foaming, and this is closely related with the fact that the presence of IL increases the solubility of CO$_2$ in the polymer, the measurement of the sorption assumed great importance. The details of the experimental procedure are described in the next section and in the experimental section of chapter 3.

c) Mathematical modelling of diffusion *(sorption experiments)*

The mathematical treatment of the results obtained from the sorption results was also carried out, following Fick's theory of diffusion through isotropic matrices. The sorption experiments were carried out for two SPLA blends, both with and without IL doping.

The choice of the mathematical approach to be made, depends on the thermophysical characteristics of the polymer, if it is in the rubbery state (above T$_g$) or in the glassy state (below T$_g$). If the diffusing substance causes an extensive swelling of the polymer changing its shape, it exhibits a "non-Fickian" behaviour, and Fick's laws of diffusion cannot be applied. In the case of the samples under study, the extensive swelling was not observed. This means that the mathematical analysis of the sorption measurements can be made using Fick's theory of diffusion through isotropic matrices [83,84].

Fick's theory of diffusion is based on the hypothesis of the rate transfer of a diffusing substance through unit area of a section is proportional to the concentration gradient normal to the section [85], and Fick's first law is given by equation 2.1 where D is the diffusion coefficient, C is the concentration of the diffusing substance and J is the flux.

$$J = -D\frac{\delta C}{\delta x}$$
(2.1)

Fick's second law of diffusion is a differential equation solution of the first law, assuming that the diffusion is one dimensional, meaning that the gradient of concentration occurs only in one direction, along the x axis (equation 2.2).

$$\frac{\partial C}{\partial t} = D\left(\frac{\partial^2 C}{\partial x^2}\right) \tag{2.2}$$

A particular solution of Fick's second law of diffusion that describes the time dependence of the diffusing material out of the sample (in this case a slab of thickness l), can be derived. Considering that there is a uniform initial distribution and the surface concentrations are equal, the boundary conditions are

$$C = 0 \text{ for } x = 0 \text{ and for } x = l \text{ at } t = 0$$

where l is the thickness of the sample, and

$$C = C_0 \text{ for } 0 < x < 1 \text{ at } t = 0$$

resulting in

$$M(t) = \frac{8 M_0}{\pi^2} \sum_{n=0}^{\infty} \frac{1}{(2n+1)^2} \, e^{\left[((-(2n+1)/1)\pi)^2 D t\right]} \tag{2.3}$$

The simplified solution of Fick's second law, that describes the time dependence of the diffusing material out of the sample, in this case has a slab shape of thickness l, and that considers an uniform initial distribution and that the surface concentrations are equal, is given by equation 2.4

$$\frac{M(t)}{M_0} = 1 - \frac{8}{\pi^2} e^{\left(\frac{-D s \pi^2 t}{l^2}\right)} \tag{2.4}$$

where $M(t)$ is the mass of the diffusing substance at time t and M_0 is the equilibrium sorption attained theoretically after infinite time [85].

The linear relationship between the amount of CO_2 dissolved in the polymer and the square root of desorption time validates the assumption that we are in presence of Fickian diffusion phenomenon.

2.2.2.2. Chapters 5 and 6

a) Preparation of DES

DES were prepared following a very simple procedure. The corresponding amounts of each component, in the proper mole ratios, were weighed and dissolved in water. The two solutions were mixed and homogenized, and later water was removed in a rotatory evaporator, at 50 °C under vacuum, until a clear viscous liquid was obtained. DES were subsequently kept in a desiccator and under vacuum.

In the case of DES reported in chapter 6, they prepared by weighing the amounts corresponding to the correct molar ratio, and heated until a viscous liquid was otained (at ca. 70 °C for choline chloride/mandelic acid mixture, and room temperature for menthol/ibuprofen mixture) under constant stirring.

2.2. Morphological Characterization

2.2.1. Scanning electron microscopy (SEM)

SEM was used along the work presented here, in order to give more information on the external morphology and to visualize the prepared polymeric materials, especially after the process of supercritical fluid foaming.

SEM is a microscopy technique, based on the use of a high-energy electron beam, which is focused in a given sample and generates different signals that are directly related with the electron-sample interactions. The accelerated electrons in that beam carry a certain kinetic energy, which is dissipated (the incident electrons are decelerated) when in contact with the sample, originating different signals depending on the electron-sample interactions [86]. These interactions can be inelastic or elastic. The originated signals can include secondary electrons, backscattered electrons, photons (characteristic X-rays), visible light (cathodoluminescence) and heat (Figure 2.2). The secondary electrons are normally used to show the morphology and topography of the sample, while the backscattered electrons are more useful when illustrating contrasts in multiphase compositions. X-rays generated in this type of experiments are very useful in elemental analysis, since they allow identification of the composition of a sample (types and relative ratio of the atoms in a sample) [86].

SEM gives detailed information on samples' texture (external morphology, and internal when the cross section is analysed), chemical composition and even the crystalline structure. It is a very powerful technique, although it requires previous sample preparation (in order to turn it conductive).
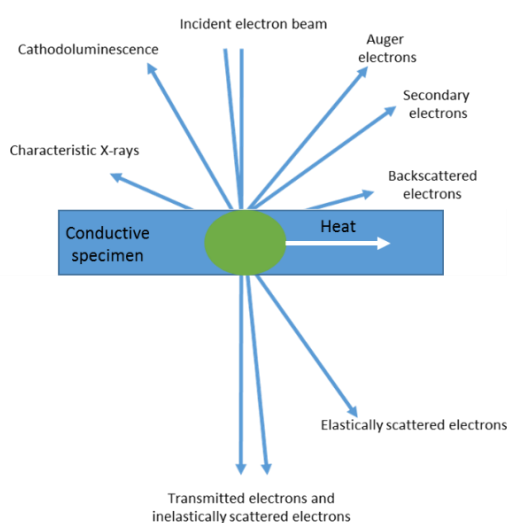
Figure 2.2- Different signals produced by the interaction of the high energy electron beam and a sample.

In this thesis SEM was used to observe differences caused by the supercritical fluid foaming process, mainly the formation of pores upon supercritical carbon dioxide exposure.

All the SEM results reported in chapters 3, 4 and 6 were obtained in a Leica Cambridge S360 scanning electron microscope. The samples were fixed by mutual conductive tape on aluminium stubs, covered with gold/palladium (Au/Pd) sputter coating. When the cross-sections of the samples were observed, prior fracturing with liquid nitrogen was required.

All the SEM experiments were performed in the partner institution ICVS/3B's associated laboratory.

2.2.2. Micro-computed tomography (Micro-CT)

Micro-CT was used in this work, in order to allow both the visualization and the morphological analysis of the processed polymeric materials.

Micro-CT has been used in the characterization of polymeric foams produced via supercritical fluid foaming [82], since it allows the analysis of the interior of the polymers, and to grasp more information on the three dimensional (3D) organization of the produced structures. It also allows the measurement of the complete 3D volume, without further sample preparation or fixation. This is a clear advantage when compared with other microscopy techniques (for example SEM), and also, this is a non-destructive technique.

Micro-CT is a technique that combines microscopy and X-ray technologies, in order to form images based on X-rays transmitted by the sample under analysis. The X-ray absorption depends on the density and thickness of the samples, and it is generally higher for elements of higher atomic number in the periodic table [87].

All the micro-CT analysis performed and reported in chapters 3, 4 and 6 were conducted in a high-resolution micro-CT Skyscan 1072 scanner (Skyscan).

In chapter 3, SPLA50 and SPLA70 blends, as well as these blends doped with 10 wt% of ionic liquid [BMIM]Cl, submitted to supercritical fluid foaming, were analysed by micro-CT. The four different samples were scanned in high resolution mode, using pixel size of 14 μm, with 1.5 seconds of exposure time. The X-ray source was set at 53 KeV, with 222 μA of current for SPLA70 and 189 μA for SPLA50. Isotropic slice data were obtained by the system and reconstructed in 2D images. These slice images were compiled and analysed to obtain quantitative architecture parameters. The morphometric analysis was performed using a micro-CT analyser (CT Analyser v1.5.1.5, SkyScan). Regions of interest were selected in each slice image and threshold to eliminate background noise and to distinguish polymer material from pore voids. The two dimensional (2D) images were visualized using a Data-viewer software (v1.4.4, 64-bit, SkyScan) and the 3D reconstructions were bult using a CTvox software (v2.3.0 r810, SkyScan).

In chapter 4, the analysis of all the SPCL foamed samples (SPCL and SPCL doped with different ionic liquids, in different wt%), were analysed following the above described procedure. The X-ray source was set at 53 KeV with 189 μA current.

In Chapter 6, were SPCL doped with different eutectic solvents was submitted to supercritical fluid foaming, the analysis was also carried out using similar parameters.

All the micro-CT experiments were performed in the partner institution ICVS/3B's associated laboratory.

2.2.3. Polarized optical microscopy (POM)

POM is a very interesting experimental technique, since it provides a unique window into the internal structure of crystalline samples, and has applications that range from collecting images to determine particle size and shape of crystals, to full optical crystallography [88]. Polarized microscopy has already been used to study the phase behaviour of ILs [89], and in this work, POM was used in chapter 5 where the thermophysical characterization of different deep eutectic solvents was carried out. POM micrographs of different prepared deep eutectic solvents were collected, at different temperatures, and together with differential scanning calorimetry results, characterizing their thermal behaviour.

The experiments were performed in an Olympus 3x51 optical microscope, equipped with a Linkman LT536 liquid nitrogen-cooled cryostage (in order to attain low temperatures). The micrographs presented in chapter 5 were taken at appropriate temperatures, using an Olympus C5060 wide zoom camera.

The POM experiments were performed in the collaboration with CQFM IN - Institute of Nanoscience and Nanotechnology/IST.

2.3. Chemical characterization

2.3.1. Karl-Fischer titration

For all the prepared materials reported in chapters 4, 5 and 6, the water content was determined by the Karl-Fischer titration method. The reagent used in Karl-Fischer titration was Hydranal Coulomat AG (Sigma-Aldrich).

The Karl-Fischer (KF) method, developed by Karl-Fischer, was developed taking into account the Bunsen reaction, used for the determination of sulphur dioxide in aqueous solutions, according to the following reaction

$$SO_2 + I_2 + 2H_2O \rightarrow H_2SO_4 + 2HI.$$
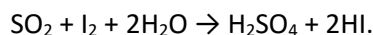
This reaction can be used for the determination of water, if the sulphur dioxide is in excess and the acids produced are neutralized by a base [90].

KF titration is able to determine free and bound water of an analyte, working over a wide concentration range from ppm to 100 %, with reproducible and correct results [90]. In this case a Coulometric titration was performed, meaning that the electric current is used; the current releases the stoichiometric corresponding amount of iodine from the iodide-containing KF reagent by electrolysis.

In this work a KF 831 Coulometer without diaphragm was used (Figure 2.3), where the main compartment contains the platinum anode, anode solution and analyte. The anode solution (KF reagent) is normally composed of an alcohol (e.g. methanol), a base (e.g. pyridine), SO_2 and I_2. There is also another separated electrode, the cathode, which is immersed in the anode solution. The platinum anode generates I_2 when current is provided through the solution and the following reaction occurs

$$H_2O + I_2 + [RNH]^+SO_3^- + 2RN \rightarrow [RNH]^+SO_4CH_3^- + 2[RNH]^+I^-$$
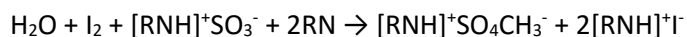
where for each mole of H_2O present, one mole of I_2 is consumed.

The detector circuit maintains a constant current between the two detector electrodes. At the equivalence point, an excess of I_2 accompanied by an abrupt voltage drop, marks the end point. So, the amount of current needed to generate the I_2 and to reach the end point of the titration is then used to calculate the amount of H_2O in a given sample.

The Karl Fischer coulomter used in this work is automated and carries the titration automatically, meaning that the titration rate and volume increments are controlled according to the signal measured by the indication system [90]. All the KF results presented in this thesis are the average of a minimum of three experiments.

Figure 2.3- Karl-Fischer Coulometer (adapted from [90]).

2.3.2. Fourier transformed infrared spectroscopy (FTIR)

Infrared spectroscopy is a well-known and established technique for the characterization of materials and chemicals, based on the interaction of light with mater in the range of $3x10^{-4}$ and $7.8x10^{-7}$ m, giving rise to alterations in the vibrational state between bonds of the atoms that compose a given sample.

In the work presented in this thesis, the sampling technique of attenuated total reflectance (ATR) was used, enabling the direct analysis of the samples in solid and liquid states (for polymeric samples and ionic liquid samples, respectively), without any further preparation.

ATR technique supposes that the infrared beam is directed onto an optically dense crystal with high refractive index, at a certain angle, and measures the alterations (attenuations) that occur in the totally internally reflected infrared beam when in contact with a sample [91].

The use of FTIR in the ATR mode has long been used in order to prove and study the interactions occurring between $scCO_2$ and polymers when processing them [76].

In chapters 3 and 4, FTIR analysis were carried out, in order to study the interactions established between starch-based polymers and the ionic liquids they were doped with.

All analysis were carried out using a Schimadzu-IR Prestige 21 spectrometer, in the transmittance mode, in the spectral region of 4400-800 cm^{-1}.

All the FTIR-ATR experiments were performed in the partner institution ICVS/3B's associated laboratory.

2.3.3. Polarity measurements

In chapter 5, the polarity of the prepared deep eutectic solvents was studied. The polarity measurements were performed using Nile Red (Figure 2.4) as a solvatochromic dye, which has been previously used to assess the polarity of weak acids and protic molecular solvents and ILs [92,93].
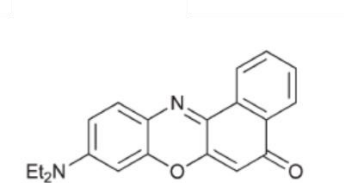
Figure 2.4- Chemical Structure of Nile Red [92].

The maximum absorbance wavelength (λ_{max}) is determined and the parameter E_{NR} is obtained using the following equation [94]

$$E_{NR} = 28591/\lambda_{max} \tag{2.5}$$

with in E_{NR} kcal/mol and λ_{max} in nm.

The different values obtained, for different solvents are all relative to the E_{NR} of the reference solvent, and allow the construction of a relative polarity scale.

Nile Red was prepared in ethanol as a stock solution. A small amount of Nile Red stock solution was added (50-100 µL) to each sample. The cuvette containing the sample+Nile Red was then placed under nitrogen atmosphere, in order to evaporate the solvent, and the UV/Vis spectra was immediately acquired. All spectra were obtained in a Beckman Coulter DU800 (Beckman Coulter) spectrophotometer, and the results are the average of at least two measurements for each sample, at room temperature.

2.4. Physical Characterization

2.4.1. Dielectric relaxation spectrosocpy (DRS)

Dielectric techniques are very useful when studying molecular mobility (dipolar reorientation and charge transport) in various materials [95]. Dielectric relaxation spectroscopy (DRS) probes the orientational and interfacial polarization and charge transport as the response

of a sample submitted to a time dependent electric field [96]. Measurements are normally carried out isothermally in the frequency domain.

The results of DRS measurements are usually analysed in the form of the complex dielectric function

$$\varepsilon*(\omega)=\varepsilon'(\omega)-i\varepsilon''(\omega) \tag{2.6}$$

whose real part is related with energy stored by the system, while the imaginary part accounts for the energy dissipated inside the material; $\omega = 2\pi f$ is the angular frequency and f refers to the frequency of the outer electrical field. Alternative representations of the dielectric response are the complex conductivity [96]

$$\sigma^*(\omega) = i\omega\varepsilon_0\varepsilon^*(\omega) \tag{2.7}$$

and the complex dielectric modulus

$$M''(\omega) = \frac{1}{\varepsilon^*(\omega)} \tag{2.8}$$

Since the propagation of the mobile charge carriers also contributes to the complex function [96], it is advantageous to analyse the dielectric response through the complex conductivity function

$$\sigma^*(\omega) = \sigma'(\omega) + i\sigma''(\omega) \tag{2.9}.$$

In order to get a better insight on the dipolar polarization caused by the reorientational motions of permanent dipoles, the imaginary part of the complex dielectric modulus can be studied

$$M^*(\omega) = M'(\omega) + iM''(\omega) \tag{2.10}$$

which is related with the real and imaginary parts of the complex dielectric permittivity, by equation 4.6

$$M''(\omega) = \frac{\varepsilon'}{[(\varepsilon')^2+(\varepsilon'')^2]} \tag{2.11}$$

In this work, DRS was used to assess the molecular mobility and the conductivity of the prepared materials in chapter 4, composed of SPCL polymeric matrices doped with ILs, and submitted to supercritical fluid foaming. DRS was also used in chapter 5, in order to assess the conductivity of several different prepared deep eutectic solvents. Details on the experimental procedures used for each measurement as well as the temperature programs are described in detail in chapters 4 and 5, respectively.

2.4.2. Density measurements

Chapter 5 reports the densities of different prepared natural deep eutectic solvents. These density values were all determined following a simple gravimetric method, of weighing calibrated volumes, at 23 °C.

2.5. Thermal characterization

2.5.1. Differential scanning calorimetry (DSC)

DSC is a thermoanalytical technique that helps to characterize the physical characteristics and transitions of different types of materials. DSC measures, as a function of temperature, the difference between the amount of heat that is required to increase the temperature of a given sample and an inert reference material, which should have a well-defined heat capacity over the range of temperatures, at which sample and reference are submitted [97].

DSC can register different processes, depending on the amount of heat that flows through the sample; the process can be exothermic (emits energy), e.g., crystallization process, or endothermic (energy absorbing) for example the melting of a solid to a liquid. So, DSC can measure the amount of heat required for different transitions, such as melting, crystallization and determine the associated melting temperature (T_m) and crystallization temperature (T_c). Another transition that DSC is sensitive to, is the glass transition, which can be defined as a change in the heat capacity when the sample goes from the glassy state to a rubbery state, and is observed as a heat flux discontinuity in the thermogram (Figure 2.5). An associated glass transition temperature (T_g) can also be obtained.

All these physical transitions resgistered and measured by DSC, are of extreme importance when working with the processing of polymers. They determine the thermal limits within which the polymer can be processed, and register any alteration in their structure. In the work reported in this thesis, DSC was essential in determining the effects of ionic liquid doping on the polymer structure (chapters 3 and 4). DSC is also a very usefull characterization technique, and when preparing novel materials or solvents (as it is in the case of deep eutectic solvents reported in chapters 5 and 6), the knowledge of their thermal behavior is extremely important. Similar studies have been reported already [98].

The details of the DSC experiments are described in the experimental sections of each chapter, as well as the respective heating programs associated with each DSC analysis.
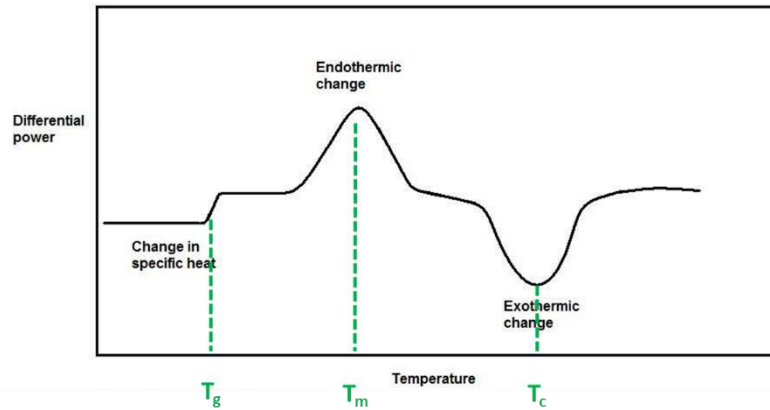
Figure 2.5- Typical DSC thermogram, registering different transitions (glass transition, melting and crystallization) with the associated temperatures T_g, Tm and Tc (adapted from [99]).

2.6. Mechanical Characterization

2.6.1. Mechanical testing

Mechanical testing, in the compressive and tensile modes, allows the determination of the mechanical behaviour under different conditions, and is usually performed in a universal testing machine [100]. The data that are obtained from this tests allow the construction of stress *vs.* strain curves, which give important properties such as the tensile strength, elongation-at-break and Young's Modulus.

Young's Modulus is an important parameter in the characterization of materials, allowing the determination of its "stiffness". It is defined as the ratio between the tensile stress and the strain (eq. 2.1, where E is the Young's Modulus, σ is the stress and ε is the strain), and can be measured considering the linear portion of the stress vs. strain curve.

$$E = \sigma/\varepsilon \tag{2.12}$$

Depending on the Young's Modulus, the material has different characteristics and behaviour, as it can be seen in Figure 2.6.
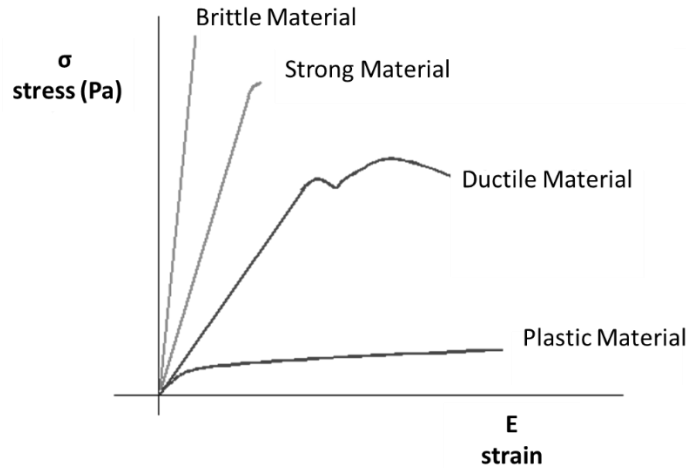
Figure 2.6- Examples of some types of materials according to their Young's Modulus (adapted from [101]).

In the tensile mode, the mechanical tests determine the behaviour of a given sample or specimen under axial tensile loading, and allow the determination of several parameters like for example the tensile strength, yield strength and elasticity modulus [100].

In the compressive mode, the tests determine the behaviour of the specimens when submitted to a compressive load, and allow the determination of several material characteristic properties like its elastic limit, yield strength and compressive strength [100].

The mechanical analysis results presented in this work in chapters 3, 4 and 6 were obtained in the compressive and tensile modes, in an INSTRON 5540 universal testing machine (Instron Int. Ltd.). In the tensile tests, the specimens used were 60 mm in length, 1 mm width and 3 mm in thickness. The crosshead speed varied from 1-5 mm/min, and for each condition, the samples were loaded until core break. The data presented in chapters 3 and 4 represent the average of at least 5 measurements, and 3 measurements for the results in chapter 6. On the other hand, compressive tests were carried out with a crosshead speed of 2 mm/min, until a maximum reduction weight of 60%.

All the mechanical analysis were performed in the partner institution ICVS/3B's associated laboratory.

2.6.2. Rheology studies

Chapter 5 reports the rheological study of different prepared natural deep eutectic solvents, in order to have information on its viscosity and rheological behaviour.

The rheological behaviour of a liquid, can obey to the so-called Newtonian behaviour, which obeys the following equation 2.8

$$\sigma = \eta \dot{\gamma} \qquad (2.13)$$

where σ is the shear stress, $\dot{\gamma}$ is the shear rate and η is the viscosity of the liquid or fluid [102]. Water is a good example of a Newtonian fluid.

In some cases the shear stress is not proportional to the shear rate, and the liquid is then called non-Newtonian, and the ratio $\sigma/\dot{\gamma}$ is then called the apparent viscosity, which is not necessarily constant. If the liquid or fluid is non-Newtonian, it can be a shear thinning liquid or a shear thickening liquid, depending on how the viscosity varies with the shear rate (Figure 2.7). In terms of viscosity, the behaviour of a Newtonian fluid is that the viscosity is constant over the entire shear rate range, a shear thinning fluid shows decreased viscosity with increasing shear rate (e.g. paint) and a shear thickening fluid shows increased viscosity with increasing shear rate (e.g. corn starch dissolved in water). Another possibility is that the fluid behaves as a Bingham plastic, like for example toothpaste, in which the viscosity appears to be infinite until a certain value of shear stress is achieved.
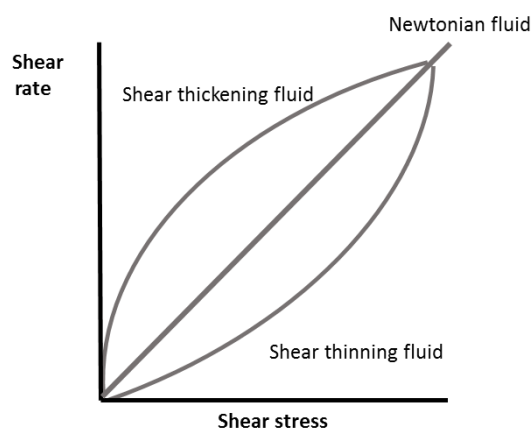
Figure 2.7 – Typical shear rate *vs.* shear stress curve obtained in rheology measurements and examples of the different fluid behaviour; shear thickening, Newtonian and shear thinning (adapted from [103]).

In chapter 5, curve flow measurements were carried out for several deep eutectic solvents, displaying the viscosity vs. shear rate, calculated from the instrument parameters. The flow behaviour of the samples were evaluated.

The experiments were carried out using a Paar Physica MCR300 (Germany) rheometer. The steady-flow measurements were carried out using controlled-stress rheometer fitted with a concentric geometry cylinder (CC10). The torque amplitude was imposed by using a logarithmic shear stress ramp, in the range of 0.1-1000 Pa. The temperature of the samples was kept at 23 °C using a water circulating bath. The results presented are the average of three different measurements for each sample.

All the rheology experiments were performed in the partner institution ICVS/3B's associated laboratory.

2.7. *In vitro* performance

2.7.1. Drug release studies

The release profile of the DES formed by menthol/ibuprofen (chapter 6) from SPCL foamed blend was studied after immersion in a phosphate buffer saline (PBS) solution at 37 $^{\circ}$C, under stirring at 60 rpm. The concentration of ibuprofen in the buffer was measured by UV/Vis spectroscopy at 220 nm, in a Synergy HT from BIO-TEK microplate reader, using a 96 wells quartz microplate.

The PBS buffer was prepared from phosphate buffered saline tablets (Sigma), with the concentration 2.7 mM, and potassium chloride 137 mM, at pH 7.4, at 25 $^{\circ}$C (these experiments were carried out in the partner institution ICVS/3B's)

2.7.2 Mathematical modelling of drug release

From Fick's law of diffusion (eq. 2.1) an equation can be derived, which models the drug release mechanism, considering that diffusion is the dominating mass transport mechanism and the drug release is diffusion-controlled.

A merely Fickian diffusion is hardly ever the case, as the water uptake of the matrixes may also play an important role in the release profile of the active compound. An heuristic equation can be applied in situations of release processes, which fall between the Fickian diffusion and the zero-order release kinetics (i.e, when the drug release rate is independent of time) [104] (eq. 2.14)

$$\frac{M_{t_0}}{M_\infty} = kt^n \tag{2.14}$$

where M_{t_0} is the absolute cumulative amount of drug released at time t_0, M_∞ is the absolute cumulative amount of drug released at infinite time, k is a constant that incorporates structural and geometrical characteristics of the controlled release system, and n is the release exponent, indicative of the mechanism of the drug release, [104]. Additionally, from this power law it is also possible to derive the kinetic constant of the system, which is characteristic of properties of the matrices prepared as it incorporates the structural and geometrical characteristics of the device.

Chapter 3

Supercritical Fluid Processing of Starch-based Polymers Doped with Ionic Liquids

3.1. Introduction

The recently and increased interest of biodegradable polymers has been previously referred, along with the clear advantages compared with conventional petroleum based polymeric materials [105,106]. Starch is an excellent candidate as a substitute and more sustainable raw material, but its poor processability, low flexibility, poor solubility, among other aspects, has limited its applications.

One approach that improves starch processability is to blend starch with other polymers, such as polyesters, like poly(lactic acid) (PLA). These types of polymer blends have already found applications in areas that go from food industry to the biomedical field [8]. The latter is one of the potential applications for this blend of starch and PLA, since none of the polymers present any toxicological concerns. Blending starch and PLA (SPLA), yields a polymer blend that presents a more hydrophobic character, lower water permeability and improved mechanical properties [107].

PLA has been used in the biomedical field for the production of scaffolds, drug delivery devices and orthopedic implants [14]. These materials need to have special structural and chemical features, one of those being the need for high porosity and 3D interconnectivity, with sufficient mechanical strength so that the structure does not collapse [108].

Several methods have been reported for the production of 3D interconnected porous scaffolds, such as solvent casting, particulate leaching, melt molding, fiber bonding or the use of supercritical fluid technology [108]. One of the preferred techniques is the supercritical fluid foaming or SCF foaming with supercritical carbon dioxide ($scCO_2$), since this method that uses a "clean" solvent and produces solvent-free porous structures [109,110], as previously described.

The success of SCF foaming is highly dependent on several factors, such as the solubility of $scCO_2$ in the polymer, the interactions that are established between CO_2 and the polymer and the changes in polymer structure that derive from those interactions (in morphology and crystallinity, for example). Therefore, it is important to collect data on the behavior of the polymer when submitted to the SCF foaming process.

In this work, in addition to studying the SCF foaming of a polymeric blend of starch and PLA, with different crystallinity degrees, the use of an ionic liquid (IL) as a foaming enhancer is also assessed. The combination of supercritical fluid technology and ILs has been suggested as a more sustainable approach to overcome some drawbacks of conventional polymer processing techniques [111]. The IL used in this work, 1-butyl-3-methylimidazolium chloride [BMIM]Cl, has been previously reported as a good solvent for natural-based polymers, and to also have a plasticizing effect [82,112–115]. Actually, SCF foaming relies on the plasticizing effect of $scCO_2$ in polymers, which can lower their glass transition temperature (T_g), thereby leading to improved processability [116]. It is clear that this effect is also dependent on the interactions established between the polymer and $scCO_2$ [117,118]. The synergy between $scCO_2$ and ILs is well known, and the fact that these solvents are able to dissolve considerable amounts of $scCO_2$, is explored in this work; the enhancement of the polymer-$scCO_2$ interactions can be achieved by IL doping [82]. The IL can later be removed from the biopolymer through solvent exchange techniques.

The main goal of the work presented in this chapter is to carry out a more detailed study on the effects of SCF foaming on the SPLA polymer blend and the effect of [BMIM]Cl doping, providing insight on the $scCO_2$ sorption process. The optimization of the SCF foaming process is very important, especially in the optimization of the modification and production of porous structures that can have applications in the biomedical field.

3.2. Materials and Methods

3.2.1 Materials

The natural based polymers used were based on a blend of corn starch/poly(lactic acid) termed SPLA, with weight percentages of poly(lactic acid) of 50 % (SPLA50) and 70 % (SPLA70), and were obtained from Novamont. The ionic liquid 1-butyl-3-methylimidazolium ([BMIM]Cl) was obtained from Sigma Aldrich. Carbon dioxide (99.998 %) was supplied by Air Liquide.

3.2.2. Sample Preparation

SPLA samples doped with IL were obtained by compression moulding. SPLA50 or SPLA70 were mechanically mixed with [BMIM]Cl in a mortar, in order to yield homogeneous mixtures with 10 wt% of IL. Care was taken to ensure that no phase separation occurred. The mixture was poured into stainless steel rings (12x2 mmm) and then compression molded using a Moore Hydraulic Press (UK) at 80 °C, 6 MPa, for 15 min. Heating is required to facilitate molding. This process yields a homogeneous composite of polymer and IL. Table 3.1 summarizes the materials prepared.

Table 3.1- Listing of the SPLA polymers prepared.

Polymer	[BMIM]Cl (wt %)	Reference
SPLA 50	-	SPLA50
SPLA70	-	SPLA70
SPLA50	10	SPLA50 10Cl
SPLA70	10	SPLA70 10 Cl

3.2.3. Supercritical fluid foaming

The porous SPLA matrixes were prepared by supercritical fluid foaming (SCF), using the conditions of 20.0 MPa, 40 °C, and different soaking times of 1, 3 and 6 h. Samples were loaded into a high pressure cell and heated to attain the desired temperature, using an electric thin band heater (OGDEN) connected to a temperature controller. Carbon dioxide was then pumped into the vessel using a high pressure piston pump (P-200A Thar Technologies), to the desired working pressure. The pressure inside the vessel was controlled with a pressure transducer. After the foaming process was completed, the cell was slowly depressurized down to ambient pressure.

3.2.4. Differential scanning calorimetry (DSC)

DSC experiments were carried out using a DSC Q100 V9.8 Build 296 apparatus. Samples were placed in aluminum pans and heated at a 10 °C/min rate from 20 °C to 200 °C, then cooled to 20 °C, and further heated to 200 °C at a 5 °C/min rate. Standard calibrations were performed using indium leads.

3.2.5. Mechanical analysis

Mechanical analysis of the polymer materials, in the compressive and tensile modes, was performed using an INSTRON 5540 universal testing machine with a load cell of 1kN (Instron Int. Ltd., UK). Compression testing was carried out at a crosshead speed of 2 mm/min, until a maximum reduction weight of 60%. For tensile tests, specimens dimensions used were 60x1x3 mm (length x width x thickness). The load was placed midway between the supports with a span (L) of 30 mm. The cross-head speed was 1-5 mm/min, and for each condition, the samples were loaded until core break. All the data presented concerning mechanical analysis is the result of the average of at least five measurements.

3.2.6. Infrared spectroscopy (FTIR-ATR)

Infrared spectra of the SPLA50 and SPLA70 with and without IL was obtained in transmittance mode, using a Shimadzu-IR Prestige 21 spectrometer, equipped with an attenuated total reflection (ATR) system in the spectral region of 44000-800 cm^{-1}, with a resolution of 4 cm^{-1}, for 32 scans.

3.2.7. Scanning electron microscopy (SEM)

The porous matrixes obtained after SCF foaming were observed with a Leica Cambridge S360 scanning electron microscope. Cross sections of the sample were observed after fracturing the samples with liquid nitrogen.

3.2.8. Micro-computed tomography (micro-CT)

The morphological structure of the samples was evaluated using a Scanco 20 equipment (Skyscan 1702) with penetrative X-rays of 53 KeV and 222 µA for SPLA70, and 189 µA for SPLA50, in high-resolution mode, with a pixel size of 14 µm and 1.5 seconds of exposure time. A CT analyser (v1.5.1.5, Skyscan) was used to calculate the parameter images from the 2D images obtained.

3.2.9. Sorption measurements

The amount of carbon dioxide sorbed in the polymer matrixes was determined by a simple gravimetric method, similar to the one described by Berens *et al.* [119]. CO_2 sorption measurements were carried out in the same experimental conditions as the foaming experiments (at 20.0 MPa, 40 °C and for 1, 3 and 6 hours of soaking time). The samples were weighed and loaded into a high pressure vessel, and then heated in a thermostatic bath up to 40 °C. CO_2 was liquefied in a cooling bath containing a water/ethylene glycol solution, before being pumped with an HPLC pump (KNAUER 1800 preparative pump 1800, with maximum flow rate of 100 mL/min), to the desired pressure. The pressure inside the vessel was measured with a pressure transducer. At the end of the experiment, the vessel was rapidly depressurized (in ca. 30 seconds), and the sample was transferred to a weighing scale, in order to record the changes in weight during desorption of CO_2 at atmospheric pressure, for a period of 1 h. Figure 3.1 is a schematic of the experimental apparatus.
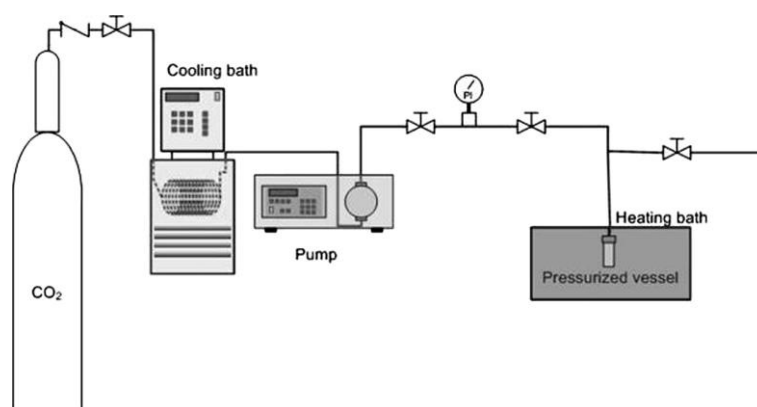
Figure 3.1- Schematic of the experimental apparatus used for the sorption measurements.

According to the Fickian diffusion behavior law, the amount of CO_2 that is dissolved in the polymer, for each sorption time period (1, 3 and 6 hours) is derived from a linear regression of the desorption data, at t=0.

3.2.10. Statistical analysis

Statistical analysis of the data obtained in the morphology analysis was conducted using IBM SPSS Statistics version 2.0 software. Shapiro-Wilk test was employed to evaluate the normality of the data sets. The results obtained in this work follow a normal distribution. In this case, one way ANOVA coupled with the Bonferroni post-hoc test was used to determine statistical significant differences. Differences between the groups with $p < 0.05$ were considered to be statistically significant.

3.3. Results and Discussion

Blending is an easy process to associate different polymers and obtain a material with improved properties and performance [120]. Of course the obtained material will strongly depend on the polymer used, and also on the processing, which is not always a trivial task, since some polymer blends present limited processability. The doping of polymer blends with plasticizers can further enhance their processability, flexibility and the ductility.

The doping of polymers with ILs may change the physicochemical properties of the polymers. In the work presented here, the potential advantages of using ILs together with SCF technology to process a starch based polymer blend are evaluated.

Two different ILs were used in order to form polymer-IL composites with SPLA50 or SPLA70, namely 1-butyl-3-methylimidazolium chloride ([BMIM]Cl) and 1-butyl-3-methylimidazolium acetate ([BMIM]Ac). However, the mixtures formed with doping SPLA with [BMIM]Ac were not homogeneous. Phase separation was observed, indicating that the interactions established between SPLA and [BMIM]Ac are not favorable (irrespective of the starch content of the polymer). When 10 wt% of [BMIM]Cl was used to dope SPLA 50 and SPLA 70, it was possible to obtain homogeneous mixtures, and several characterization methods were used to study the interactions established between the polymer and the IL.

3.3.1. FTIR-ATR analysis

FTIR spectroscopy in the ATR mode was used in order to evaluate the chemical interactions between SPLA 50 or SPLA 70 with [BMIM]Cl. The resulting spectra and peak assignments are presented in Figure 3.2 and Table 3.2.
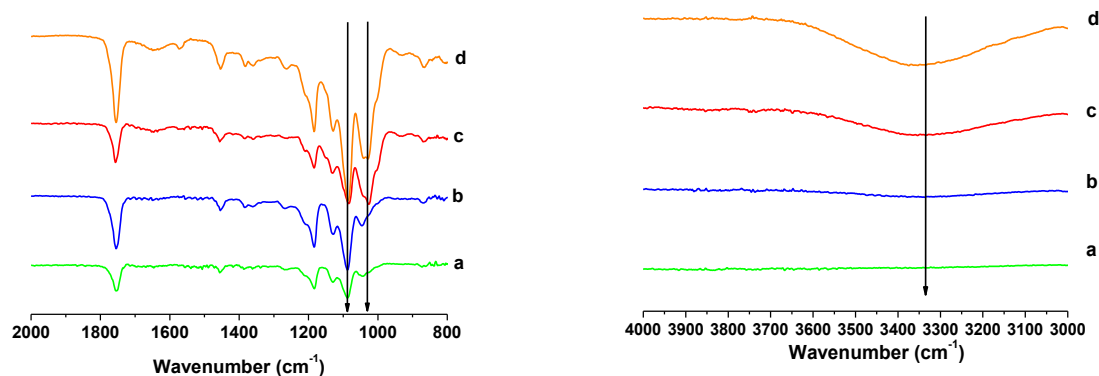
Figure 3.2- FTIR-ATR spectra of the samples SPLA50 **(a)**, SPLA70 **(b)**, SPLA50 10 Cl **(c)** (SPLA50 doped with 10 wt% of [BMIM]Cl) and SPLA70 10Cl **(d)** (SPLA70 doped with 10 wt% of [BMIM]Cl).

Table 3.2- FTIR characteristic peaks of starch, PLA and [BMIM]Cl.

	Wavenumber (cm^{-1})	Characteristic peak	Reference
Starch	1080; 1362-1338	C-O stretching	121
	1413	O-H bending	
	1456	CH$_2$ bending	
	925	CH$_2$ rocking	
PLA	1044;1094;1128; 1184	CH$_3$ rocking	122123
	1362-1356	C-COO stretching	
	1455	CH$_3$ bending	
	1751	C=0 bending	
[BMIM]Cl	1578	C=O acetate carboxylate	82
	3000-3600	O-H stretching	

The differences that are observed between SPLA50 and SPLA70, reflected in the differences in the intensity of the peaks attributed of the PLA component, can be explained by the differences in composition of the two starch-based polymers. Those have higher intensity in the case of SPLA70.

As for SPLA 50 and SPLA70 doped with 10 wt% of [BMIM]Cl, it is possible to detect alterations in the peak located at ca. 1040 cm^{-1}, which is attributed to the CH$_3$ rocking mode of PLA, and is related to the interactions between the PLA component and the IL, which is in agreement with data found in the literature [124].

There is also a considerable increase in the intensity of the peak located at 1080 cm^{-1}, attributed to the carboxyl (–COOH) group of starch, suggesting that the interactions between starch and the IL are stronger when compared to the PLA component, corroborating previously reported data [115].

For the samples doped with IL, there is also an increase in the intensity of the peak located at 3000-3300 cm^{-1}, reflecting an increase in hydrogen bonding and confirming the interactions between SPLA and [BMIM]Cl [82].

3.3.2. DSC analysis

The thermal behavior of the composites formed between SPLA and the IL were also assessed by DSC, in order to assess their thermal behavior. Figure 3.3 shows the thermograms obtained, and Table 3.3 shows values for the glass transition temperature (T_g), melting temperature (T_m) and degree of crystallinity (X_c).
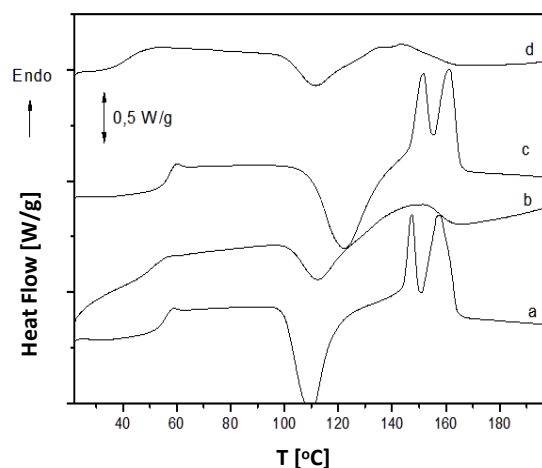
Figure 3.3- DSC thermograms for the samples SPLA50 **(a)**, SPLA50 10Cl **(b)**, SPLA70 **(c)** and SPLA70 10Cl **(d)**.

Table 3.3- Thermal properties obtained by DSC for all the polymers under study.

Samples	T_g (°C)	T_m (°C)	X_c (%)
SPLA 50	58.0±0.2	157.8±0.2	31.3±0.5
SPLA50 10Cl	57.1±0.9	150.6±3.6	18.9±1.1
SPLA70	59.4±0.3	155.5±7.6	42.2±0.4
SPLA70 10Cl	52.4±2.4	147.2±2.4	34.1±0.5

The DSC data revealed two overlapping endothermic processes, as seen by the melting peaks, located between 140 °C and 160 °C, which can be due to different crystal structures of PLA present in the blends. The melting temperature of SPLA50 is also lower than that of SPLA70, which is probably related with the lower weight content of PLA in the case of SPLA50 (or the corresponding higher starch content). In the thermograms of the SPLA samples doped with IL, only one endothermic process associated with melting is observed, revealing that the IL present changes the crystalline structure of both SPLA50 and SPLA70.

The T_g values obtained for SPLA50 and SPLA70 are in good agreement with literature data [122]. For the samples doped with [BMIM]Cl, a decrease in T_g is observed, suggesting that the IL can act as a plasticizing agent.

The crystallinity degree was determined from the thermograms, by quantifying the heat associated with the melting of the polymer (Eq (3.1))

$$X_C = \left(\frac{\Delta H_m}{\Delta H_m^0 * w}\right) * 100$$
(3.1)

where ΔH_m is the specific melting enthalpy of the sample, ΔH_m^0 is the melting enthalpy of 100 % crystalline PLA (93 J/g [123]) and w is the weight fraction of PLA in the blend (50 % in the case of SPLA50 and 70 % in the case of SPLA70). The polymer crystallinity refers to the overall level of crystalline components relative to amorphous component. X_c decreases significantly in the presence of [BMIM]Cl, indicating a clear effect of the IL in the decrease in crystallinity of both polymers.

3.3.3. Mechanical tests analysis

Mechanical tests were also performed to assess the effects of IL doping on SPLA50 and SPLA70, including a possible plasticizing effect. Previous studies performed by Jacobsen *et al.* [125] report the effects of different plasticizers on the mechanical properties of PLA, including a decrease in the maximum tensile stress and in the elasticity modulus.

Figure 3.4 shows the results from the mechanical analysis, and Table 3.4 a summary of the mechanical properties of the samples under study.

The results obtained show that the Young's modulus is affected by the presence of IL/plasticizer, which may indicate increased polymer chain mobility. The tensile tests also reveal lower elongation at break for the polymers in the presence of the IL, and this effect is more pronounced in the case of SPLA50, confirming what was previously observed in the FTIR-ATR data, i.e. that the IL establishes stronger interactions with the starch component of SPLA.

[BMIM]Cl has been reported to be an efficient plasticizer for starch [115], allowing a better processability, the decrease in the Young modulus of starch caused by the presence of [BMIM]Cl was attributed to the reduction of the hydrogen bonds between starch chains when the IL is present [115]
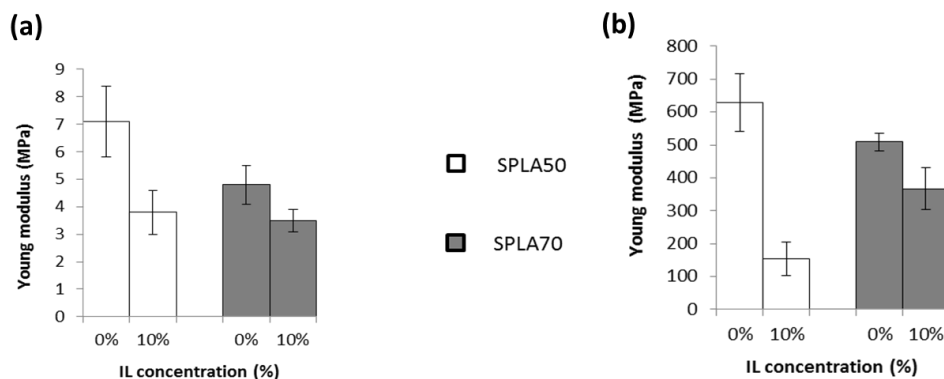
Figure 3.4- Effect of [BMIM]Cl doping on the mechanical properties of SPLA50 and SPLA70 in the compressive mode **(a)** and tensile mode **(b)**.

Table 3.4- Summary of the mechanical properties of the polymers studied.

Polymer	Compressive	Tensile	
	E (MPa)	E (MPa)	Elongation at break (%)
SPLA50	7.1±1.3	624±76.5	2.3±0.2
SPCL50 10Cl	3.7±0.7	142±51.7	1.0±0.5
SPLA70	4.8±0.6	502±27.6	2.4±0.8
SPLA70 10Cl	3.5±0.5	354±61.5	0.8±0.1

3.3.4. Supercritical fluid foaming

The development of porous degradable structures has received great attention for different applications, such as insulation foams, packaging and tissue engineering. A wide range of fields may benefit from novel lightweight materials with enhanced properties.

SPLA50 and SPLA70, pure or doped with IL, were submitted to SCF foaming with $scCO_2$ at 20.0 MPa and 40 °C. Different soaking times were studied, to evaluate the effect of the CO_2 diffusion on the properties of SPLA.

The cross-sections of the samples treated were analyzed by scanning electron microscopy (SEM) and micro-computed tomography (microCT), in order to evaluate the effect of soaking time/CO_2 diffusion on the morphological characteristics of the prepared matrices.

If tissue engineering and biomedical applications are envisaged for these materials, there is the need to remove any residual IL present in the final matrix. In this case, the IL used in this study can be easily leached out, by immersing the materials in water or ethanol or by performing a conventional Soxhlet extraction [126].

3.3.4.1. Morphological analysis

One of the most noticeable changes in the samples submitted to foaming regards morphology. SEM allowed the observation of the pores and cross sections of samples SPLA50 and SPLA70 doped with IL, submitted to foaming for different soaking times (Figure 3.5). SEM analysis shows that the presence of [BMIM]Cl is essential for the foaming of SPLA50. The IL acts as a foaming enhancer (and plasticizer), since visually, there is no evidence of foaming of SPLA50 without the presence of IL, regardless of the soaking time. Nevertheless, a more quantitative analysis was carried out to assess the impact of the foaming process.

Micro-CT allows the quantification, at high resolution, of the micro-structural morphology of the inner structure of the SPLA matrices prepared (Figure 3.6). The micro-CT analysis reveals that upon doping with [BMIM]Cl, it is possible to obtain porous structures via SCF foaming, and that this effect is more pronounced in the SPLA50 matrix. Also, the soaking time has an influence in the final structures obtained. It is expected that with increasing soaking time, more CO_2 molecules will diffuse into the bulk of the samples, resulting in higher porosity. Quantitative data may also be obtained from the microCT images obtained with the appropriate

CTAn software. The porosity was determined for all samples, with and without IL doping, and the results are presented in Figure 3.7.
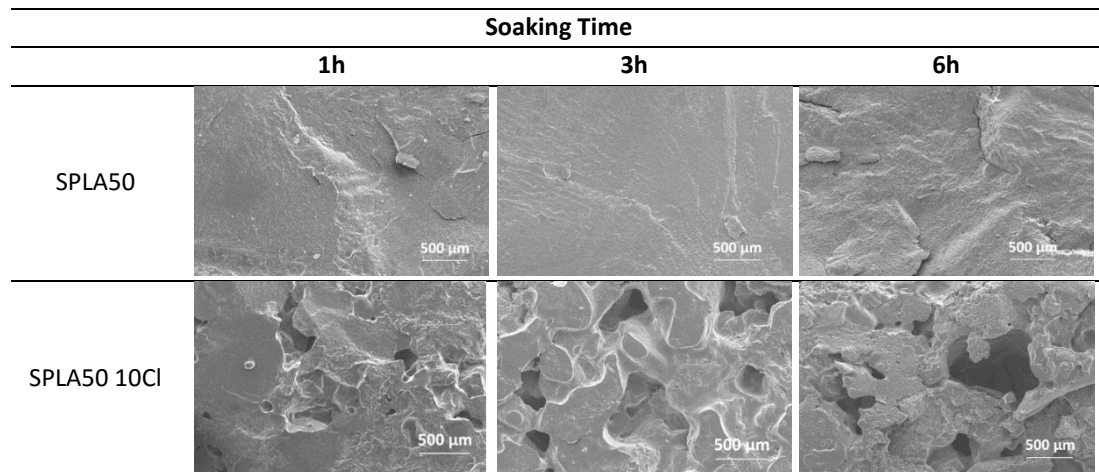
Figure 3.5- SEM micrographs of SPLA50 and SPLA50 10Cl, submitted to SCF foaming for different soaking times.
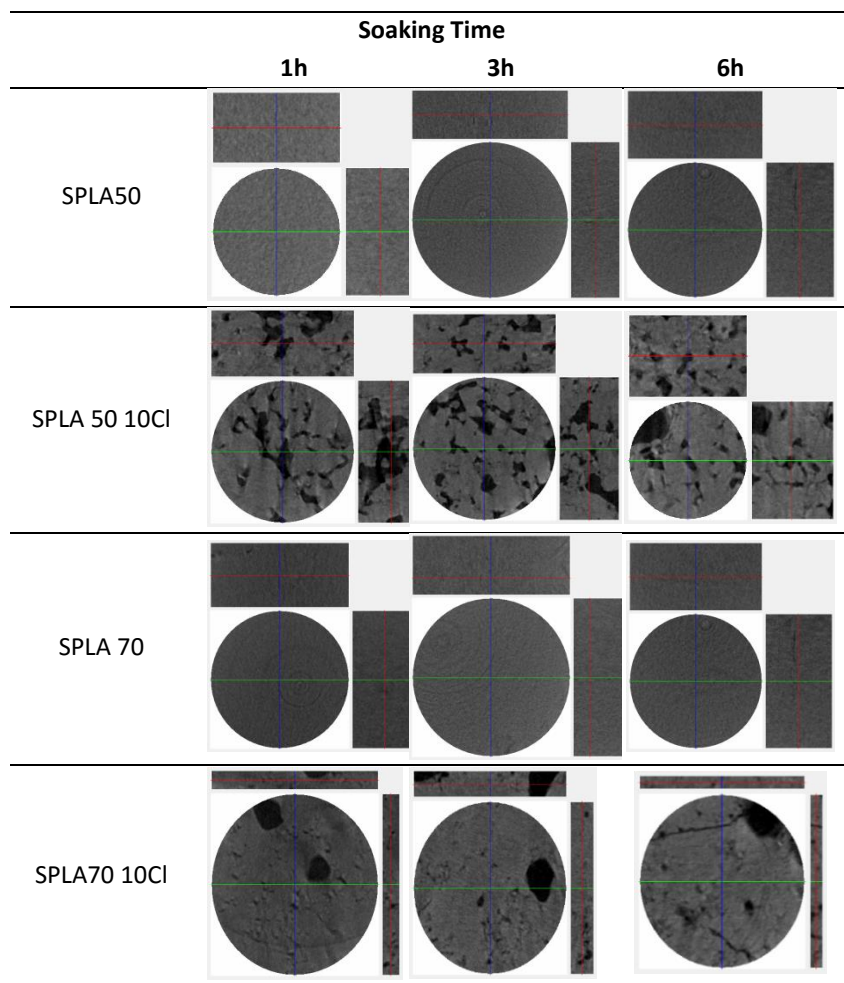
Figure 3.6- Micro-CT analysis of the polymers studied.
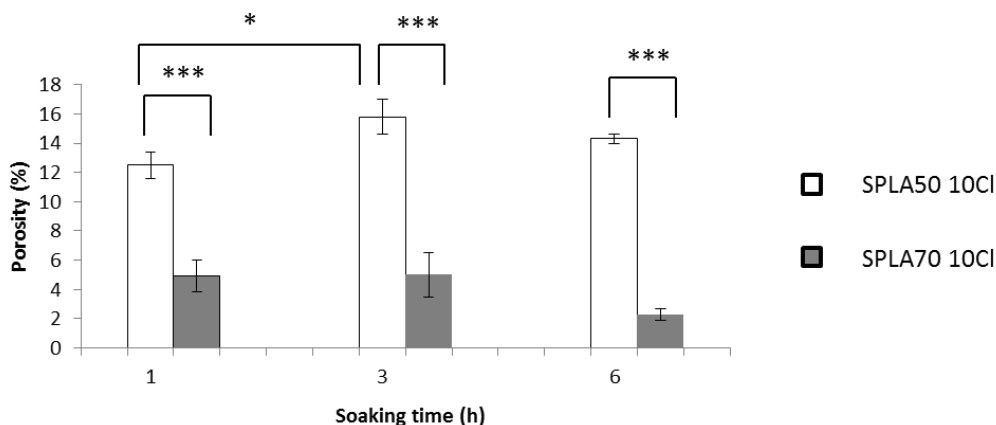
Figure 3.7- Porosity dependence on soaking time for SPLA polymers doped with [BMIM]Cl. Asterisks are referent to statistical analysis.

Statistically significant differences were observed, comparing the two polymers for all soaking times tested. Regarding the effect of soaking time on the porosity, only in the case of SPLA50 10 Cl was observed and increase on porosity when the soaking time increased from one to three hours.

There are different mechanisms involved in the gas foaming process. The solubility of CO_2 in the polymeric matrix will, in this case, control the gas bubble nucleation and the porous structure formation. In this sense, favorable interactions established between the polymer chains and CO_2 will enhance the foaming process. At the same time, the inherent crystallinity of the polymer samples also influences the foaming ability. In the case of semi-crystalline polymers, the crystalline domains do not contribute to CO_2 sorption.

Thermal analysis, of the "raw" polymers SPLA50 and SPLA70, as well as the processed ones, was carried out to verify changes in polymer crystallinity before and after the foaming process. The results presented in Figure 3.8, show that the soaking time is an important parameter which affects crystallinity by promoting the decrease in the crystalline domains, and that the decrease in crystallinity is more noticeable when IL is present.

Moreover, it was possible to see a higher crystallinity in SPLA70 than in SPLA50, as it would be expected, due to the higher fraction of starch present in the SPLA50 blend. Liao and co-workers [127] have discussed in their work the competitive effect of CO_2 sorption and CO_2-induced crystallization. The CO_2 dissolved within the matrix induces physical changes in the polymer, which are translated in different crystalline structures within the foamed polymer. According to our results, crystallinity of SPLA50 and SPLA70 decreased after CO_2 exposure at high pressure, which may be explained by the rapid crystallization of the polymer after foaming due to the CO_2 diffusion out of the matrix. This fast crystallization does not promote the formation of highly ordered structures, rendering matrices with lower crystallinity.

As it was previously said, the solubility of CO_2 in the polymeric blends controls the pore nucleation and structure formation. Therefore, it is expected that the sorption degree of the matrices may also be related with the porosity of the structures obtained from SCF foaming. The

determination of the amount of CO_2 dissolved in the polymeric blends was determined by a simple gravimetric method, and its mathematical analysis is presented in the following section.
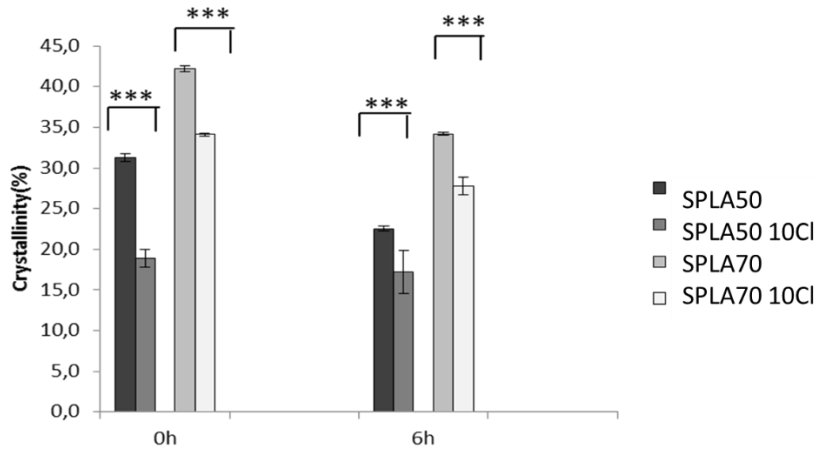
Figure 3.8- Crystallinity of the different samples under study, before and after the foaming process (soaking time of 6 hours).

3.3.4.2. Carbon dioxide sorption measurements- Mathematical analysis

The solubility of CO_2 in the polymer is of great importance and it is intimately related with pore nucleation and structure formation mechanisms. It is expected that the porosity of the SPLA is then related with the sorption and the amount of CO_2 dissolved in the matrices. The CO_2 sorption measurements were carried out, using a simple gravimetric method and a mathematical treatment of the sorption of CO_2 by the polymers in study was performed.

The choice of the mathematical approach to be made, depends on the thermophysical characteristics of the polymer, if it is in the rubbery state (above T_g) or in the glassy state (below T_g). If the diffusing substance causes an extensive swelling of the polymer (changing its shape), it exhibits a "non-Fickian" behaviour, and Fick's laws of diffusion cannot be applied. In the case of the samples under study, the extensive swelling of SPLA50 and SPLA70 (doped with IL and not doped with IL) was not observed. This means that the mathematical analysis of the sorption measurements can be made using Fick's theory of diffusion through isotropic matrices [83,84] (*see Methods and Experimental*).

A simplified solution of Fick's second law, that describes the time dependence of the diffusing material out of the sample, in this case a slab shape of thickness l, and that considers an uniform initial distribution and that the surface concentrations are equal, is given by equation 3.2

$$\frac{M(t)}{M_0} = 1 - \frac{8}{\pi^2} e^{\left(\frac{-Ds\pi^2 t}{l^2}\right)} \tag{3.2}$$

where $M(t)$ is the mass of the diffusing substance at time t and M_0 is the equilibrium sorption attained theoretically after infinite time [85].

The linear relationship between the amount of CO_2 dissolved in the polymer and the square root of desorption time validates the assumption that we are in presence of Fickian diffusion phenomena.

The sorption experiments were carried out for SPLA50 and SPLA70, with and without IL doping. The sorption degree was obtained as the ratio between the mass of CO_2 in the sample and the total mass (mass of CO_2 plus the mass of the polymer sample). The maximum sorption degree was determined by plotting the sorption degree as a function of $t^{1/2}$, and the value for time zero was extrapolated and assumed to be the maximum sorption value (Figure 3.9). The apparent sorption and desorption coefficients of the different samples were determined using equation 3.2, and the results are presented in Table 3.5.
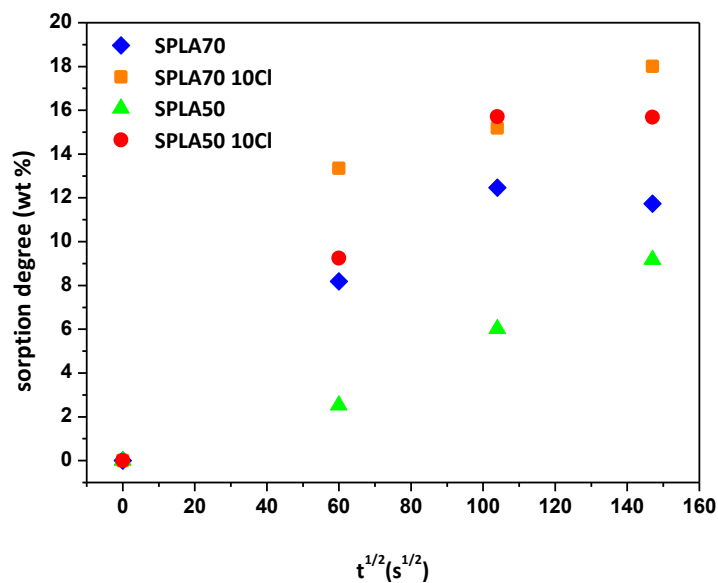
Figure 3.9- Sorption curves for samples under study.

Table 3.5- Sorption degree, apparent sorption and desorption coefficients, for the samples under study.

Sample	T (ºC)	P (MPa)	Thickness (mm)	Max. Soprtion degree (%)	Apparent sorption coeff. (m²/s)	Apparent desorption coeff. (m²/s)
SPLA50	40	20.0	2	9.17	4.14x10⁻¹¹	1,84x10⁻⁰⁹
SPLA50 10Cl	40	20.0	2	15.71	2.07x10⁻¹⁰	1,83x10⁻⁰⁹
SPLA70	40	20.0	2	12.46	6,95x10⁻¹¹	1,39x10⁻⁰⁹
SPLA70 10Cl	40	20.0	2	18.01	1,51x10⁻¹⁰	1,59x10⁻⁰⁹

The highest sorption degree was obtained for SPLA70 10Cl, the fact that the value for this parameter is not much higher than that for SPLA50 10Cl, indicates that the PLA content in the polymer (and hence, its crystallinity) does not have a pronounced effect on the sorption of CO_2. The presence of the IL increases the sorption degree, as expected, in both SPLA50 and SPLA70, with an increase in the sorption value of ca. 6%.

If $ln(M(t)/M_0)$ is plotted as a function of t/l^2, the calculation of the sorption and desorption coefficients is possible. Figure 3.10 shows the plots of the sorption and desorption results. The calculated apparent sorption diffusion coefficient values in the presence of IL are ca. 10-fold higher than without IL doping, and this is observed for both SPLA50 and SPLA70. Furthermore, the apparent desorption diffusion coefficient is higher than the apparent sorption diffusion coefficient, as it was previously reported. This can be attributed to the fact that the desorption process is much faster than the sorption. When CO_2 is being released from the matrix, the polymeric chains present higher mobility because they have already been exposed to CO_2[85].

The fact that SPLA50 presents a lower apparent diffusion coefficient, compared with SPLA70, is in agreement with the foaming results. Due to the lower desorption diffusion coefficient, the diffusion of the CO_2 out of the polymer in the decompression stage is more difficult. The expansion effect is more evident for SPLA50 resulting in a higher foaming degree and consequently higher porosity.
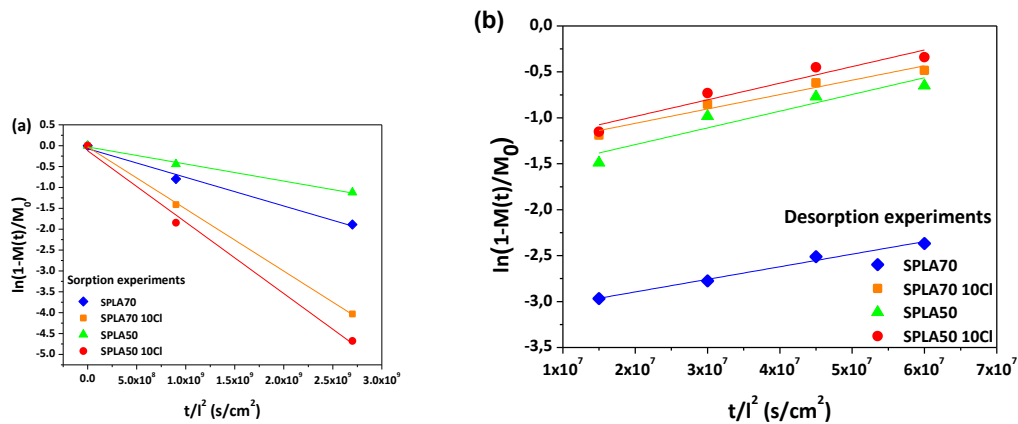
Figure 3.10- Representation of $ln(M(t)/M_0)$ vs. t/l^2 for the different sorption experiments carried out.

3.4. Conclusions

We characterized the semi-crystalline polymer blends SPLA50 and SPLA70 when submitted to supercritical fluid foaming, a method that allows the production of 3D porous and interconnected structures. Furthermore, we looked at how the doping of these polymers with the ionic liquid [BMIM]Cl affected the resulting foamed structures.

Spectroscopic data obtained by FTIR-ATR showed that [BMIM]Cl has stronger interactions with the starch component than with the PLA component.

From the thermal analysis carried out by DSC, it was possible to determine that the glass transition temperature (T_g) of the polymers decreased upon IL doping more significantly in the case of SPLA50, confirming the role of the IL as a plasticizer. This can also be concluded from the decrease in the Young's modulus, demonstrated in both compressive and tensile mode.

The decrease in crystallinity, also observed upon IL doping of SPLA50 and SPLA70 blends, can explain the enhancement of the foaming in the presence of IL.

Sorption experiments allowed the determination of the apparent sorption and desorption coefficients. The values obtained point to a plasticizing effect of both the IL and CO_2 on the obtained polymer blends.

The foaming effect is dependent on the mobility of the polymeric chains of SPLA (meaning, its crystallinity), and is dependent on the apparent diffusion coefficient of CO_2 in the polymer (sorption). The facts that SPLA50 has a lower crystallinity, compared with SPLA70, and also has a lower desorption coefficient, could be the reasons behind higher porosity and foaming efficiency found for this polymeric blend.

Chapter 4

Starch-based polymer-IL composites formed by compression moulding and supercritical fluid foaming for self-supported conductive material

4.1. Introduction

Natural-based or bio-based polymers have gained attention in recent years to be used as more than substitutes for plastics, due to their attractive characteristics. They combine high strength and stiffness, with carbon neutrality, biocompatibility, and renewability, making them more sustainable. Their applications range from packaging to biomedical purposes, meaning that they are highly versatile. They can be composed of starch, cellulose and aliphatic polyesters, for example.

The major difficulty of working with this type of polymers, is that they have very limited processability. They are very difficult to dissolve in common solvents such as water and organic solvents, due to the extensive and strong inter and intra-molecular hydrogen bonds that maintain the polymeric structure.

In the last decades, extensive research has been devoted to finding solvents that were able to dissolve bio-based polymers and natural polymers. One solvent type that was found to be able to dissolve bio-based polymers were ionic liquids (ILs). ILs have been reported as suitable solvents for cellulose, lignocellulosic materials, starch, chitin or chitosan [34,128,129], but most of the literature that can be found is focused on cellulose [34,130,131]. There is also some work referent to the modification of polymers such as cellulose and starch using ILs as solvent [37,132,133].

The advantage of using ILs to dissolve or modify natural based polymers, comes from the possibility of ILs to decrease the intermolecular forces within the polymers, which increases their flexibility, having an impact in the processability of these polymers mainly by decreasing their melting temperatures.

In fact, there are some studies dealing with the interactions established between ILs and polymers, like for example the interactions of cellulose with imidazolium based ILs [134] responsible for their dissolution, finding that the anion of ILs can establish hydrogen bonds with the hydroxyl groups of natural based polymers. Other studies refer the ability of ILs to be used as plasticizers of polymers [135–137].

One of the ways to process a polymer, is to use supercritical fluid technology, for example via supercritical fluid (SCF) foaming. This is an alternative method to obtain porous materials, which is also regarded as "greener" when compared to other foaming processes. However, the efficiency of the SCF foaming is dependent on the solubility of carbon dioxide in the polymer. Previous work [82,138] reported the ability of ILs coupled with supercritical CO_2 (scCO_2), to have a plasticizing effect on starch based polymer blends, and increased foaming efficiency.

In the work reported in this chapter, the same strategy was used, and a starch-based polymer blend, composed of starch and poly-ε-caprolactone (SPCL), was doped with two different imidazolium-based ionic liquids , 1-butyl-3-methylimidazolium acetate ([BMIM]Ac) and 1-butyl-3-methylimidazolium chloride ([BMIM]Cl). The samples were processed by means of SCF foaming and the effect of both the IL doping and the SCF foaming was assessed and the thermophysical characterization was carried out.

4.2. Materials and Methods

4.2.1 Materials

The polymer used in this work, consists of a blend of corn starch/poly(ε-caprolactone), SPCL (30 wt% of starch), in a granular form was obtained from Biocycle. The ILs used for the polymer doping were 1-butyl-3-methylimidazolium acetate ([BMIM]Ac) and 1-butyl-3-methylimidazolium chloride ([BMIM]Cl), obtained from Sigma-Aldrich. Carbon dioxide (99.998 %) was supplied by Air Liquide.

4.2.2. Sample Preparation

SPCL samples doped with IL were prepared by mechanical mixing in a mortar. The appropriate amounts of SPCL and each IL were weighed, to obtain mixtures with 10 and 30 wt% of IL. The final mixtures were all homogeneous without phase separation.

Disc shaped samples of SPCL and SPCL with 10 and 30 wt% of each IL were prepared by compression moulding, using stainless steel rings (12x2 mm) as a mould; the homogeneous mixture was poured into the mould and the samples were compression moulded in a Moore Hydraulic Press (UK), at 80 ^{o}C, 6 MPa, for 15 minutes (heating is required to facilitate material moulding).

The final sample is a homogeneous composite of polymer-IL. Table 4.1 shows a summary of the prepared materials.

Table 4.1- Prepared samples of SPCL and SPCL+IL and references.

Sample	IL	IL wt%	Reference
	-	-	SPCL
	[BMIM]Ac	10	10Ac
SPCL	[BMIM]Ac	30	30Ac
	[BMIM]Cl	10	10Cl
	[BMIM]Cl	30	30Cl
	-	-	SPCL^{F}
	[BMIM]Ac	10	10Ac^{F}
SPCL+SCF foaming	[BMIM]Ac	30	30Ac^{F}
	[BMIM]Cl	10	10Cl^{F}
	[BMIM]Cl	30	30Cl^{F}

4.2.3. Water Content Determination

Water content of the samples and pure ILs was determined by Karl-Fischer titration using an 831 KF Coulometer with a generator electrode without diaphragm with Hydranal Coulomat AG as the analyte. The results presented here, are the average of a minimum of three experiments.

4.2.4. Compressive and Tensile Mechanical Analysis

Compressive and tensile mechanical analysis was performed using an INSTROM 5540 universal testing machine (Instron Int. Ltd., UK) with a load cell of 1kN. Compressive tests were carried out at crosshead speed of 2 mm/min, until a maximum reduction in sample weight of 60%. In the tensile mode, the dimensions of the sample used were 60 mm of length, 1 mm width and 3 mm thickness. The load was placed midway between the supports with a span of 30 mm. The crosshead speed was 1-5 mm/min, and for each condition the specimens were loaded until core break. The data presented here are the result of at least five measurements.

4.2.5. Supercritical Fluid Foaming

The porous matrices were prepared via supercritical fluid (SCF) foaming, with $scCO_2$ at 20.0 MPa, 40 ^{o}C, for 1 hour.

Samples were loaded in a high pressure vessel and heated to the desired temperature with an electrical thin band heater (OGDEN), connected to a temperature controller. Carbon dioxide was pumped into the vessel using a high pressure piston pump (P-200A, Thar Technologies), until the desired pressure was attained. The pressure inside the vessel was measured with a pressure transducer. The system was left for one hour, in order to promote the foaming of the matrices and afterwards it was slowly depressurized.

4.2.6. Scanning electron microscopy (SEM)

The matrices obtained after SCF foaming were observed by a Leica Cambridge S360 scanning electron microscope. Cross sections of the sample were observed after fracturing the samples with liquid nitrogen.

4.2.7. Micro computed tomography (micro-CT)

The morphological structure of the samples was evaluated using a Skyscan 1702 (Skyscan, Belgium) with penetrative X-rays of 53 KeV and 189 µA, in high resolution mode with a pixel size of 11 µm and 1.5 seconds of exposure time. A CT analyser (v1.5.1.5, Skyscan) was used to calculate the parameter images from the 2D images obtained.

4.2.8. Infrared spectroscopy (FTIR-ATR)

Infrared spectra of the samples were obtained in the trasmittance mode, using a Shimadzu-IR Prestige 21 spectrometer equipped with an attenuated total reflection (ATR) system, in the spectral region of 44000-800 cm^{-1}, with a resolution of 4 cm^{-1} for 32 scans.

4.2.9. Differential scanning calorimetry (DSC)

The DSC analysis were performed on a Q2000 isothermal differential calorimeter (TA Instruments, Tzero^{TM} DSC technology) in the range of -150 ^{o}C to 200 ^{o}C at a heating rate of 10 ^{o}C/min. The DSC analysis of pure ILs and samples submitted to SCF foaming were carried out between -90 ^{o}C to 200 ^{o}C. The samples were packed in a TA aluminium pan (the set was not hermetically sealed to allow free water evaporation). The cycle list includes a step (for the clearer observation of the glass transition) of cooling down to -90 ^{o}C, and heating to -70 ^{o}C, at a rate of 10 ^{o}C/min, holding at this temperature for 120 minutes (annealing), afterwards there is a cooling to -90 ^{o}C followed by a final heating to 40 ^{o}C, at 30 ^{o}C/min.

4.2.10. Dielectric Relaxation Spectroscopy (DRS)

For the DRS measurements, samples in the form of discs (10x2.1 mm) of SPCL and SPCL+IL with and without foaming, were placed between two stainless steel electrodes in a parallel capacitor. IL samples were placed between two gold electrodes, using two 50 μm silicon spacers to maintain sample thickness. The sample cell was mounted on a cryostat BDS 1100. The temperature control was ensured by a Quatro Cryosystem and performed within ±0.5 ^{o}C. Measurements were carried out using an Alpha-N analyser, covering a frequency range of 10^{-1} Hz to 1 MHz. After a first cooling ramp from room temperature to -120 ^{o}C, isothermal spectra were collected from -120 ^{o}C to 5 ^{o}C in steps of 2 ^{o}C, from 5 ^{o}C to 50 ^{o}C in steps of 5 ^{o}C, and from 50 ^{o}C to 120 ^{o}C in steps of 10 ^{o}C. All the modules were supplied by Novocontrol.

4.3. Results and Discussion

Starch based polymers, doped with ILs can be an interesting approach for the development of polymeric materials with improved properties and applications.

In this work, the semi-crystalline polymeric blend of SPCL was doped with two different ILs, [BMIM]Ac and [BMIM]Cl, in different weight percentages (10, 30 wt%), and the effect of the IL on the foaming of SPCL will be further discussed.

It is important to refer that after mixing the SPCL and IL a homogeneous powder was obtained, since the content of IL is very low it was adsorbed in the polymer and the mixture could therefore be handled without loss of IL. Even after the compression moulding, the obtained samples remained homogeneous, and no leaks were observed during the experiments.

It is well known that some ILs are hygroscopic ([BMIM]Cl is especially hygroscopic) and starch also has an hydrophilic nature, so the careful control of the water content in the samples in needed since it is known to affect some of the thermophysical characteristics under study. The water content in samples of SPCL and [BMIM]Ac was 1.9 % and with [BMIM]Cl 2.6 %.

4.3.1. Mechanical properties

One of the possible effects that the IL may have in the mechanical properties of the polymer is the increase in the mobility of polymer chains.

Mechanical tests in compressive and tensile mode were performed in order to quantify this effect, and results are presented in Table 4.2 and Figure 4.1.

Table 4.2- Results for the mechanical analysis of pure SPCL and SPCL doped with the two different ILs.

Sample	Compression	Tensile	
	E (MPa)	E (MPa)	Elongation at break (%)
SPCL	6.2±0.7	352±44.6	5.7±1.4
10Cl	2.2±0.3	114±35.8	5.0±1.1
30Cl	0.8±0.3	104±26.4	4.7±0.5
10Ac	5.2±0.5	223±29.3	8.9±1.9
30Ac	2.6±0.4	133±53.3	8.0±2.1
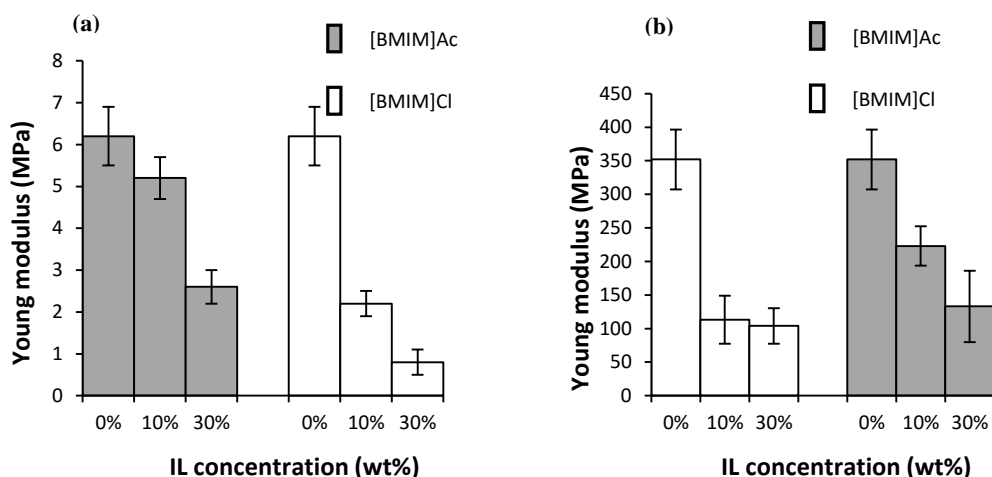
Figure 4.1- Effect of IL presence and IL concentration in the Young's modulus of SPCL matrices in compressive mode **(a)** and tensile mode **(b)**.

These results show that the Young's modulus is different for pure SPCL and for SPCL doped with ILs, which was observed both in compressive and tensile modes, indicating that IL does in fact have an effect in polymer chain mobility.

The tests in the compressive mode showed that the Young's modulus is lower for the sample of SPCL with 30% of [BMIM]Cl. The lowest concentration of [BMIM]Ac does not change significantly the mechanical properties compared to pure SPCL.

The tensile tests revealed higher elongation at break for SPCL with [BMIM]Ac in comparison with both unmodified samples and those containing [BMIM]Cl, which is another indication of stronger interactions between this IL and the polymer.

It is also important to refer that both the compressive and tensile tests were carried out at different crosshead speeds, in order to ensure that the crystallinity of the samples under study is not dependent on the stimulus they are being submitted to. No differences were found for the different tests.

4.3.2. Supercritical fluid foaming processing

Previous work reported the ability to foam polymeric blends prepared by compression moulding, at 20.0 MPa and 40 ºC [82,138]. In the present work, the same methodology was adopted.

SEM and micro-CT were used to analyse the effects of SCF foaming in the samples under study (Figure 4.2).

From the micro-CT analysis morphological parameters, such as porosity, can be obtained (Table 4.3). The foaming process increases the porosity of SPCL, especially when the IL is present. Porosity is higher when SPCL is doped with 30 wt% of [BMIM]Cl. There are several works reported in literature referring the high solubility of $scCO_2$ in imidazolium-based ILs, and also showing that polymeric matrices doped with ILs promote the foaming process [138]; it is then safe

to affirm that the foaming efficiency in this case is closely related with the $scCO_2$ solubility in the ILs [BMIM]Ac and [BMIM]Cl.

Table 4.3- Porosity of the samples under study, foamed and unfoamed, obtained by micro-CT analysis.

Sample	Soaking time (hours)	Porosity
SPCL		0.2±0.3
10Cl		6.2±3.3
30Cl	0	3.8±1.4
10Ac		2.4±0.7
30Ac		2.1±0.9
SPCL[F]		14.3±1.9
10Cl[F]		20.0±3.4
30Cl[F]	1	38.8±1.0
10Ac[F]		32.8±4.5
30Ac[F]		40.9±4.8
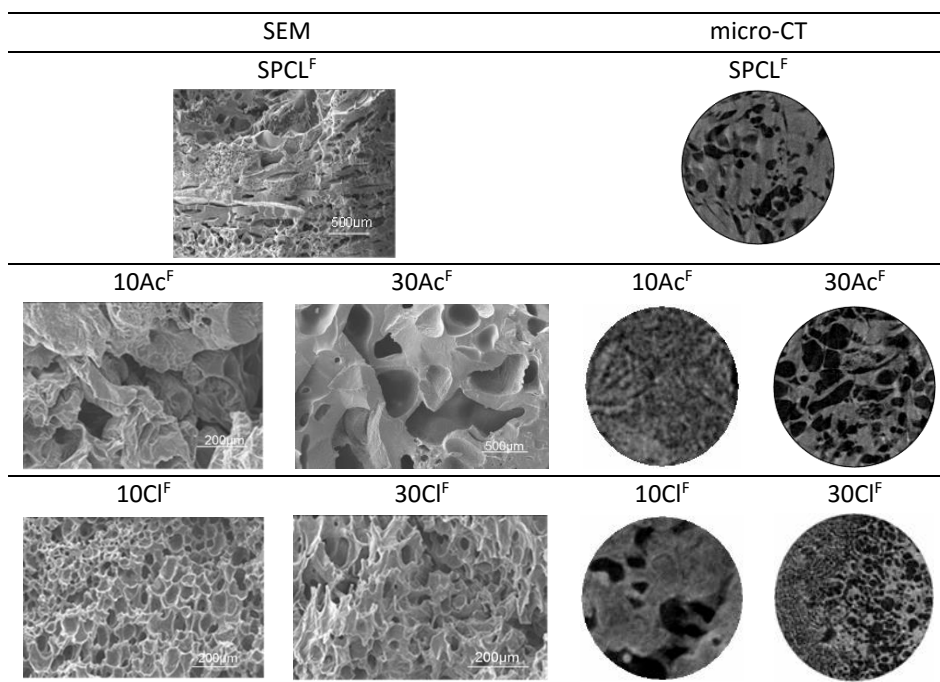
Figure 4.2- SEM and micro-CT 2D images of the cross section of the foamed samples. It must be noted that the SEM images of 10Ac[F], 10Cl[F] and 30Cl[F] have a scale of 200 μm and the SEM images for SPCL[F] and 30AC[F] have a scale of 500 μm.

The images presented in Figure 4.2 show that in the presence of IL, there is an increase in the porosity of SPCL, and that it is dependent of the amount of IL used (or its concentration).

Also, SPCL doped with 30 wt% of [BMIM]Ac results in bigger pores compared to samples doped with [BMIM]Cl.

4.3.3. FTIR-ATR

The existence of interactions established between SPCL and the ILs was studied by Fourier transformed infrared spectroscopy in the attenuated total reflectance mode (FTIR-ATR). Figure 4.3 shows the collected spectra, and Table 4.4 the characteristic peaks of starch, poly-ε-caprolactone, [BMIM]Ac and [BMIM]Cl.
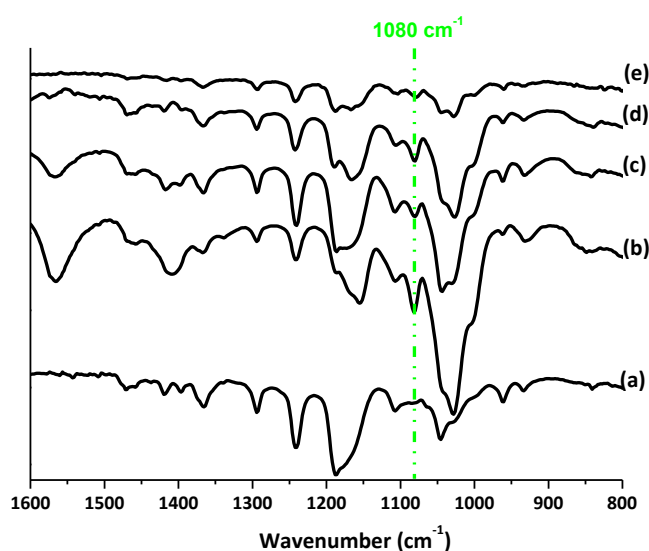
Figure 4.3- FTIR. ATR spectra of SPCL **(a)**, 10Ac **(b)**, 10Cl **(c)**, 30Ac **(d)** and 30Cl **(e)**.

Table 4.4- Characteristic FTIR peaks of starch, PCL and the ILs used in this work.

	Wavenumber (cm^{-1})	Characteristic peak	Reference
starch	1080; 1362-1338	C-O stretching	[139]
	1413	O-H bending	
	1456	CH$_2$ bending	
	925	CH$_2$ rocking	
PCL	961	CH$_2$ rocking	[139]
	1366	C-O stretching	
	1418	O-H stretching	
	1471	C-H bending	
[BMIM]Ac	1173	Imidazolium cation	[121]
	1379	C-O acetate carboxylate	
	1578	C=O acetate carboxylate	
[BMIM]Cl	1173	C=C deformation	-

The collected spectra show the interactions between polymer and the ILs, especially the highlighted peak at ca. 1080 cm^{-1} attributed to the vibrations of starch, that are altered in the presence of IL. This means that the main interactions are established between the starch moiety and IL, since the characteristic peaks attributed to the PCL moiety are not visibly altered.

The peaks located ca. 1170 cm^{-1} are significantly more intense when there is IL presence in the samples. This is due to the fact that this peak is attributed to the vibrations of the imidazolium cation, present in both ILs used in the doping of SPCL.

4.3.4 Thermal characterization by DSC

The thermal behaviour of the samples under study was assessed by DSC. Figure 4.4 shows the resulting thermograms for samples before SCF foaming.

The thermogram in Figure 4.4 (a) shows the presence of an endothermic transition located at ca. 60 $^{\circ}$C (run 2), that occurs in the same region as the melting of the SPCL polymer blend, and is in close agreement to the value for melting temperature (T_m) found in literature for PCL [122], meaning that it is referent to the melting of the PCL component. In the subsequent cooling run (run3) an exothermic transition is observed, with a peak at ca. 30 $^{\circ}$C that is associated with the crystallization. All samples under study crystallize around that temperature.

For the samples containing IL, the minimum of the melting is slightly shifted to lower temperatures (run 4, Figure 4.4 (c)), which can be due to relatively lower spherulite size and/or the sperulites thickness in these materials [140], or even with less dense crystalline regions, that can be due to the IL incorporation in the polymer that interfere with chain packing.

Figure 4.4 (b), shows a close up of the DSC collected after the annealing, showing a heat flux discontinuity, typical of the glass transition and associated with a T_g. The annealing allows the accentuation of the heat flux jump, and allows a better identification of the T_g, which for all the samples is located around the same temperature. The T_g of SPCL, determined from the midpoint, does not seem to undergo significant changes upon IL doping (independent of the IL), and is in good accordance with the T_g value of PCL obtained from literature [122].

The thermal behaviour of SPCL doped with ILs is mainly determined by the PCL constituent, which was seen by the agreement between both T_m and T_g values obtained for SPCL and compared with pure PCL. This is further supported by the fact that no IL rich regions are found in the thermogram, since no other heat flux steps are present in the thermograms that could be assigned to the ILs. Figure 4.4 (d) shows the thermogram of IL, [BMIM]Ac, where the effect of the water content is visible, shifting the T_g to higher values upon dehydration (plasticizing effect of water).
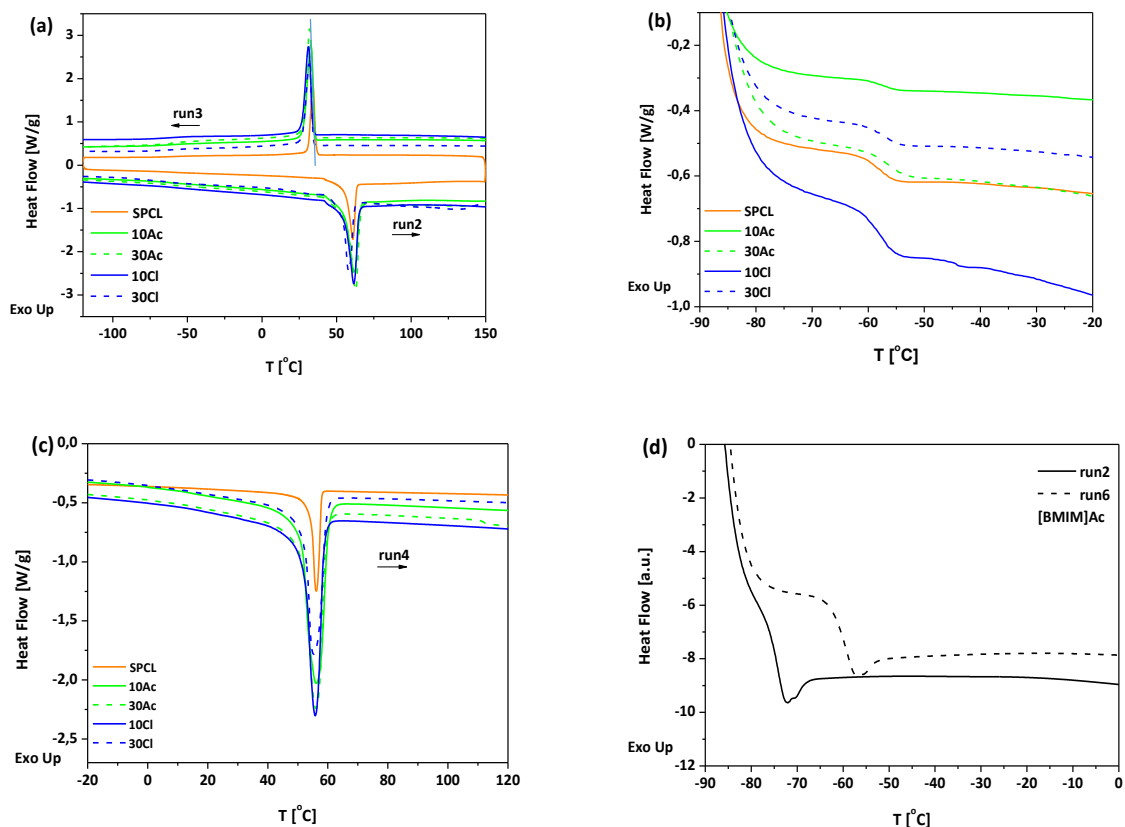
Figure 4.4- DSC thermograms of the samples under study; Melting (endothermic) and crystallization (exothermic) process are clearly observed **(a)**, scale up of the glass transition region obtained after annealing at -70 °C **(b)**, clear vision of the melting peak obtained in the second heating run **(c)**, scale up of the glass transition region for IL [BMIM]Ac **(d)**.

FTIR-ATR results presented above, confirmed IL-matrix interactions, but they proved not to be evident from the DSC analysis. The infrared results showed alterations in the peak attributed to the C-O vibration of the starch component in the presence of IL, meaning that it interacts with that moiety. In DSC, the transition attributed to starch was not identified, meaning that DSC is "blind" to starch, and only transitions associated to PCL are visible. So, it is not surprising that no alterations are observed in the DSC thermograms upon IL doping of SPCL. Moreover, the invariance of the glass transition and T_g for samples with and without IL, can be interpreted as the IL presence not interfering with the cooperative mechanism that is the origin of the glass transition of SPCL.

A small decrease in the T_m of SPCL samples doped with IL is observed, which means that IL incorporation affects crystallization. Nevertheless after the thermal heating to 200 °C the crystallization and further melting are no longer affected by IL presence.

Figure 4.5 shows the DSC thermograms of the samples that were submitted to SCF foaming, which were collected under very similar conditions (*see experimental, 4.2.9.*). The thermograms are again dominated by the melting and crystallization events. The endothermic broad band located at ca. 100-120 °C is related with the evaporation of residual water, and it is more evident for samples 10Ac^F and 30Cl^F (Figure 4.5 (a)).

In the low temperature region, the typical heat flux discontinuity associated with the glass transition is observed, although it is ill-defined. In order to enhance this transition, these samples were submitted to annealing at -70 $^{\circ}$C, after which a temperature scan was carried out. In Figure 4.5 (b) the glass transitions can be observed, confirming a presence of a T_g at ca. 63 $^{\circ}$C, not undergoing significant changes for all the samples under study.
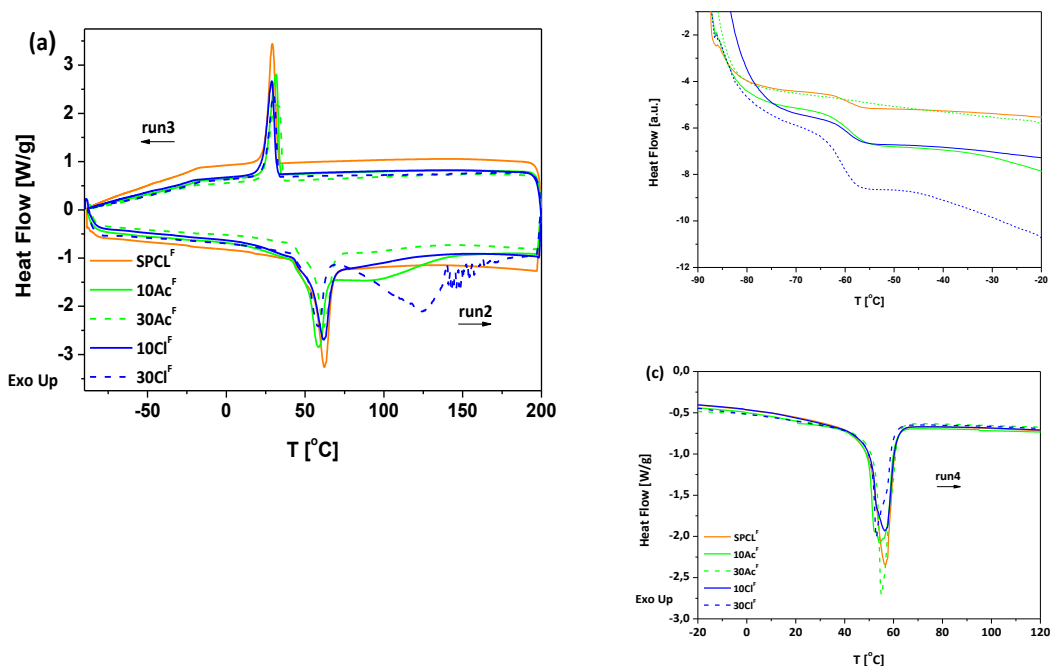
Figure 4.5- Thermograms for samples submitted to SCF foaming. Melting and crystallization are observed **(a)**, clear vision of T_g detected after annealing at -70 $^{\circ}$C **(b)**, detailed vision of the melting in the subsequent heating run **(c)**.

The melting region (Figure 4.5 (c)) reveals that there is a slight shift of the minimum of T_m to lower temperatures, for samples $10Ac^F$ and $30Cl^F$, the higher value of Tm is 62.2 $^{\circ}$C (attributed to $SPCL^F$), while the lower occurs at 58.2 $^{\circ}$C (for $30Cl^F$). After the first heating scan (run 2) all the samples undergo crystallization near 30 $^{\circ}$C (run 3), and both crystallization and further melting occur at temperatures very near to which was observed previously for the unfoamed materials. Therefore, this seems to be caused by the presence of IL rather than by SCF foaming.

4.3.5 Dielectric Relaxation Spectroscopy Studies

In this work, dielectric relaxation spectroscopy (DRS) was used to assess the molecular mobility and the conductivity of the prepared materials. DRS probes orientational and interfacial polarization and charge transport as the response of a sample to a time dependent electric field[141] (*see chapter 2*). The use of DRS for the study of polysaccharides and IL has been employed by other authors, and there are several studies concerning dielectric properties of starch and

ionic liquids[142–145] and on the impact of the incorporation of plasticizing agents in conductivity in electrolyte polymers[146].

The initial water content of the samples was measured and values between 1.9 % and 3.0 % were obtained. It is expected that the water presence will have some influence in the conductivity measurements, nevertheless that influence of is expected to be relatively constant in all samples.

Figure 4.6 shows the resulting spectra of real conductivity, $\sigma'(f)$ of the samples under study, in order to assess the influence of the presence of IL. The conductivity isotherms represented in Figure 4.6 correspond to -80 ^{o}C and 0 ^{o}C.

SPCL is a semi-crystalline material, which has been also previously observed from DSC analysis. At -80 ^{o}C, this polymeric blend is below its T_g, meaning that there are no appreciable cooperative motions of the matrix, which explains why no significant conductivity is noticed for SPCL with no exhibition of a plateau of direct conductivity, σ_{dc} (Figure 4.6 (a)). The same behaviour is exhibited by the samples doped with [BMIM]Ac, since the at -80 ^{o}C, we are also below the T_g of [BMIM]Ac. On the other hand [BMIM]Cl is well above its T_g and conductivity in samples of SPCL doped with this IL (10Cl and 30Cl) is higher, even showing a conductivity plateau, meaning that direct conductivity (σ_{dc}) takes place.

Therefore, in samples of SPCL doped with [BMIM]Cl, the conductivity is dominated by the IL response, which increases with increased concentration. This means that the charge transport mechanism that is the base of conductivity, is not related by the segmental motions of the polymer matrix itself, being caused by the IL presence.

At 0 ^{o}C, the SPCL matrix and both ILs are above their T_g values, and that is reflected in the conductivity enhancement observed (Figure 4.6 (b)). Although the samples doped with [BMIM]Ac show an increase in conductivity, the doping with [BMIM]Cl has a greater effect in conductivity enhancement.

According to the work of Ramesh *et al.* [147], the doping of polymer matrices with IL results in the weakening of the interactions between starch polymer chains via hydrogen bonds; in the present work, the same was observed by FTIR-ATR analysis. So the increase in conductivity is also a consequence of the higher polymer flexibility and enhanced segmental mobility, which facilitates the ionic transport, providing more conductive pathways [147].

One very interesting observation is that, at 0 ^{o}C, the conductivity of 30Cl is very close to the one of pure ILs, with the advantage of being more stable over all the tested frequency range, since the measurements of ILs' conductivity are repeatedly affected by electrical interferences. Although the SPCL matrix itself does not contribute to the conductivity, it acts as a solid support for the IL, creating a self-supported conductive material. This can open doors for applications of these starch based materials.
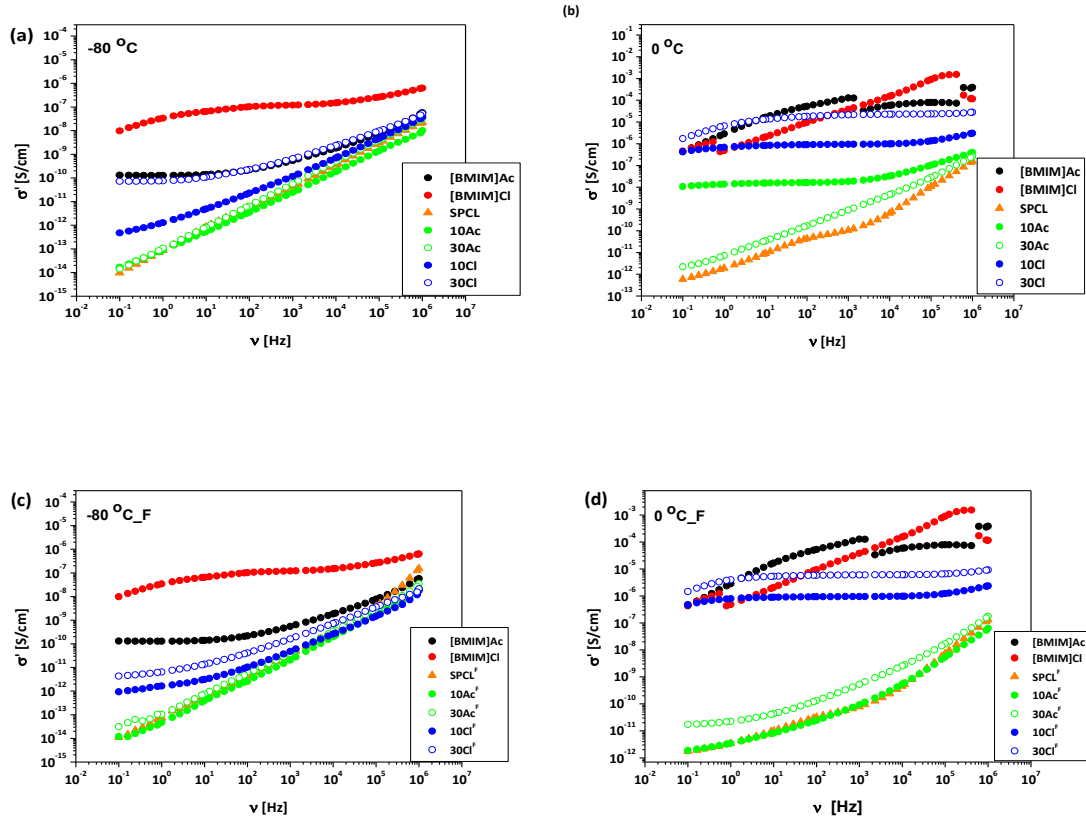
Figure 4.6- Conductivity spectra of SPCL and SPCL samples doped with IL; isothermal curves collected at -80 °C **(a)**, 0 °C **(b)**, -80 °C after SCF foaming **(c)** and 0 °C after foaming **(d)**. All spectra were collected in the presence of residual amounts of water.

Another interesting fact is that the same behaviour is observed for the samples subjected to SCF foaming (Figure 4.6 (c) and (d)). This is an evidence of the presence of an interconnected and porous structure produced by the SCF foaming process; if the structure did not presented this structure, the conductivity pathways would be interrupted resulting in decreased conductivity and σ_{dc} would not be observed.

The dielectric response of the materials under study can also be evaluated in terms of the dielectric modulus (*see chapter 2, section 2.2.7.*). Figure 4.7 shows the temperature dependence of the imaginary part of the dielectric modulus for all the samples, and is taken from the isothermal dielectric spectra.
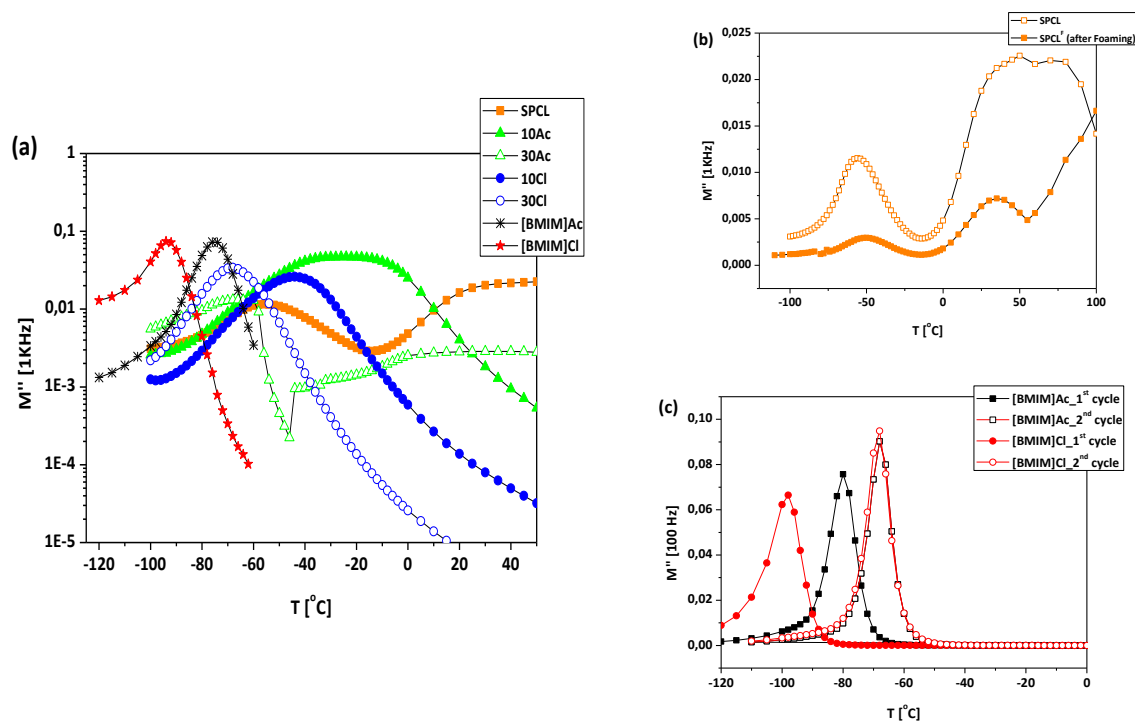
Figure 4.7- Representation of the imaginary part of the dielectric modulus; at 1 MHz **(a)**, for the different samples and ILs (in logarithmic scale to allow comparison of data that varies several order of magnitude), SPCL before and after SCF foaming at 1 KHz **(b)**, temperature dependence of ILs, at lower frequency (100 Hz) before and after heating to 120 °C **(c)**.

The dielectric response of a material to an alternating electrical field has contributions from dipolar relaxation (reorientational polarization of permanent dipoles), from conductivity, and also from interfacial polarization. The study of this dielectric response through the dielectric modulus offers some advantages, since it supresses the electrode polarization effect, due to the blocking of charges in the electrode-dielectric surface, allowing the identification of the dipolar relaxation phenomenon. The dipolar contribution emerges at lower temperatures, and the conductivity effect at higher temperatures (lower frequencies of the isothermal dielectric spectra).

Figure 4.7 (a) shows peaks in the temperature range of -100 °C to -25 °C, attributed to dipolar relaxation and with the motions related with the dynamic process of glass transition, complementing the DSC analysis.

There are some subtle differences between the samples, that were not detected from the DSC analysis, one of which is that the maximum of $M''(T)$ for [BMIM]Cl is located at the lowest temperature.

In Figure 4.7 (c), where the modulus results for the ILs are presented for a lower frequency (100 Hz), the peak of [BMIM]Cl emerges at ca. -100 °C, confirming its low T_g and why it is not detected in the DSC studies (DSC runs start at -90 °C). Upon water removal the peak shifts for significantly higher temperatures up to ca. -70 °C, undergoing a strong effect of the drying when compared with IL [BMIM]Ac.

The representation of the dielectric modulus, also shows that in the first heating run, the peaks of samples 10Ac and 10Cl are slightly shifted to higher temperatures relatively to SPCL and to the pure ILs, indicating some mobility hindrance. This can be due to the interaction established between IL and the starch moiety, which slows down the dipoles reorientational motions. On the other hand, samples 30Ac and 30Cl show peaks slightly shifted to lower temperatures, which can be attributed to the water that interacts mainly with the IL; the plasticizing effect of water in the ILs has been previously demonstrated for [BMIM]Ac (Figure 4.4 (d)), and is now demonstrated to [BMIM]Cl. Therefore, attention must be paid when evaluating the effect of adding or blending ILs with polymers, when ILs have high hydrophilicity.

At higher temperatures, the dielectric response is mainly dominated by the conductivity contribution. In Figue 4.7 (b) it is shown the dielectric modulus spectra of SPCL and SPCL submitted to SCF foaming. The dielectric response increases significantly when approaching the melting temperature, seen as discontinuity on $M''(T)$ at ca. 60 °C. The region of the glass transition emerges as a well-defined peak for both materials. It is also possible to see that, besides differences in intensity probably caused by differences in sample thickness (foamed sample is thicker), the overall dielectric behaviour is the same for both materials.

4.4. Conclusions

This work intended to give a more detailed description of materials composed by biopolymer blends and ionic liquids (ILs), prepared via supercritical fluid foaming, a combination that was used before, with satisfactory results in the production of foamed bio-based materials.

The presence of IL, doped in the polymeric blends, has proved to be essential to obtain foamed structures with the desired morphological characteristics, mainly porosity, which was observed by SEM and micro-CT. The feasibility of the foaming process coupled with the use of ILs has been previously studied, but some details on the characteristics of the obtained materials are presented here.

FTIR-ATR results have proved the existence of interactions between the used ILs and the polymeric blend.

DSC analysis revealed that the glass transition and melting events occur at temperatures homologue to poly-ε-caprolactone (PCL), with no phase transformations assigned to the starch component. For the samples doped with IL, a variation on the melting temperature occurs to lower temperatures, probably due the incorporation of IL that impairs the close packing of the crystalline PCL phase. The glass transition undergoes no effect upon IL addition, which goes against what is usually described in literature, where the addition of low molecular weight compounds, including ILs, can lower the glass transition temperature (T_g) due to a plasticizing effect. Actually, the reason for this observation may be due to the IL having a greater influence over the starch component, to which DSC is not sensitive. The interactions of IL and starch are confirmed by FTIR-ATR and the plasticization effect was instead proved for water over ILs.

The dielectric measurements revealed some subtle differences in the mobility of the different prepared materials. It confirmed the lower T_g for the IL [BMIM]Cl, and a mobility enhancement of SPCL doped with ILs compared to SPCL alone. On the other hand, it showed

that blends doped with the lower content of IL show some hindrance in the mobility, possibly due to the interaction of the dipolar moieties of ILs with starch.

Concerning conductivity, it was observed that the conductivity of SPCL doped with IL depends mostly on the IL, without being enabled by the segmental motions of the polymeric matrix itself. SPCL doped with 30 wt% of [BMIM]Cl, showed conductivity values compared with the ones of pure IL, but with an enhanced stability. This can open door to potential applications of these materials as self-supported conductive systems, made of bio-based polymers.

Although the use of ILs is considered as more sustainable, the most recent studies on these solvents show that although they present negligible vapour pressure, it is not safe to say that they are non-toxic and green. If the final objective of the produced materials reported in this work, was to use them for biomedical applications the removal of IL upon foaming the polymer must be assured, and other types of ILs or solvents should also be considered as possible candidates.

Chapter 5

Properties and Thermal Behavior of Natural Deep Eutectic Solvents

The results in this chapter were previously submitted as: **R. Craveiro**, I. Aroso, V. Flammia, T. Carvalho, M. T. Viciosa, M. Dionísio, S. Barreiros, R. L. Reis, A. R. C. Duarte, A. Paiva, *(submitted to RSC Advances)* .

The conductivity measurements and part of the DSC measurements were performed by Veronica Flammia and Tânia Carvalho. The density and rheology measurements were performed by Ivo Aroso. The POM analysis was performed by María Viciosa.

5.1. Introduction

As it has been said along this thesis, the search for new solvents that can replace common organic solvent media assumes great importance, not only because of the related negative environmental effects, but also if applications in the area of biomaterials are envisaged, more biocompatible and biodegradable solvents are necessary.

Since the beginning of research in the area of deep eutectic solvents (DES) [43] up to now, they have already found many applications, covering many different areas such as extraction solvents, in synthesis, as biological solvents, among others [17,39,54,57–59,62,148,149]. DES appeared alongside a new generation of ionic liquids (ILs) that intended to be more sustainable, biodegradable and biocompatible. DES are normally composed of choline chloride (ChCl, a quaternary ammonium salt), carboxylic acids and other hydrogen bond donors (HBD), such as urea, citric acid or glycerol. DES present many advantages relative to ILs, since they are much more easily prepared, they are biodegradable, and they are cheaper than ILs, mainly due to the abundance of the raw materials [62,150]. Still, one of their disadvantages is related with the fact that some of them are not liquid at room temperature and present high viscosities [62].

One very interesting hypothesis, recently stated by Choi *et al.* [63], was that the presence of DES could also be found in natural and biological media. This would be an alternative to the aqueous and lipid media that are found in most organisms, composed of primary metabolites, and was termed as natural deep eutectic solvent - NADES. This hypothesis gained chemical and physical evidence, when it was found that those primary metabolites, such as sugars, organic acids and amino-acids (for example) were able to form DES, when mixed in appropriate molar ratios. Dai and co-workers [62,65] reported an extensive list of NADES based on those primary metabolites, and described some of their physicochemical properties. These authors have already described these solvents and their applications, as well as Paiva *et al.* [61], who reported the use of NADES as extractions solvents, as well as data on their cytotoxicity which was found out to be lower than that of ILs.

The fact that NADES are natural and bio-based, biodegradable, constituted of renewable raw materials, easy to prepare and have low cytotoxicity, has envisaged applications as solvents to be used with biopolymers for biomedical applications, for example.

Nevertheless, to use these solvents a better understanding on their thermal and physicochemical properties is needed, to fully explore their potential applications and understand their organization. A detailed characterization of NADES can lead to further scientific developments. Dai *et al.* have characterized some NADES by nuclear magnetic resonance (NMR) spectroscopy and concluded that water played an important role in NADES formation. In addition, Dai and co-workers also determined the thermal and physical characteristics of some of NADES with water in its composition [151]. Florindo *et al.* also reported the strong influence of water in the properties of choline chloride:carboxylic acids DES. The thermal properties of NADES are also presented, with special attention to the glass transition temperature (T_g) and decomposition temperature (T_d) [152]. Following their work, NADES composed of different sugars, organic acids and choline chloride, in the ratios reported and according to the procedures described were prepared.

The work presented in this chapter, intends to give a more detailed characterization on some of the most widely used NADES, namely their thermal behaviour, conductivity, density, viscosity and polarity.

5.2. Materials and methods

5.2.1. Materials

Choline chloride, D-(+)-xylose, D-(+)-glucose, citric acid monohydrate, nile red and Hydranal Coulomat AG were acquired from Sigma-Aldrich. D-(+)-sucrose was acquired from Fluka, and L-(+)-tartaric acid was from Fischer scientific. All chemicals were used without further purification.

5.2.2. Preparation of NADES

NADES were prepared according to Table 5.1. The corresponding amounts of each component, in the proper molar ratios, were weighed and dissolved in water. The two solutions were mixed and homogenized, and later water was removed in a rotatory evaporator, at 50 ºC under vacuum, until a clear viscous liquid was obtained. NADES were subsequently kept in a desiccator and under vacuum.

Table 5.1 – NADES prepared in this work, and the corresponding mole ratios of components and sample names.

NADES		mole ratio	Sample Name
component 1	component 2		
Choline Chloride	D-(+)-glucose	1:1	ChCl:gluc (1:1)
Choline Chloride	citric acid	1:1	ChCl:ca (1:1)
Choline Chloride	D-(+)-sucrose	4:1	ChCl:suc (4:1)
Choline Chloride	D-(+)-sucrose	1:1	ChCl:suc (1:1)
Choline Chloride	D-(+)-xylose	2:1	ChCl:xyl (2:1)
Choline Chloride	D-(+)-xylose	3:1	ChCl:xyl (3:1)
Citric acid	D-(+)-sucrose	1:1	ca:suc (1:1)
Citric acid	D-(+)-glucose	1:1	ca:gluc (1:1)
D-(+)-glucose	L-(+)-tartaric acid	1:1	gluc:ta (1:1)

5.2.3 Water content determination

The water content of the NADES mixtures was determined by Karl-Fischer titration, using an 831 KF Coulometer with generator electrode and without diaphragm. The water content values presented for each NADES are an average of at least three measurements.

5.2.4. Differential scanning Calorimetry (DSC)

The experiments leading to the determination of the degradation temperatures of NADES (T_d), were performed in a DSC Q100 equipment (TA Instruments-ELNOR). The experiments were conducted under nitrogen atmosphere, with samples with a mass of 5-10 mg in packed aluminium pans. The samples were heated at a constant heating rate of 20 °C/min, from -40 °C up to 250 °C, and the results presented are an average of at least three measurements.

The thermal behaviour of NADES and its individual components was later studied with a DSC Q2000 (TA Instruments, Tzero™ DSC technology). Measurements were performed under dry high purity helium, at a flow rate of 50 mL/min. Less than 5 mg of each samples were packed in a TA aluminium pan (the set was not hermetically sealed to allow free water evaporation). At least two scans of cooling and heating were performed at 20 °C/min, in the temperature range of -90 °C to 120 °C. Each sample was kept for an additional 1 min at 120 °C at the end of the scan, in order to ensure water removal. They were also kept for an additional 10 min at -90 °C at the end of each scan, in order to obtain a better signal for the glass transition temperature (T_g), when present.

5.2.5. Polarized Optical Microscopy (POM)

By using light microscopy with cross polarizers, it is possible to obtain information on the isotropy of a sample (in this case NADES) at different experimental conditions.

Polarized optical microscopy was performed on an Olympus Bx51 optical microscope equipped with a Linkman LTS36 liquid nitrogen-cooled cryostage. The microstructure of the samples was monitored by taking microphotographs at appropriate temperatures, using an Olympus C5060 wide zoom camera. A drop of each sample was positioned on a microscope slide and inserted in the hot stage. Before each measurement, the samples were heated at 120 °C and kept at least 10 minutes at this temperature to allow water removal. After this thermal treatment, a cover slip is put on the top of the sample. Cooling and heating treatment were carried out at a rate of 20 °C/min.

5.2.6. Density measurements

Density of NADES was measured following a simple gravimetric method, using a calibrated volume at 23 °C.

5.2.7. Conductivity measurements

The conductivity measurements were performed using dielectric relaxation spectroscopy (DRS). NADES samples were placed between two stainless steel electrodes of 10

mm diameter, in a BDS parallel capacitor, using two 50 μm silicon spacers to maintain sample thickness. The sample cell was mounted on a BDS 1100 cryostat and exposed to a gas stream that resulted from the evaporation of liquid nitrogen in a Dewar. The temperature control was ensured by a Quatro Cryosystem and performed within ± 0.5 $^{\circ}$C. The measurements were performed in an Alpha-N analyser, covering a frequency range from 10^{-1} Hz to 1 MHz. After an initial cooling ramp from room temperature to 0 $^{\circ}$C, isothermal spectra were collected from 0 $^{\circ}$C to 40 $^{\circ}$C in steps of 5 $^{\circ}$C. All the modules were supplied by Novocontrol.

5.2.8 Polarity Measurements

Polarity measurements were carried out using Nile Red as a solvatochromic probe. A stock solution was prepared in ethanol. The NADES samples were placed in a quartz cuvette and the Nile Red stock solution was added (50-100 μL). The cuvette containing the solution was then placed under nitrogen atmosphere, in order to evaporate the solvent, and the UV/Vis spectra was immediately acquired, at 23 $^{\circ}$C. Spectra of Nile Red samples with different amounts of water were also recorded, in order to determine the influence of water in the polarity measurements.

5.2.9. Rheology measurements

The viscosity and the rheological behaviour of NADES were studied using a rheometer (Paar Physica MCR300, Germany). Steady-flow measurements were carried out using a controlled-stress rheometer fitted with a concentric cylinder geometry (CC10). The torque amplitude was imposed by using a logarithmic ramp shear stress, in a range of 0.1 to 1000 Pa. The temperature of the samples was kept at 23 $^{\circ}$C, using a water circulating bath. All the present results are an average of at least three measurements.

5.3. Results and Discussion

5.3.1. Thermal Characterization

All the presented NADES' thermal stability was evaluated, up to 250 $^{\circ}$C, by DSC. All samples present a T_d above 120 $^{\circ}$C (Table 4.2); NADES composed by sugars present lower T_d values, and the ones with carboxylic acids in its composition have higher T_d values, which is in accordance with results presented by Dai *et al.* [62]. Further information on the thermal behaviour of each NADES are also presented in Table 5.2.

The initial water content for each NADES is also presented in Table 5.2, which can be up to 5.5 %. For all the NADES, the presence of water can be detected in the thermograms by a broad endothermic peak with its onset located at 27 $^{\circ}$C, detected in the first scan (data not shown); this peak corresponds to water evaporation, and is not visible in subsequent scans meaning that all the water was removed in the first heating scan.

For all the NADES under study, a discontinuity in the heat flux is also observed for lower temperatures, corresponding to the glass transition. The detection of a glass transition from which a T_g value can be determined allows us to classify all the NADES tested as glass formers.

All NADES exhibit different glass transition temperatures (T_g) in the first and last scans. In all cases, the T_g was lower in the first scan, and was shifted to higher temperatures in the following scans, until constant. The reason for this can be due to the plasticizing effect of water [142] (Figure 5.1). The variation of the onset of the T_g ranges from 10 $^{\circ}$C to 30 $^{\circ}$C, depending on the hydrophilicity of NADES (more pronounced in those with ChCl).

The thermogram for gluc:ta (1:1) presented in Figure 5.1 (a) as an example of the data obtained by DSC measurements. It is seen that T_g is the only detected thermal event, which is also what occurs for most of the NADES studied. A POM microphotograph of gluc:ta (1:1) is also shown, at a temperature lower that T_g, confirming the vitrification of the sample.

Also in Figure 5.1 (b), the thermogram for NADES ca:gluc (1:1) is presented, showing a different thermal behaviour. In this case, two glass transitions are observed, clearly visible after water removal, suggesting a phase separation which is also observed by the POM microphotographs below and above the T_g.

Table 5.2- Water content and thermal properties of the NADES under study, degradation temperature (T_d), melting temperature (T_m) and glass transition temperature (T_g). The pure compounds are also included for comparison.

NADES	H₂O content (%)[a]	T_d (°C)	$T_{c, melt}$ (°C)[b]	$T_{c\,cold}$ (°C)[b]	T_m (°C)[b]	$T_{g\,First\,Scan}$ (°C)	$T_{g\,Last\,Scan}$ (°C)[b]
ChCl:gluc (1:1)	5.5	129.8	-	-	-	-60.4	-28.4
ChCl:ca (1:1)	0.2	171.3	-9.7	-	76.0	-36.7	-21.4
ChCl:suc (4:1)	0.2	141.7	-33.9	51.8	79.2	-76.9	-42.0
ChCl:suc (1:1)	0.2	126.8	-	-	-	-47.6	-15.8
ChCl:ta (2:1)	1.9	130.8	-	-	-	-67.3	-41.6
ChCl:xyl (3:1)	0.2	165.2	20.1	59.9	78.5	< - 80[c]	-46.4
ChCl:xyl (2:1)	4.4	172.7	-	56.9	78.3	< - 80[c]	-51.2
ca:suc (1:1)	1.2	121.2	-	-	-	-45.4	-14.0
ca:gluc (1:1)	0.5	130.1	-	-	-	-30.4	9.8/48.7
gluc:ta (1:1)	0.4	117.5	-	-	-	-31.7	-18.3
Glucose	-	-	-	-	-	-	-39.2[d]/-37.0[e]
Sucrose	-	-	-	-	-	-	-39.1[d]
Xylose	-	-	-	-	-	-	-43.8
citric acid	-	-	-	-	64.2	-	-38.2
tartaric acid	-	-	-	-	-	-	-40.1[d]
ChCl	-	-	46.5—33.2	-	90.8	-	-

[a] after the preparation and storage.

[b] data referent to last scan (dry sample).

[c] the onset of the glass transition is beyond the limit of detection.

[d] glass transition is ill defined

[e] sample with 12.8 wt% of water
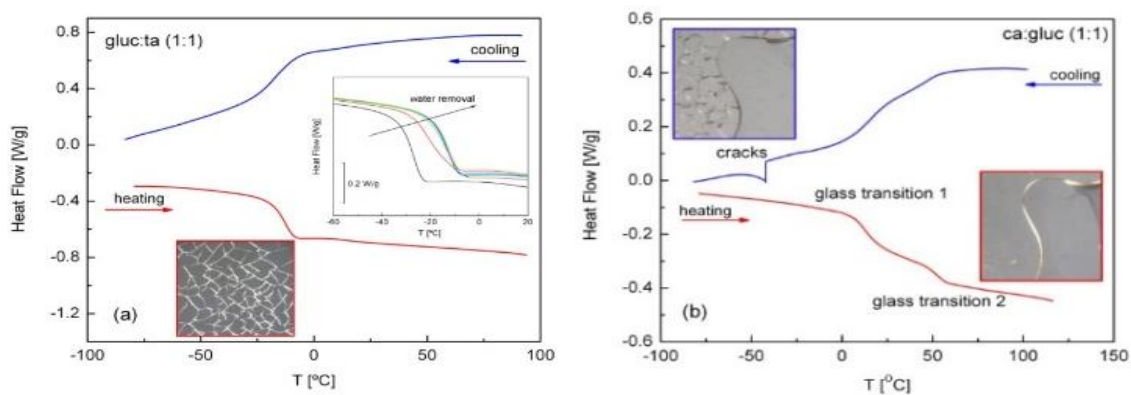
Figure 5.1- Thermograms for different NADES (after water removal) and corresponding POM micrographs; gluc:ta (1:1) **(a)**, ca:gluc (1:1) **(b)**. The inset in Figure 5.1 (a) shows the effect of water presence in the T_g and its subsequent removal.

Figure 5.1 (a) further shows for gluc:ta (1:1) a POM micrograph where micro-cracks appear on heating the NADES at -57 °C (below the T_g), covering all the sample. With further heating (above the T_g), those micro-cracks start to disappear, and a homogeneous dark POM micrograph is obtained (data not shown), characteristic of a supercooled isotropic liquid.

For ca:gluc (1:1), two glass transition events are detected in the DSC thermogram, suggesting that two glasses are formed upon cooling. Although this NADES has a liquid appearance at room temperature, the POM micrograph taken at -55 °C (below both T_g values) reveal the coexistence of two different glasses; the micro-cracks only emerge in a defined region of the sample (Figure 5.1 (b)). Similar behavior was found out in other low molecular weight glass formers [153,154]. These two separate regions are still present at higher temperatures (above the two T_g), meaning that phase separation persists when the sample is in its supercooled liquid state.

Regarding the NADES that present melting, a more complex thermal behaviour is observed. Figure 5.2 presents the thermogram obtained for ChCl:xyl, which shows exothermic and endothermic peaks, corresponding to melting and crystallization (respectively). This is also observed for ChCl:ca (1:1), that upon water removal undergoes a partial crystallization on cooling from the liquid state (*melt crystallization*) [155]. On the other hand, ChCl:xyl (2:1) fails to crystalize on cooling, but crystallizes upon heating from the glass state (*cold crystallization*). This type of crystallization is observed when an amorphous material is reheated above its glass transition [155]. It is interesting to note that ChCl:suc (4:1) and ChCl:xyl (3:1) undergo both melt and cold crystallization, as well as glass transition.

All the NADES that show a melting peak have associated T_m close to 80 °C, and only NADES with ChCl in its composition show crystallization phenomena, which may indicate that ChCl is the component that determines crystallization. It is important to note that the melting phenomenon is purely thermodynamic in nature, while crystallization is also controlled by factors such as nuclei formation and crystal growth [156].
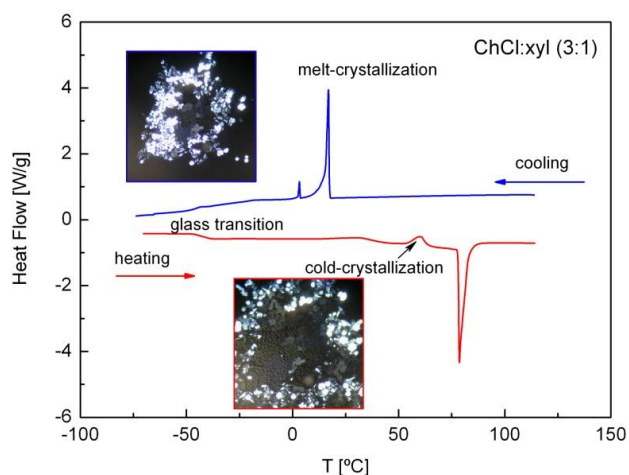
Figure 5.2- Thermogram for NADES ChCl:xyl (3:1) (after water removal) with the corresponding POM microphotographs.

POM microphotographs of ChCl:xyl (3:1) and ChCl:ca (1:1), which are semi crystalline at room temperature, are shown in Figure 5.3. The dispersed crystals of the NADES are observed. For both NADES, there is recrystallization after melting.
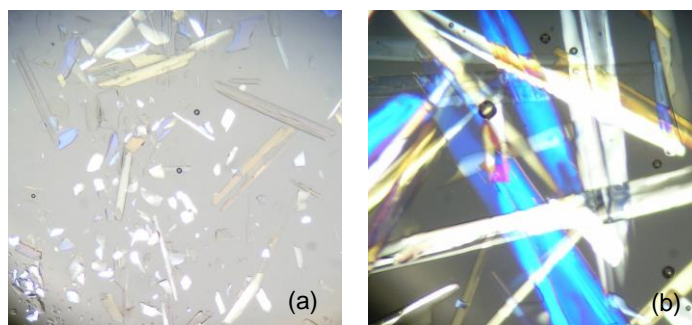
Figure 5.3- Microphotographs taken by POM at 25 °C at a magnification of 40x of ChCl:xyl (3:1) **(a)** and ChCl:ca (1:1) **(b)**.

As previously said, the presence of water and its quantification in NADES, assumes great importance when studying its thermophysical properties. In the studies performed by Dai *et al.* [62], they concluded that some of the NADES could not form a liquid mixture at room temperature and they added known amounts of water in order to obtain them in the liquid state. That amount of water was later included as a molar fraction in the final composition of the NADES.

This is the case of ChCl:xyl (2:1), which is liquid with 4.4 wt% of water. In Table 5.2, it is observed that ChCl.xyl (2:1) has a T_m of 78.3 °C. This value was obtained on the last scan of DSC, when all water was already removed. This stresses the fact that in some cases water is essential for the formation of a liquid NADES at room temperature. Another case is ChCl:gluc (1:1), which is only stable with water, precipitating upon water removal. These observations were corroborated by the work of Dai *et al.* [62].

To further assess the importance of water in the formation of NADES, ChCl:ca (1:1), ChCl:suc (4:1) and ChCl:xyl (3:1) are also presented in Table 5.2 with only 0.2 wt% of water, even though they are not liquid at room temperature.

Nevertheless, it is worth to show the influence of the water amount of NADES in the thermal properties. ChCl:xyl (2:1) was prepared with different known water amounts (the water amounts were measured by Karl-Fischer titration), and the DSC were acquired in the same conditions as before. The results are presented in Table 5.3, and clearly demonstrate the plasticizing effect of water, where with increasing amounts of water present in the sample, the T_g value decreases. NADES are obtained by the complexation of a hydrogen acceptor and a hydrogen-bond donor. Therefore, water will have a significant influence in the complex, altering the properties of the NADES, thus interfering in the liquidus and solidus lines of the eutectic phase diagram. In fact, Dai and co-workers observed a strong interaction between the hydroxyl groups of water with the hydroxyl groups of xylose and choline and the chloride anion [151]. The destabilization of the supramolecular structure of NADES by water, increases the mobility of the both components of NADES translated in the decrease in the T_g.

As for ChCl:xyl (2:1), with the addition of 4% (wt.) of water to the NADES, T_m suffers a depression of 1 °C, nevertheless at higher contents of water the opposite effect occurs and an increase in the melting temperature is observed. This values are in accordance with Dai *et al.* which reported a T_g of -81.8 °C for ChCl:xyl (2:1) with 7.74% water content. The influence of water content in the T_g, observed for NADES, is not seen in the pure components for which almost no variation occurs in the respective T_g (Table 5.2). For a sample of glucose after the addition of 12.8% (w/w) of water content, a small change in the glass transition temperature occurs.

Table 5.3- Influence of the amount of water in the T_g value, measured by DSC; data specific for the NADES ChCl:xyl (2:1).

ChCl:xyl (2:1)	$T_{g\ Last\ Scan}$ (°C)	T_m (°C)
2.2 % H_2O	-58.55	77.12
4.01% H_2O	-59.15	76.22
4.98 % H_2O	-61.26	77.02

5.3.2. Density

All the NADES under study present higher density that water, about 20% higher, and NADES that contain ChCl in their composition are the ones with comparatively lower densities (Table 5.4).

Table 5.4- Density of the NADES under study.

NADES	density (g/mL)
ChCl:gluc (1:1)	1.27
ChCl:ca (1:1)	1.30
ChCl:ca (2:1)	1.25
ChCl:suc (4:1)	1.22
ChCl:suc (1:1)	1.35
ChCl:ta (2:1)	1.26
ChCl:xyl (2:1)	1.23
ChCl:xyl (3:1)	1.22
ca:suc (1:1)	1.43
ca:gluc (1:1)	1.45
gluc:ta (1:1)	1.46

5.3.3. Conductivity

The conductivity of the NADES under study was assessed by DRS. This technique mainly probes, for a sample under the influence of an oscillating electric filed, the reorientational movements of dipoles and propagation of mobile charge carriers [157]. The migration of the charge carriers occurs due to a translational diffusion through hopping movements of electrons, holes and ions, giving rise to conductivity [157].

The conductivity of each NADES was measured from 10^{-1} Hz to 10 KHz, in the temperature range of 0-40 °C, in steps of 5 °C.

The conductivity data obtained by DRS (*equations 2.6 to 2.11, Chapter 2*), can provide information about the charge transport mechanism of a material [158]. In this work, the results obtained are based in the real part of conductivity, which shows a universal behavior for a variety of disordered conductive materials, i.e., it exhibits a plateau at lowest frequencies and high temperatures. At that plateau, the conductivity is independent of the frequency, and extrapolating $\omega \rightarrow 0$, the direct conductivity (σ_{dc}) can be determined. At higher temperatures, conductivity becomes frequency dependent [159]. This can be illustrated in Figure 5.4 that shows the isotherms for NADES ca:suc (1:1).
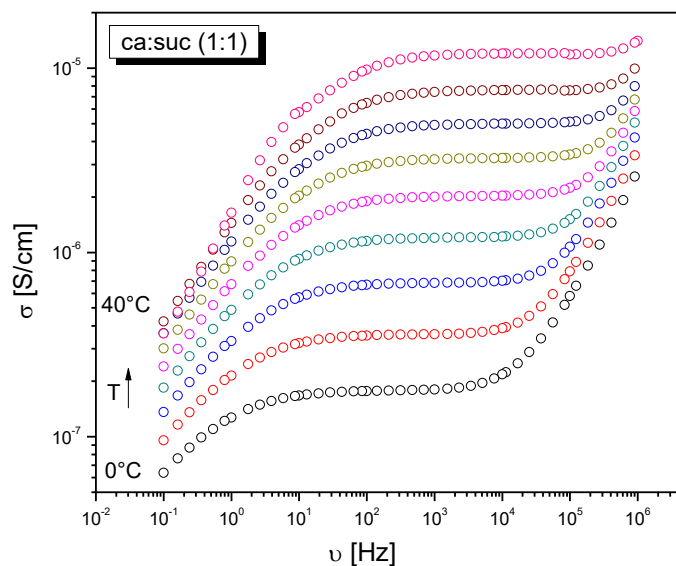
Figure 5.4- Isotherms of conductivity dependence with frequency, for the NADES ca:suc (1:1).

The conductivity values (σ_{dc}) presented in Table 5.5 were obtained from this plateau, for each isotherm (σ_{dc} is an average of the values at the plateau). The NADES ChCl:suc (1:1) and ChCl:suc (4:1) exhibit the higher conductivities, that are the same order of magnitude as the conductivity of some ILs, e.g., [BMIM]PF$_6$ which has a conductivity of 2.46x10^{-3} S/cm, at 35 ^{o}C [160]. The other NADES under study exhibit conductivities at least one order of magnitude lower.

Table 5.5- Conductivity data (σ_{dc}) for the NADES under study, at different temperatures.

σ_{dc} (S/cm)	0 ºC	5 ºC	10 ºC	15 ºC	20 ºC	25 ºC	30 ºC	35 ºC	40 ºC
ca:gluc (1:1)	1.80x10^{-7}	4.24x10^{-7}	8.47x10^{-7}	1.96x10^{-6}	2.63x10^{-6}	4.19x10^{-6}	6.39x10^{-6}	9.06x10^{-6}	1.19x10^{-5}
ChCl:suc (4:1)	2.92x10^{-4}	4.19x10^{-4}	5.79x10^{-4}	7.75x10^{-4}	1.02x10^{-3}	1.28x10^{-3}	1.54x10^{-3}	1.80x10^{-3}	2.05x10^{-3}
ca:suc (1:1)	1.77x10^{-7}	3.60x10^{-7}	6.80x10^{-7}	1.20x10^{-6}	2.01x10^{-6}	3.22x10^{-6}	4.96x10^{-6}	7.51x10^{-6}	1.19x10^{-5}
gluc:ta (1:1)	1.01x10^{-5}	1.59x10^{-5}	2.57x10^{-5}	4.16x10^{-5}	6.39x10^{-5}	1.27x10^{-4}	2.35x10^{-4}	5.00x10^{-4}	1.23x10^{-3}
ChCl:ca (1:1)	3.43x10^{-5}	4.97x10^{-5}	7.13x10^{-5}	9.93 x10^{-5}	1.37x10^{-4}	1.82x10^{-4}	2.30x10^{-4}	2.73x10^{-4}	3.10x10^{-4}
ChCl:suc (1:1)	2.22x10^{-4}	4.23x10^{-4}	6.04x10^{-4}	8.36x10^{-4}	1.08x10^{-3}	1.35x10^{-3}	1.55x10^{-3}	1.74x10^{-3}	1.81x10^{-3}
ChCl:gluc (1:1)	6.72x10^{-6}	1.06x10^{-5}	1.51x10^{-5}	2.00x10^{-5}	2.41x10^{-5}	2.55x10^{-5}	2.54x10^{-5}	2.55x10^{-5}	3.04x10^{-5}
ChCl:xyl (2:1)	2.43x10^{-5}	3.35x10^{-5}	4.52x10^{-5}	5.70x10^{-5}	7.20x10^{-5}	9.31x10^{-5}	9.24x10^{-5}	9.34x10^{-5}	9.17x10^{-5}
ChCl:xyl (3:1)	3.28x10^{-6}	5.73x10^{-6}	1.17x10^{-5}	2.05x10^{-5}	3.37x10^{-5}	5.57x10^{-5}	8.66x10^{-5}	1.12x10^{-4}	1.75x10^{-4}

From Table 5.5, it is observed that the amplitude of variation of the σ_{dc} is relatively low within the temperature range under study. But in the case of NADES ca:gluc (1:1), ca:suc (1:1) and ChCl:xyl (3:1), it is possible to simulate the σ_{dc} dependence with temperature, by the Vogel-Fulcher-Tammann (VFT) equation.

The VFT equation normally describes the temperature dependence of the relaxation time, associated with the dynamic glass transition, but it was found to describe quite well the $\sigma_{DC}(1/T)$ for a variety of materials, including ILs [156,161,162].

The VFT equation was fitted to $\sigma_{DC}(1/T)$, according to the equation

$$\sigma_{dc} = \sigma_{\infty} exp^{(-\frac{B}{T-T_0})} \tag{5.5}$$

where B is an empirical parameter accounting for the plot curvature, σ_{∞} is the high temperature limit of the conductivity and T_0 is the Vogel temperature at which the conductivity goes to zero. When the VFT equation is used to simulate the glassy dynamics relaxation time, T_0 is interpreted as the glass transition temperature of an ideal glass, i.e., a glass obtained with an infinitely slow cooling rate [163].

Figure 5.5 shows the results for the VFT fitting, in the solid lines, evidencing that the temperature dependence of the conductivity is well described by the VFT equation. Table 5.6 shows the VFT fitting parameters.
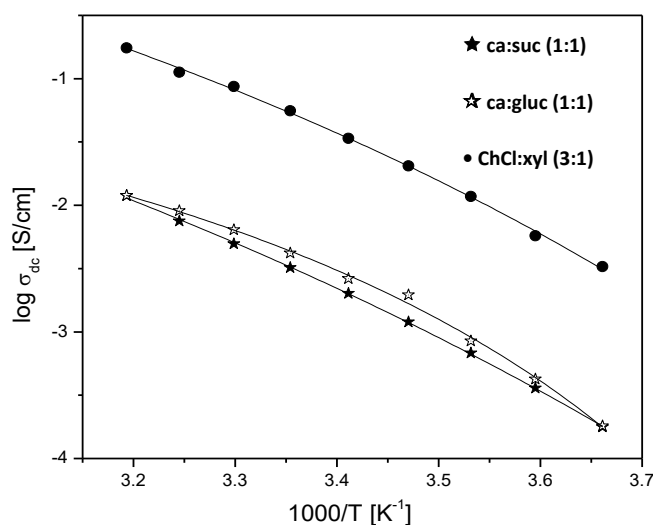
Figure 5.5- Temperature dependence of the pure conductivity, σ_{dc}, of NADES. ChCl:xyl (3:1), ca:suc (1:1) and ca:gluc (1:1). The solid lines were obtained by fitting with the VFT equation.

Table 5.6- Fit parameters obtained according to the VFT law for the conductivity (eq. 5.5).

	σ_∞ (S/cm)	B (K)	T_0 (K)
ChCl:xyl (3:1)	1063±812	1107±301	136±2
ca:suc (1:1)	556±333	1556±223	127±1
ca:gluc (1:1)	1.3±0.7	397±84	227±6

Note*: The uncertainties are the statistical errors given by the fitting program. For each material, the similarity between B and T_0 estimated through $\sigma_{dc}(T)$ indicates a parallelism between these two quantities.*

From these results, there is an indication that the ion conducting motions are governed by the glassy dynamics, as it was already found for similar systems [156,161,162]. When the Vogel temperature (T_0) and the glass transition temperature are compared, there is the same variation; T_0 (in Kelvins) is higher for ca:suc (1:1) and ca:gluc (1:1), while the lower value is for ChCl:xyl (3:1) the same order observed for the T_g of these samples. This corroborates the association between the charge transport mechanism and the dynamic glass transition.

5.3.4. Polarity

The polarity of the NADES under study was measured using Nile Red as a solvatochromic dye, which has been previously used to assess the polarity of weak acids and protic molecular solvents and ILs [93,164].

The maximum absorbance wavelength (λ_{max}) for each NADES sample was measured and the parameter E_{NR} was determined (Chapter 2, equation 2.9) [94].

Solvents with higher polarity shift the λ_{max} of the dye to higher wavelength values, yielding lower E_{NR} values. The changes measured in the λ_{max} values of Nile Red, relative to the value that the dye exhibits in the reference solvent (in this case, ethanol), make it possible to calculate the relative polarity of a sample of interest.

The results of the polarity measurements are depicted in Figure 5.6, where the polarity of the IL [BMIM]BF$_4$ was also included for comparison. According to equation 2.9 (Chapter 2), the experimental value for the polarity of [BMIM]BF$_4$ (in this work) yields a λ_{max} of 556 nm, which differs less than 1% from the value reported in literature [93].

From the presented results, it is seen that NADES composed of organic acids are the most polar, and the least polar are composed by sugars, which is in agreement with results previously reported by Dai *et al.* [62]. In particular, between the NADES that are composed by carboxylic acids, gluc:ta (1:1) is slightly more polar than gluc:ca (1:1). This can be related to chemical structure and also with the pKa, tartaric acid is stronger (pKa=2.98) than citric acid (pKa=3.14). As expected, a higher proportion of organic acid brings about an increase in the polarity of NADES.

Another factor that needs to be taken into account is the water content of the sample. Dai *et al.* have shown the influence of the amount of water in NADES in their polarity [62]. In this work, to account for that effect, measurements of Nile Red solutions with different amounts of

water from 0.1 % up to 15 % were performed. A bathocromic shift is visible, since with increasing the water content the λ_{max} shifts for higher wavelengths. The deviation of nile red λ_{max} was under 1.2 % (Figure 5.7), and the variations of the value of E_{NR} have a small extent. Also, increasing the water content results in lower E_{NR} values, and consequently higher polarity.
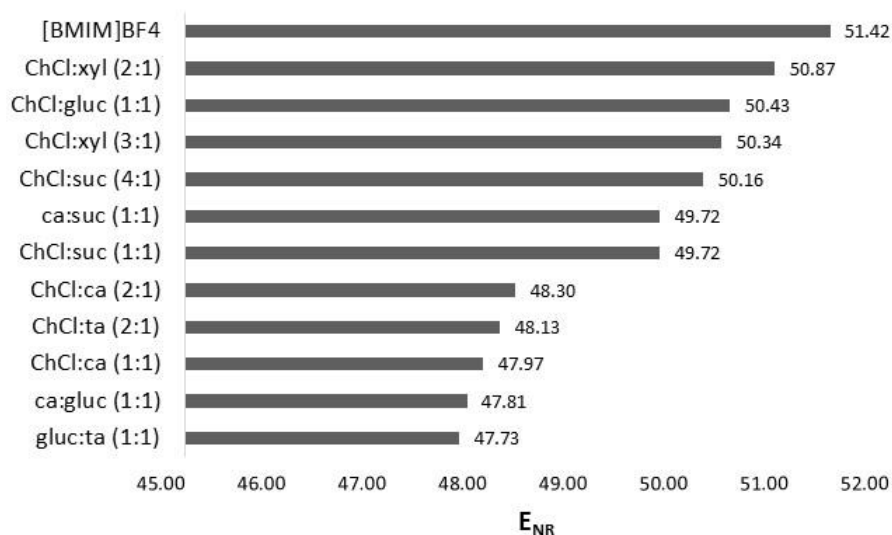
Figure 5.6- E_{NR} values of the NADES under study, and also for IL [BMIM]BF₄ (included for comparison).
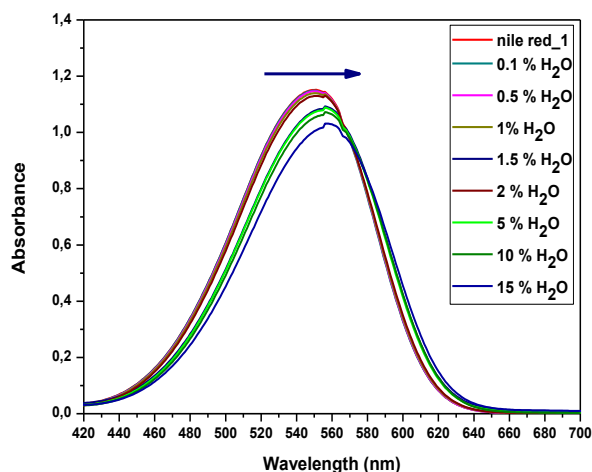
Figure 5.7- Influence of the water content in the nile red absorbance spectrum in the visible region.

The same is observed in the case of ChCl:xyl (2:1), where the variation of water content results in small variations in the E_{NR} value. Although the variations in the ENR values are small with the increasing water content, they can significantly alter the polarity scale of the different studied NADES.

The same tendency was observed in the studies of Dai *et al.* [62], that report changes in the polarity of NADES 1,2-propanediol:choline chloride:water (1:1:1). The authors suggest that the dilution of the NADES (up to 50% of water content) with water causes dramatic a change in the structure of the NADES, due to the rupture of the hydrogen bonding network formed between the two components of the NADES.

Table 5.7- Influence of the water content of ChCl:xyl (2:1) wavelength of maximum absorption (λ_{max}) of nile red, and in the respective E_{NR} value.

Water content ChCl:xyl (2:1) (%)	Nile Red λ_{max} (nm)	E_{NR} (Kcal/mol)
3.8	563	50,78
4.3	564	50,69
6.0	570	50,16

5.3.5. Rheology

The viscosities of the NADES under study were assessed by curve flow measurements, with exception for ca:suc (1:1), that exhibits almost a solid-like behaviour where the measurements could not be performed. Figure 5.8 is shows some of the results obtained, for ca:gluc(1:1) and ChCl:ca (1:1).

NADES ca:gluc (1:1) exhibits a shear-thinning behaviour, which is characterized by a decrease of the viscosity with the increasing shear rate. This effect is also observed for ChCl:ca (1:1) (Figure 5.6 (b)), with changes in viscosity of two orders of magnitude, when the shear stress varies from 0.1 to 1000 s^{-1}. For the later NADES, the behaviour is not always the same, since in the range of 0.1 to 1 s^{-1} there is an increase in viscosity. However, at higher rates than 1 s^{-1} the apparent viscosity approaches a Newtonian plateau where viscosity is independent of shear rate.

(a)   **(b)**
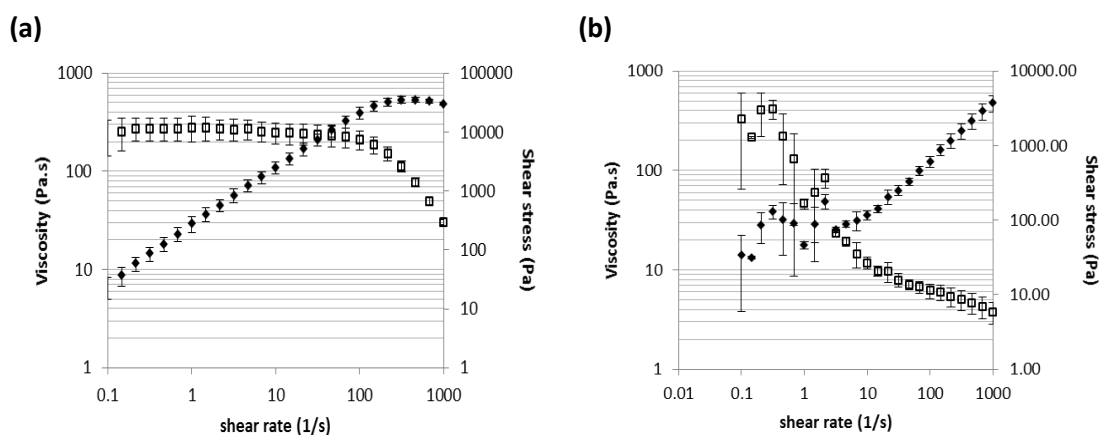
Figure 5.8- Flow curves for ca:gluc (1:1) **(a)** and ChCl:ca (1:1) **(b)**, at 23 °C. Open symbols refer to viscosity and closed symbols to shear stress.

The shear stress also shows changes with the shear rate; there is an initial increase of the shear stress, however this dependence does not intersect the origin and therefore the behavior of these samples cannot be considered Newtonian. This means that viscosity cannot be directly calculated from the slope of the mathematical relation

$$\sigma = \eta\dot{\gamma}$$

where σ is the shear stress, η is the viscosity and $\dot{\gamma}$ is the shear rate.

The behaviour of the NADES under study is characterized by the existence of a yield stress or apparent yield stress, σ_0, determined at $\dot{\gamma}$=0. The apparent yield stress was determined for all the NADES under study and is presented in Table 5.8.

Table 5.8- Apparent yield stress and viscosity of the NADES studied, at 23 °C.

NADES	Yield stress (σ_0) (Pa)	Viscosity (η_0) (Pa/s)
ChCl:gluc(1:1)	2.8	2.35
ChCl:ca (1:1)	80.4	3.39
ChCl:suc (4:1)	84.9	6.81
ChCl:suc (1:1)	118.6	7.10
ChCl:xyl (2:1)	7.4	1.28
ca:gluc (1:1)	108.3	227.02
gluc:ta (1:1)	218.6	49.64

When the magnitude of the external yield stress exceeds the value of σ_0, the fluid is able to flow. Additionally, when the apparent viscosity approaches a Newtonian plateau, it is possible to determine the zero shear viscosity η_0 (Table 5.7).

The results shown here show that the viscosity is highly dependent on the NADES composition. It is also important to note that the viscosity is dependent on the amount of water of the NADES, and this results refer to samples that contain the water content shown in Table 5.5.

Kulkarni *et al.* have shown an extensive report on the viscosity of ILs, and most of the ILs tested is much lower than the values obtained for NADES (<1 Pa/s) [165]. This shows one of the main limitations in applying NADES to certain areas, the very high viscosity. This can be tuned by adding specific amounts of water to the NADES mixture, but the impact of water in the other physico-chemical properties would need to be taken into account. So, a deeper knowledge of the viscosity dependence of NADES with the percentage of water needs to be acquired.

5.4. Conclusions

This chapter presents data on the thermophysical properties on several natural deep eutectic solvents. The determination of properties such as density, viscosity, polarity, conductivity and the thermal behavior are essential for a better understanding of these novel solvents, and for the unveiling of potential applications. The NADES presented in this study are composed of choline chloride and organic acids and sugars, all primary metabolites of organisms.

One very important conclusion that can be drawn from this study is that the composition of NADES has a great influence on the properties measured, including the water content. For that reason, the effect of the amount of water present in those properties was also evaluated.

Regarding the thermal behavior, it is observed that all NADES under study are glass formers, which was confirmed by DSC measurements and observed in POM microphotographs).

Some NADES show particular behavior, such as ca:gluc (1:1), that exhibits two different glass transitions (attributed to the two constituents of the NADES), revealing that that NADES is not totally homogeneous. This is also observed in POM microphotographs. Other NADES, such as ChCl:xyl (3:1) exhibit melt crystallization and cold crystallization, but a deeper understanding on the molecular mechanisms responsible by these phenomena is needed to fully describe them. Furthermore, the choline chloride presence may be related with the crystallization events that occur in NADES where it is present.

The density of all NADES understudy is higher than the density of water, for the temperatures studied. Also, they are all more polar than IL [BMIM]BF$_4$, being that NADES composed of organic acids are more polar than those composed of sugars.

Conductivity was assessed by means of DRS spectroscopy, and some NADES show conductivities close to the ones of some ILs, which may lead to electrochemical applications. In some cases, the temperature dependence of conductivity was well described by the VFT equation (in NADES ChCl:gluc (1:1), ChCl:suc (1:1) and ChCl:xyl (3:1)). It is safe to say that the charge transport mechanism that is responsible for conductivity is closely associated with the phenomenon of dynamic glass transition.

As referred previously, one of the drawbacks of NADES, and one of its possible limitations to some applications, is that they have high viscosities. In this study, all the NADES present viscosities higher than those of ILs, but it is important to note that it depends on the NADES composition and the water content.

Chapter 6

Processing of Starch-based
Polymers with Deep Eutectic
Solvents via Supercritical Fluid
Foaming

6.1. Introduction

Natural deep eutectic solvents (NADES) are considered part of a new generation of "green" solvents, mainly due to the fact that their constituents are natural metabolites (sugars, amino-acids, organic acids, among others) [61,62]. Their synthesis is also simple and sustainable, since it consists in the simple mixing and sometimes heating of two or more components, without any further synthetic and purification steps.

The applications of this type of eutectic solvents are starting to emerge and already cover many areas, including their use as extraction solvents and reaction media [65].

Much of the work presented in this thesis covers strategies to enhance the processability of starch-based polymer blends. The doping of the polymer blend with an ionic liquid (IL) followed by supercritical fluid (SCF) foaming proved efficient in obtaining structures with enhanced porosity and better mechanical properties. These final polymeric materials can have a myriad of applications, ranging from self-supported conductive materials to applications in the biomedical field [138,166]. Nevertheless, the use of ILs may not be always convenient, mainly due to the toxicity and negative environmental effects that are now being associated with some ILs [42,167].

Since NADES share many of the characteristics of ILs, their use in the processing of the polymer blends previously reported appeared to be a promising strategy. The use of NADES for the doping and possible foaming enhancement effect should be advantageous when compared with the use of ILs, given that NADES are overall more sustainable solvents, with an acceptable biodegradable and sometimes non-cytotoxic profile [61,168].

Another interesting approach is to use DES as bioactive or therapeutic solvents. This is also a strategy that has been previously used with ILs [169–173], and is now being adopted in the field of DES, since they can also be formed by one or more bioactive compounds with different therapeutic activity. Examples of these therapeutic DES (or THEDES) are presented by Stott *et al.* [45] and Carriazo *et al.* [174], who report on the formation of a DES composed by menthol (anesthetic and permeation enhancer compound) and ibuprofen (a model non-steroidal, anti-inflammatory drug, NSAID). Ruβ *et al.* [175] also reported the formation of a DES composed by ChCl and (*R*)-(-)-mandelic acid (known for its antibacterial activity). This has one major advantage, namely the possibility of using the therapeutic agent in its liquid form instead of a crystalline solid form, overcoming the problems related with the polymorphism [176], which limits the use of pharmaceutical ingredients.

In this work, a biocompatible, polymeric blend of starch:poly-ε-caprolactone (SPCL) was used and doped with NADES and the effect on the SCF foaming of the polymer was accessed.

SPCL was also doped with two different THEDES, one composed by choline chloride and mandelic acid, and the other by menthol and ibuprofen. Their ability to foam SPCL was also assessed, and the potential use of the foamed structure as a drug delivery device (therapeutic agent carrier) was also studied. Ultimately, the bioactive compounds will remain in the porous matrix obtained by supercritical fluid foaming, and since the matrix is a polymeric and biocompatible porous support, the controlled release of the compound into a medium will be achieved.

6.2. Materials and methods

6.2.1. Materials

The polymeric blend used consists of corn starch with poly-ε-caprolactone, SPCL (30 wt% of starch), in a granular form obtained from Biocycle.

The compounds used for the preparation of NADES and THEDES were choline chloride (ChCl), D-(+)-xylose, D-(+)-glucose, citric acid monohydrate (Sigma-Aldrich), D-(+)-sucrose (Fluka), L-(+)-tartaric acid (Fischer scientific), (*R*)-(-)-mandelic acid (ma; Alfa Aesar), (*R*,*S*)-(±)-menthol (Aldrich). Ibuprofen (ibu) was obtained from precipitation and subsequent washing of the ibuprofen sodium salt (Fluka; the procedure is described in Chapter 2). The Karl-Fischer titration reagents were Hydranal Coulomat AG (Sigma-Aldrich). All chemicals were used without further purification.

6.2.2. Preparation of DES

DES were prepared according to Table 6.1. All samples were prepared by weighing the corresponding amounts of each component, in the proper mole ratios. With the exception of THEDES, the components were dissolved in water, and the two solutions were mixed, homogenized, and later water was removed in a rotatory evaporator, at 50 °C under vacuum, until a clear viscous liquid was obtained, which was subsequently kept in a desiccator.

In the case of THEDES, ChCl:ma(1:2) was prepared by weighing the amounts corresponding to the correct molar ratio, and heated until a viscous liquid was otained (ca. 70 °C), under constant stirring. The THEDES composed of menthol:ibu (3:1) was prepared in a similar way, but the components were stirred at room temperature and a clear liquid was obtained.

Table 6.1- Summary of the DES prepared.

| DES | | mole ratio | Sample Name |
component 1	component 2		
Choline Chloride	citric acid	1:1	ChCl:ca (1:1)
Choline Chloride	D-(+)-sucrose	4:1	ChCl:suc (4:1)
Choline Chloride	D-(+)-sucrose	1:1	ChCl:suc (1:1)
Choline Chloride	D-(+)-xylose	2:1	ChCl:xyl (2:1)
Choline Chloride	D-(+)-xylose	3:1	ChCl:xyl (3:1)
Citric acid	D-(+)-sucrose	1:1	ca:suc (1:1)
Citric acid	D-(+)-glucose	1:1	ca:gluc (1:1)
D(+) Glucose	L-(+)-tartaric acid	1:1	gluc:ta (1:1)
choline chloride	*R*-(-)-mandelic acid	1:2	ChCl:ma (1:2)
(*R*,*S*)-(±)-menthol	ibuprofen	3:1	menthol:Ibu (3:1)

NADES rows: first 8; THEDES: last 2.

6.2.3. Water Content Determination

The water content of the samples and all the DES prepared was determined by Karl-Fischer titration using an 831 KF Coulometer with a generator electrode without diaphragm. The results presented are the average of a minimum of three measurements.

6.2.4. Sample Preparation

In a first approach, to determine the foaming ability of NADES, the polymeric blend SPCL was doped with 10 wt% of each NADES, and homogeneous mixtures of SPCL-NADES were obtained. The mixtures were then submitted to compression moulding. Disc shaped samples were prepared, using (12x2 mm) stainless steel rings as a mould, using a Moore Hydraulic press, at 80 °C, 8 MPa, for 15 min. A final homogeneous sample was obtained.

SPCL polymers doped with 10 and 30 wt% of menthol:ibuprofen (3:1) THEDES were prepared in the same manner, but at lower temperatures (ca. 40-50 °C).

6.2.5. Mechanical Tests

Mechanical analysis of the samples was performed using an INSTRON 5540 universal testing machine with a load cell of 1kN (Instron Int. Ltd., UK). The mechanical properties of the different SPCL-NADES systems were evaluated, in the tensile mode. Specimens of dimensions 60x1x3 mm (length x width x thickness) were used. The load was placed midway between the supports with a span (L) of 30 mm. The cross-head speed was 1:5 mm/min. For each condition, the specimens were loaded until core break. The results presented are the average of at least three measurements.

6.2.6. Supercritical fluid foaming

Samples of different SPCL-NADES and SPCL-THEDES were foamed with supercritical carbon dioxide (scCO$_2$). Samples were loaded into a high pressure vessel. CO$_2$ was then pumped into the vessel using a compressor (Newport Scientific Inc.), up to 20.0 MPa (pressurization takes ca. 10 minutes), at 40 °C. The pressure was controlled using a pressure transducer. The vessel was kept at those conditions for one hour, after which the system was slowly depressurized down to ambient pressure, at 0.67 MPa/min.

In the case where images of the pressurization and depressurization process were obtained, for samples of SPCL and SPCL+gluc:ta (1:1), a high pressure view cell with sapphire windows was used, to allow the visualization of the process. Images were collected after predetermined times. Samples were submitted to longer periods of foaming (90 minutes for SPCL, and 180 minutes for SPCL+gluc:ta).

6.2.7. SEM

The matrices obtained after SCF foaming were observed with a Leica Cambridge S360 scanning electron microscope. Cross-sections of the sample were observed after fracturing the samples with liquid nitrogen.

6.2.8. Micro-CT

The morphological structure of the samples was evaluated using a Skyscan 1702 (Skyscan, Belgium) with penetrative X-rays of 53 KeV and 189 µA, in high resolution mode with a pixel size of 11 µm and 1.5 seconds of exposure time. A CT analyser software (v1.5.1.5, SkyScan) was used to calculate the parameter images from the 2D images obtained. 2D images of the cross-sections were visualized using Data-Viewer software (v1.4.4 64-bit, Skyscan), and the 3D reconstructions were built using CTvox software (v2.3.0 r810, Skyscan).

6.2.9. DSC

The DSC analysis were performed with a Q2000 isothermal differential calorimeter (TA Instruments, Tzero™ DSC technology). The samples were packed in a TA aluminium pan (the set was not hermetically sealed to allow free water evaporation).

The DSC analysis of mandelic acid was carried out from -90 °C to 180 °C, at a rate of 10 °C/min. In the case of choline chloride, measurements were carried out between -90 °C and 120 °C, at a rate of 20 °C/min. In the case of the mixture ChCl:ma (2:1), a slower rate was used in order to register with more precision the alterations caused by the formation of the eutectic, and the DSC thermogram was obtained between -10 °C and 180 °C, with a rate of 1 °C/min.

In the case of menthol and ibuprofen, DSC data were collected between -90°C and 120 °C at a rate of 10 °C/min. In the case of the mixture menthol:ibu (3:1), the DSC analysis was performed between -90 °C and 100 °C, at a rate of 10 °C/min, as well as between -90 °C and 100 °C, but with a holding step at -20 °C for a period of 120 minutes (annealing) and then cooling down to -90 °C, followed by heating and cooling scans.

6.2.10. Controlled Release Tests

The release profile of the THEDES mentol:ibu (3:1) from the SPCL was studied after immersion in a phosphate buffer saline (PBS) solution at 37 °C, under stirring at 60 rpm. The concentration of ibuprofen in the buffer was measured by UV/Vis spectroscopy at 220 nm, in a Synergy HT from BIO-TEK microplate reader, using a 96 wells quartz microplate.

The PBS buffer was prepared from phosphate buffered saline tablets (Sigma), with the concentration 2.7 mM, and potassium chloride 137 mM, at pH 7.4, at 25 °C (these experiments were carried out in the partner institution ICVS/3B's).

6.3. Results

In the first part of this work, the ability of different NADES to enhance the SCF foaming process of SPCL was evaluated, as well as the ability to obtain homogeneous porous 3D structures.

This work comprises also the use of SCF foaming to impregnate THEDES in SPCL matrices, and their possible use for controlled drug release applications.

The NADES used in this work were prepared according to the literature [62], but it was observed that they presented a high water content, since some are highly hygroscopic. The percentage of water in each NADES was determined by Karl-Fischer titration and results are presented in Table 6.2.

The water content can influence the thermophysical properties of the DES, and when working with these solvents, one must previously know the amount of water present, in order to rationalize the results.

Table 6.2- Water content of all the DES prepared.

DES	Sample	Water content (wt%)
NADES	ChCl:ca (1:1)	7.7
	ChCl:suc (4:1)	8.1
	ChCl:suc (1:1)	6.4
	ChCl:xyl (2:1)	7.0
	ChCl:xyl (3:1)	5.6
	ca:suc (1:1)	6.4
	ca:gluc (1:1)	8.2
	gluc:ta (1:1)	7.5
THEDES	ChCl:ma (1:2)	4.3
	menthol:ibu (3:1)	0.11

6.3.1. Natural deep eutectic solvents as foaming enhancers

6.3.1.1. Mechanical Tests

Figure 6.1 presents the results obtained in the mechanical tests performed in tensile mode, showing the Young's modulus (green bars) and the elongation at break (blue symbols). The results obtained for SPCL doped with two ILs (used in work reported in Chapter 4), are included for comparison.

The mechanical response of SPCL doped with NADES shows that NADES lowers the Young's modulus and decreases the elongation at break relative to SPCL alone or SPCL doped with ILs. The addition of plasticizers increases intermolecular space between the polymeric chains, reducing the energy required for the chains' movement. This typically results in a

decrease of the Young's Modulus [177,178]. ILs have been reported to have this effect [179,180] and as seen in Figure 6.1, the results obtained with some of the NADES conform to that trend. On the other hand, the increased mobility of the polymer chains may allow for more ordered arrangements and an increase in the crystallinity of the polymer, thereby leading to a decrease in the elongation at break. All the NADES tested as well as [BMIM]Cl decrease to a higher or lower extent the elongation at break of SPCL, but [BMIM]Ac has the opposite effect.
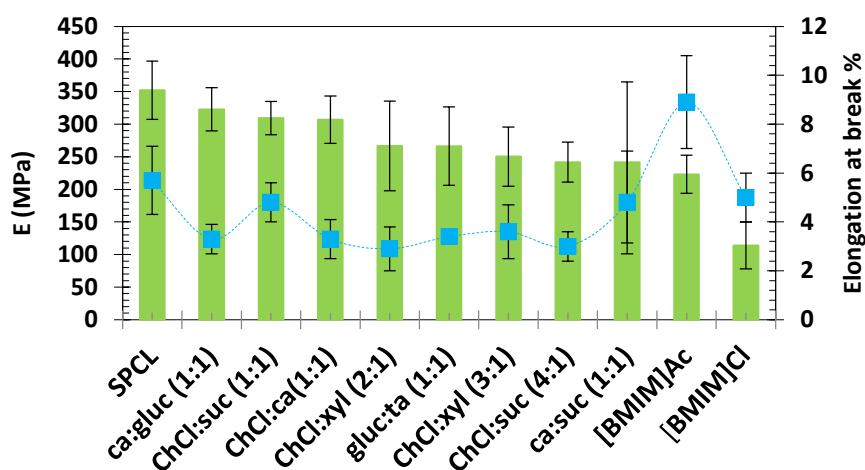
Figure 6.1- Young's modulus (bars) and elongation at break (symbols) for SPCL doped with various NADES. Results for undoped SPCL and SPCL doped with two imidazolium-based ILs are included for comparison.

6.3.1.2. Supercritical Fluid Foaming (SCF Foaming)

In order to illustrate the SCF foaming of SPCL and the effect of the presence of NADES, images were collected during pressurization and depressurization, using a high pressure view cell. Results are presented in Figures 6.2 and 6.3.

Pressurization
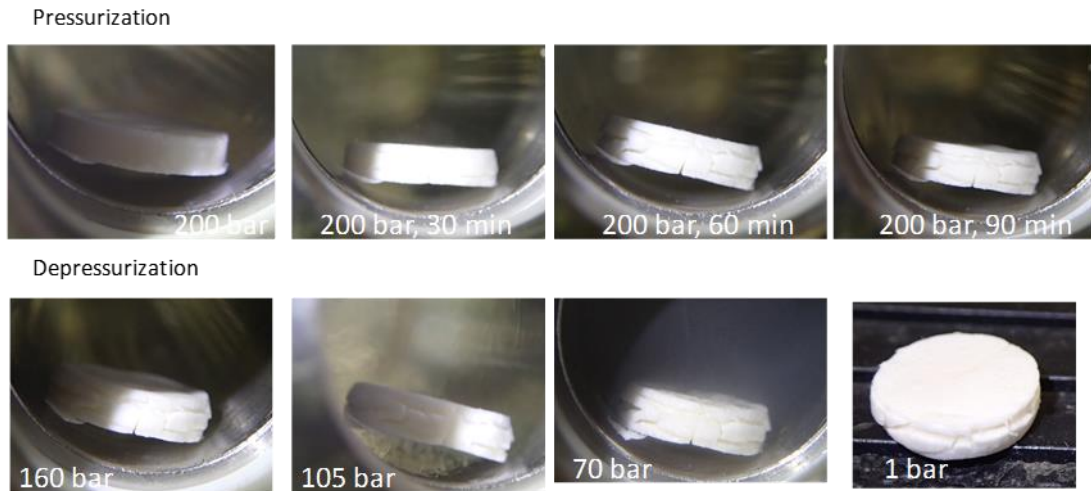
Depressurization

Figure 6.2- Effect of pressurization and depressurization on the SCF foaming process of SPCL.

In the SCF foaming process of SPCL without the presence of NADES, it is clear that the polymer sample cracks and that the foaming that may occur is not homogeneous.

Regarding the sample of SPCL doped with gluc:ta (1:1), shown in Figure 6.3, differences can be observed as soon as pressurization occurs. In the first images, the effect of the diffusion of scCO$_2$ into the bulk of the sample is clearly seen, accompanied by a change of the colour of the sample, as well as swelling. The main parameters to take into account in SCF foaming with CO$_2$ are the concentration of CO$_2$ in the polymer, which is closely related with the solubility of CO$_2$ in the polymer, and the depressurization rate[181].

The depressurization rate $\delta P/\delta t$ affects polymer relaxation and can lead to different foamed materials. It can be hypothesized that during CO$_2$ diffusion into the polymer matrix, the swelling occurs, depending on the time, temperature and pressure, while the formation of the 3D internal structure occurs during depressurization, intimately dependent on the depressurization rate.

Pressurization
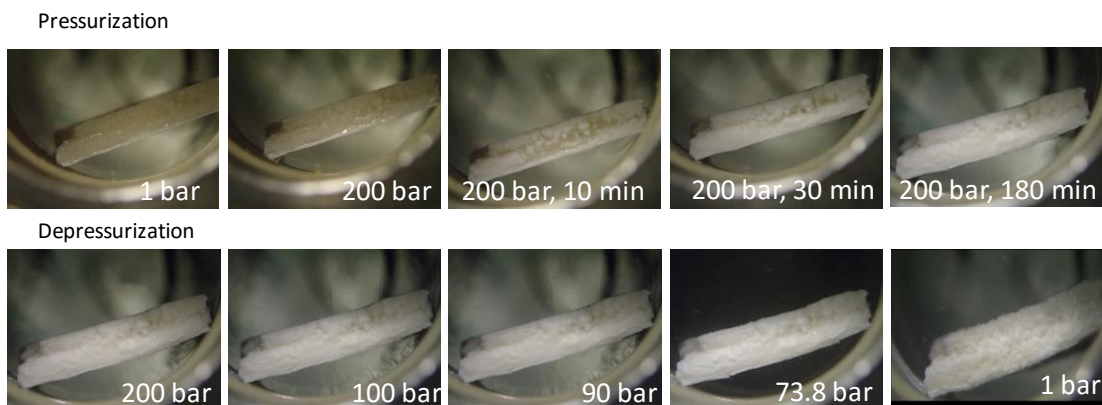
Depressurization

Figure 6.3- Effect of pressurization and depressurization on the SCF foaming process of SPCL doped with NADES gluc:ta (1:1).

6.3.1.3. SEM and micro-CT

The analysis performed by SEM and micro-CT allows the visualization of the foaming effects. Figure 6.4 shows that the porosity of the structures obtained depends on the NADES used for the doping of SPCL.

A more quantitative micro-CT analysis was also performed. This technique allows the visualization of the foamed structures in all three axes. The results are presented in Table 6.3. This analysis shows that NADES affect the SCF foaming of the SPCL polymer blend by increasing porosity and creating interconnected 3D structures. It also shows that the extent of these effects is highly dependent on the NADES used. An increase in porosity of up to 52% is observed for SPCL-ChCl:suc (1:1), which means that NADES may have even higher potential to promote SCF foaming than ILs. In fact, Duarte *et al.* [182]doped SPCL with 10% of [BMIM]Ac, conducted SCF foaming under the same operating conditions as used here and at different soaking times, but obtained a maximum porosity of 40% , lower than obtained using ChCl:suc (1:1) instead.
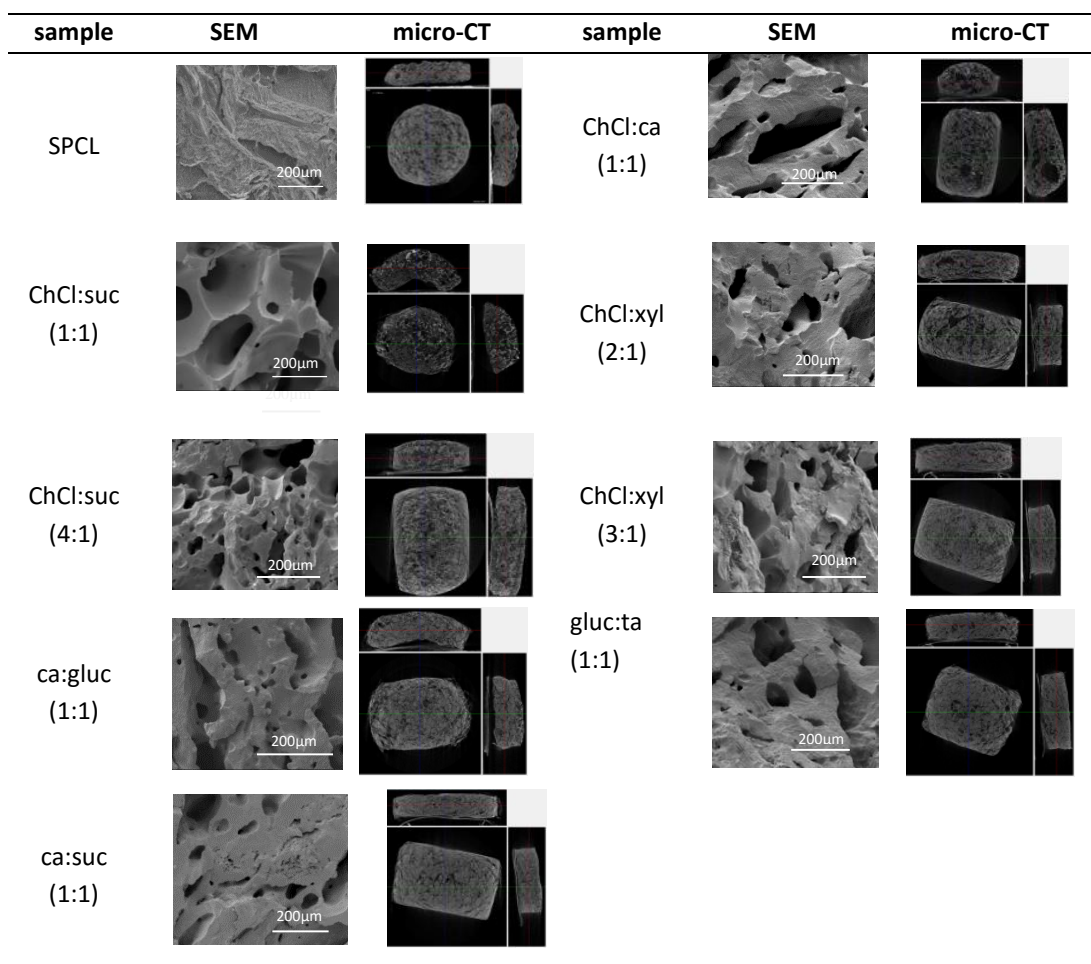
Figure 6.4- SEM and micro-CT images of the SPCL+NADES materials, after SCF foaming.

Table 6.3- Morphological parameters obtained for SPCL and SPCL+NADES foamed samples.

Sample	Porosity (%)	Mean pore size (μm)	Interconnectivity (%)
SPCL	4.1±0.9	-	-
ChCl:suc (1:1)	51.7±6.0	209±35	59.5±1.9
ChCl:suc (4:1)	8.2±1.3	129±4.9	5.0±1.0
ChCl:ca (1:1)	42.8±1.9	350±21	34.6±4.9
ChCl:xyl (2:1)	21.5±3.0	243±54	13.5±7.3
ChCl:xyl (3:1)	5.0±1.0	111±3	3±1.0
ca:gluc (1:1)	5.3±0.9	108±3	5.8±1.8
gluc:ta (1:1)	14.9±2.4	182±3	9.3±1.5
ca:suc (1:1)	4.7±1.1	166±39	7.2. ±3.5

As shown in Table 6.2, the NADES used in this work have an average of 7-8 % of water when prepared. It is important to discuss the possible influence of the water content in the SCF foaming, since it can have a plasticizing effect in the structures. If the data on water content and the extension of foaming are considered together, water appears not to have a relevant effect as a plasticizing agent. This is well illustrated by ca:gluc (1:1), which has a water content of 8.2 wt% but on the other hand promotes low porosity, low mean pore size and low interconnectivity. This indicates that in the SCF foaming process the NADES/SPCL interaction prevails over the effect of water.

Li *et al.* [183] reported the solubility of CO_2 in aqueous DES systems, in which the water content varied from 20 to 80%. In general, they observed that high concentrations of water have an anti-solvent effect, decreasing the solubility of CO_2 in the mixture.

There are, however, few works reporting the solubility of CO_2 in DES or eutectic mixtures [184]. Leron *et al.* [185] have obtained for the CO_2 solubility in ChCl:glycerol the value 2.6 mol CO_2/kg, at 6.0 MPa and 40 $^{\circ}$C. They also reported that the solubility of CO_2 in DES follows a linear relationship with pressure, and is inversely proportional to temperature, a trend that was already observed for CO_2-IL systems.

The solubility of CO_2 in the systems presented in this work has not yet been reported in the literature, but a rough comparison can be made with CO_2-IL systems. In the work presented in chapter 3 on the preparation of SPCL porous matrices using the [BMIM]Cl, it was shown that the extent of foaming is related with the sorption degree of CO_2 in the polymers, which is influenced by the solubility of CO_2 in the IL [138]. The CO_2-NADES systems seem to present a good solubility of CO_2, demonstrated by foaming enhancement.

6.3.2. Therapeutic deep eutectic solvents (THEDES)

Deep eutectic mixtures of bioactive and therapeutic compounds were also prepared in this work, based on the reports of Stott *et al.* [45] and Carriazo *et al.* [174]. The resulting mixtures were termed therapeutic deep eutectic solvents (THEDES). A schematic of the preparation of THEDES is depicted in Figure 6.5.
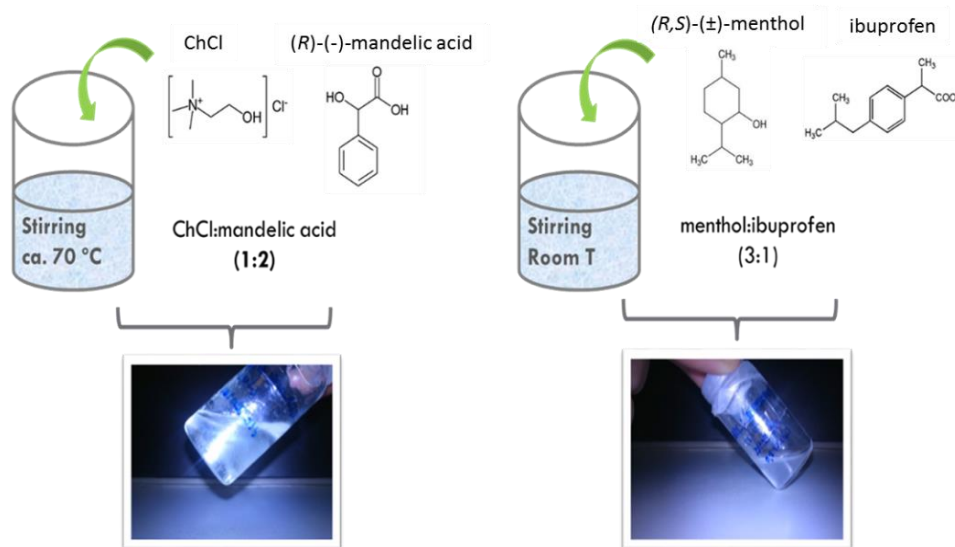
Figure 6.5- Schematic of the preparation of ChCl:ma (1:2) and menthol:ibuprofen (3:1) THEDES. ChCl:ma is liquid above ca. 70 °C and menthol:ibu (3:1) is liquid at room temperature.

6.3.2.1. Thermal behaviour of THEDES

The THEDES composed of ChCl and mandelic acid (1:2) was homogeneous, but it was only liquid above 70 °C. In order to characterize the thermal behaviour of this THEDES, a DSC analysis was performed, for both the pure starting compounds and the resulting THEDES. It can be observed that the thermal behaviour of the ChCl:ma THEDES is very different from that of the individual components.

In the thermogram of ChCl (Figure 6.6), the main thermal events that can be observed are melting and crystallization. The melting of ChCl is located between 80 °C (first heating scan, run1) and 89 °C (subsequent heating scans). ChCl is a highly hydrophilic compound, and because of that, the plasticization effect due to the presence of water is expected. The variation of melting and crystallization temperatures, as well as the differences in the base line, illustrate this effect.
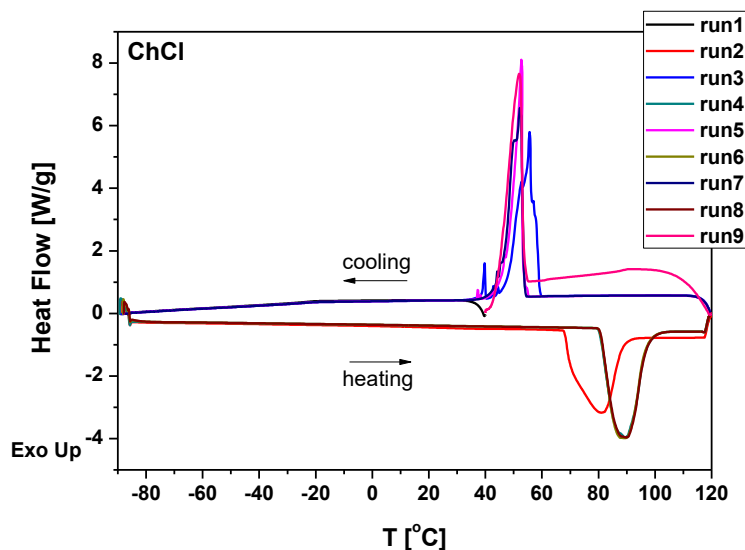
Figure 6.6- Thermogram of ChCl used in the preparation of ChCl:ma (1:2).

In the case of mandelic acid (Figure 6.7), the thermal events identified are melting, crystallization and glass transition. The temperatures associated with these transitions vary with the scans. T_m varies between 109 and 133 ^{o}C (first and last scan), whereas T_c varies between 117 and 85 ^{o}C. Also, in the first scan, no T_g is observed and in the last scan it is located at 28 ^{o}C.

Contrary to what was observed for ChCl, the behaviour of mandelic acid is not attributed to the plasticization effect of water. When the variations of T_m or T_g are caused by the presence of water in a sample (plasticization effect of water), this is also accompanied by variations in the base line of the thermogram, since the sample is losing mass during the thermal treatment.

In the case of mandelic acid, there are no visible alterations in the baseline of the tehrmogram, and the variations in the T_m are attributed to differences in the crystallinity of the sample during the thermal treatment. In the beginning, there is no amorphous region in the sample, which is well illustrated by the absence of a T_g in run2. In the subsequent scans there is an increase of the heat flux step associated with glass transition, indicating that the extent of the amorphous region is increasing. This varies concomitantly with the decrease of crystallinity. The last two scans (run 11 and 12) evidence this phenomenon very well. The material does not crystallize (run11), and subsequently a glass transition is clearly observed with no further melting (run 12). This means that at these conditions the material is completely amorphous. The other T_g's observed in runs 4, 6, 8 and 10 refer to semi-crystalline mandelic acid.
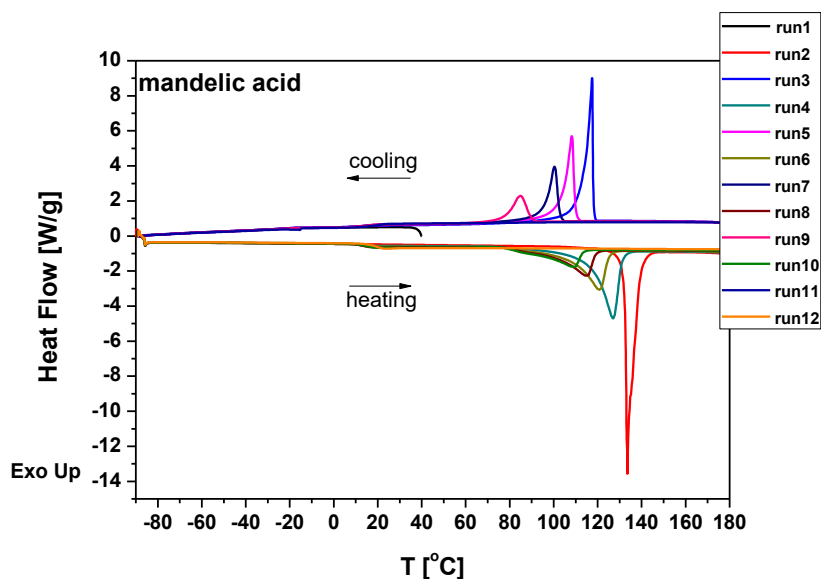
Figure 6.7- DSC thermogram of mandelic acid used in the preparation of ChCl:ma (1:2).
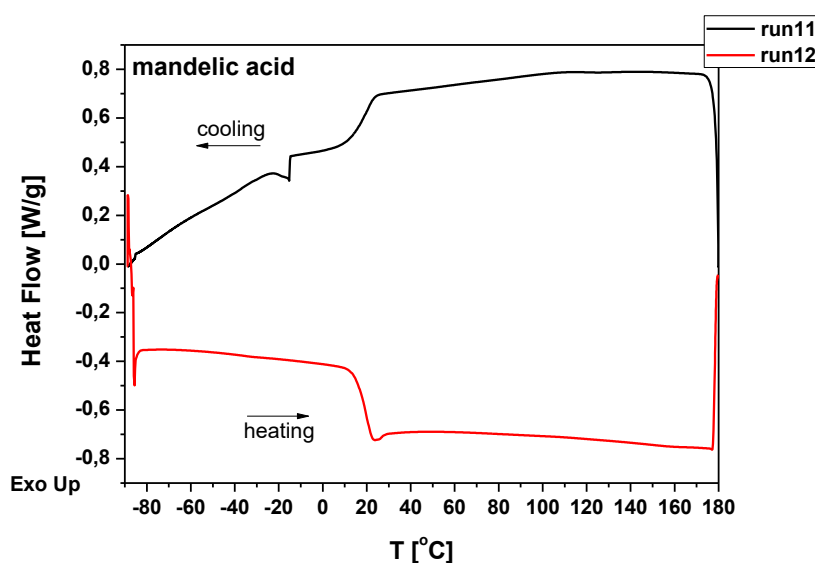
Figure 6.8- Detail of the DSC thermogram of mandelic acid, showing run11 and run12.

The thermogram of ChCl:ma (1:2) is presented in Figure 6.9. It is clear that the thermal behaviour of ChCl:ma (1:2) is different from that of the individual components. The melting occurs at temperatures between 78 and 79 °C, and crystallization between 16 and 19 °C (first and last scan values), which are different from the values for both individual components.

The different shape of the crystallization peak in Figure 6.9 is attributed to the ChCl component, and is reported as a phenomenon of the sample being self-heating during the crystallization process, due to the fact that is a highly energetic process [186].
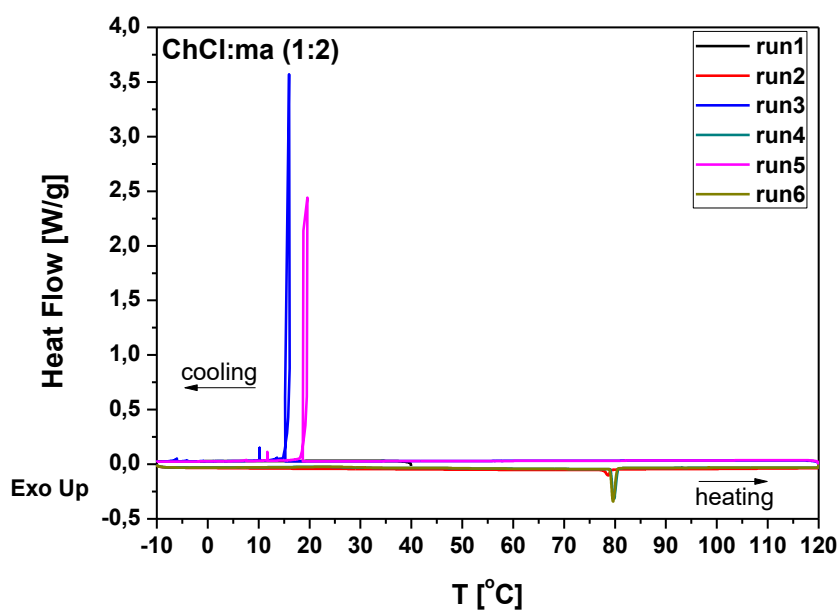
Figure 6.9- DSC thermogram of THEDES ChCl:ma (1:2).

A similar DSC analysis was performed for menthol:ibuprofen (3:1)THEDES.

The thermogram of menthol (Figure 6.10) shows two asymmetric peaks located at 29 and 35 °C attributed to melting. These values are in good agreement with data from literature [187]. The existence of two melting peaks is attributed to the existence of two different polymorphs of racemic menthol – α and β – as reported by Corvis *et al.* [187].

The crystallization peak in the first scan (run 1), is located at 16 °C, and T_c of the subsequent scans is located at 6 °C. This is probably related with the fact that crystallization is a kinetic event, and that in run 1 the starting temperature (40 °C) is different than that of the subsequent runs (120 °C).

In the thermogram of ibuprofen (Figure 6.11), in the first heating scan (run2) melting is observed. A heat flux discontinuity, attributed to the glass transition, is observed at 77 °C (T_m) which is in good agreement with the literature [154]. In this scan, and in the subsequent scans, no other thermal events are detected, with the exception of a heat flux step attributed to a glass transition with T_g located at -41 °C. This means that the sample becomes amorphous after heating to 120 °C.
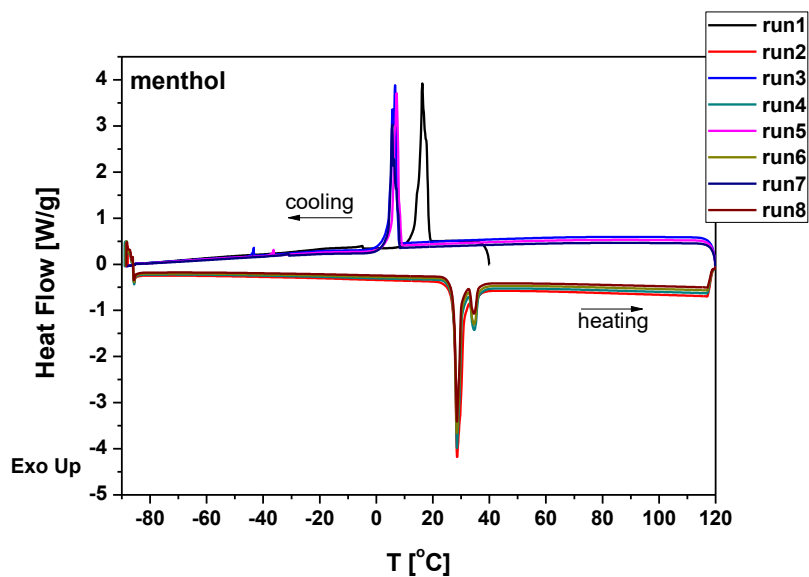
Figure 6.10- DSC thermogram of menthol used in the preparation of menthol:ibu (3:1).
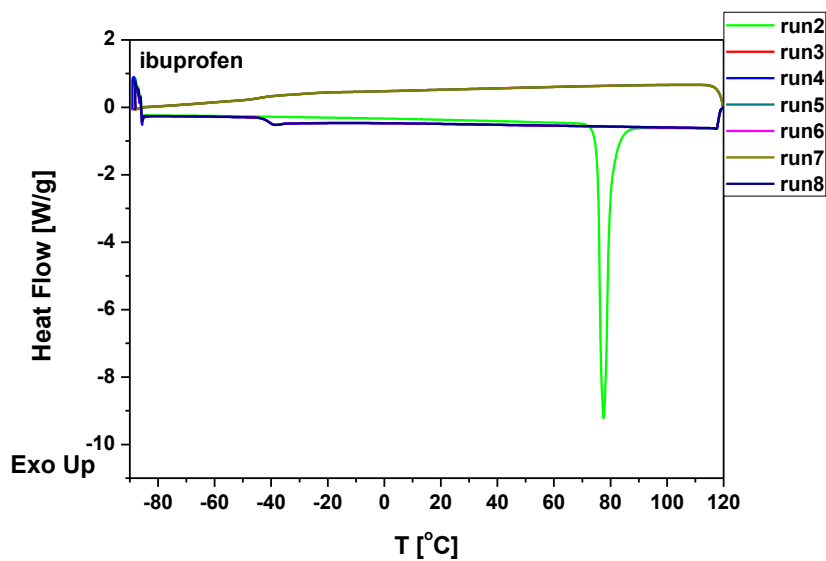
Figure 6.11- DSC thermogram of ibuprofen used in the preparation of menthol:ibu (3:1).

From the thermograms for menthol:ibu (3:1), shown in Figure 6.12, of, it is clear that the thermal behaviour of the THEDES is different from the behavior of the individual components. The THEDES was analysed before and after suffering annealing.
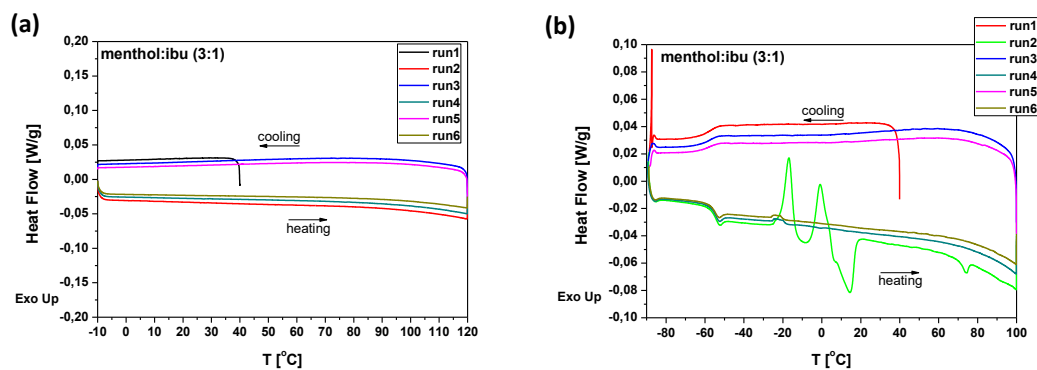
Figure 6.12- DSC thermogram of menthol:ibu (3:1) THEDES before annealing **(a)** and after annealing **(b)**.

Figure 6.11 (a) shows there are no thermal events in the temperature range between -10 and 120 °C. However, after submitting the THEDES to annealing (see experimental for details), the thermal behaviour is very different (Figure 6.12 (b)).

After annealing at -20 °C for 120 minutes, a T_g located at -53 °C is observed. Two crystallization events can also be observed, with T_c at -17 and -1 °C, resulting from "cold crystallization process" (*see chapter 5*), which are attributed to the presence of racemic menthol. The melting located at 14 °C is also attributed to menthol. T_m located at 74 °C is attributed to ibuprofen. These findings indicate that after annealing the THEDES is not totally amorphous, and the conditions at which relevant events occur suggest the presence of some crystallinity attributed to both of its components. However, if menthol:ibu (3:1) THEDES is afterwards heated to 120 °C, it becomes amorphous, as seen in subsequent scans in Figure 6.11 (b) where there are no thermal events registered by DSC, apart from the glass transition.

These DSC experiments also provide evidence that there are interactions established between the two components of ChCl:ma (1:2) and menthol:ibuprofen (3:1), as manifested in T_g, T_m and T_c values that are different from the ones obtained for menthol and for ibuprofen.

6.3.2.2. SEM and Micro-CT of foamed SPCL doped with THEDES

The foaming methodology that was used in this work has been used previously in the foaming of polymeric blends doped with ILs [82,138]. The conditions used for the SCF foaming process were 20.0 MPa, 40 °C, 1 hour pressurization, followed by slow depressurization.

To study the effects of SCF foaming on the morphology of SPCL blends doped with the two THEDES, SEM and micro-CT experiments were performed.

In Figure 6.9, SEM micrographs of SPCL doped wth ChCl:ma (1:2) and with menthol:ibu (3:1), before and after foaming, are presented. By looking at Figure 6.4, for undoped SPCL, and Figure 6.13, in which pores are clearly visible, it can be concluded that THEDES act as foaming enhancers.

Micro-CT analysis was also performed for SPCL doped with menthol:ibu (3:1), and morphological parameters,were obtained (Figure 6.14 and Table 6.4). The porosity is higher when compared to undoped SPCL (Table 6.3), and increases with the increase in the amount of THEDES. In the same manner as with ILs, this foaming enhancement caused by the presence of

THEDES is thought to be related with the higher solubility of CO_2 in THEDES, causing a more extensive foaming effect.
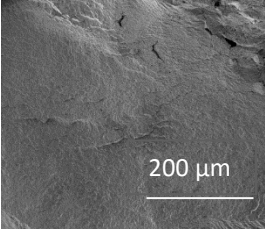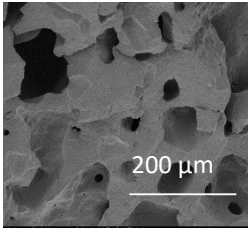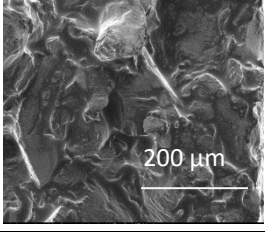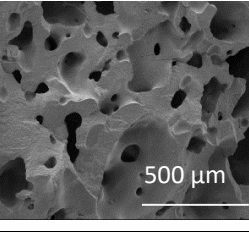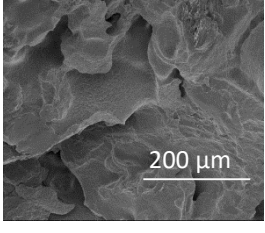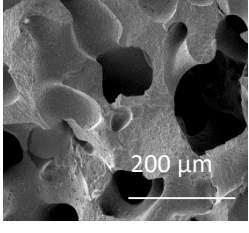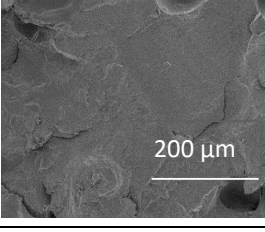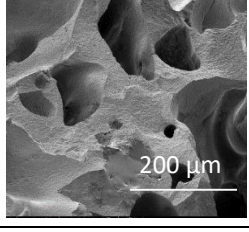
THEDES	wt %	No foaming	Foaming
ChCl:ma	10		
	30		
menthol:ibu	10		
	30		

Figure 6.13- SEM micrographs of the SPCL samples doped with different amounts of ChCl:mandelic acid and menthol:ibuprofen THEDES in different wt% amounts, before and after the foaming process. The micrograph of SPCL foamed with 30 % of ChCl:ma (1:2) has a different magnification, as indicated..

10% menthol:ibuprofen　　　　**30% menthol:ibuprofen**
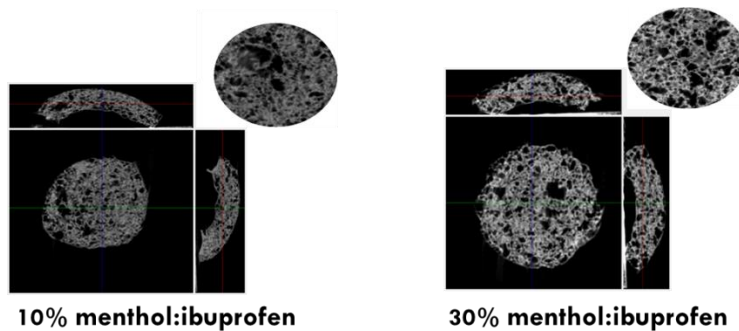
Figure 6.14- Micro-CT 2D images of the cross section of SPCL foamed samples, doped with 10 and 30% wt% of menthol:ibu (3:1).

Table 6.4- Micro-CT results for SPCL samples doped with different amounts (% w/w) of menthol:ibu (3:1), and submitted to SCF foaming.

Samples	Porosity (%)	Mean pore size (µm)	Interconnectivity (%)
10% menthol:ibuprofen	28.1±2.1	157±11	27.7±9.9
30% menthol:ibuprofen	37.7±2.0	188±12	15.1±2.4

6.3.2.3. Controlled Release tests

In addition to having a foaming enhancer effect on SPCL polymeric blends, the doping with DES (both NADES and THEDES) and processing with scCO$_2$ can result in the impregnation of the polymeric material. I.e. the presence of DES is not only important in the creation of a porous structure, as shown by the results above, but the DES can also be entrapped within the porous material.

Given that the DES can have therapeutic activity (THEDES), the creation of a sustained drug delivery system can be achieved, where the polymer acts as a biocompatible carrier.

In order to determine if the THEDES were still present in the SPCL after foaming, and if a controlled release system was obtained, controlled release tests of the THEDES menthol:ibu (3:1) were carried out. Figure 6.15 shows the results obtained for foamed SPCL doped with 10 and 30 wt% of menthol:ibu (3:1).

The fact that the presence of THEDES is detected in the controlled release tests shows that the impregnation in the SPCL matrix, using SCF foaming, is successful. However, for the first 4 hours, the results only show very subtle differences between SPCL doped with 10 or 30 wt% of THEDES. This is also observed for the foamed and not foamed samples. Also, it is observed that after 72 hours, 100% of release of ibuprofen is attained.

The release of ibuprofen is relatively fast, and if the first period of time is analysed (insets in Figure 6.11), almost 50% of the total amount of ibuprofen is released into the medium after 4 hours, and only after that a controlled release is observed.

The reason for this behaviour could rely on the preparation of the sample. When the polymer is doped with THEDES and then submitted to compression moulding, heterogeneous samples can be formed, where the amount of THEDES doped in the SPCL may not be evenly distributed. It is possible that THEDES is only on the surface of SPCL, which may lead to low amounts of menthol:ibu (3:1) impregnated in SPCL. The optimization of the preparation of SPCL+THEDES samples should be an important parameter to control when developing these materials. In this respect, the sintering method might be a good alternative for preparing these impregnated polymers.
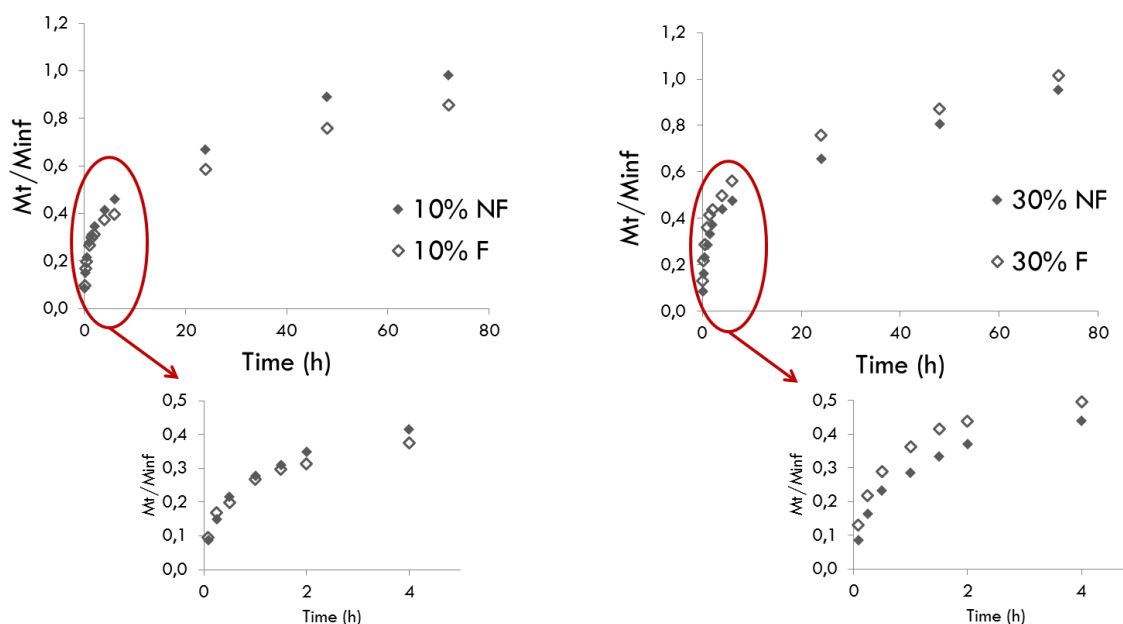
Figure 6.15- Controlled release profile of ibuprofen from SPCL matrices doped with 10 and 30 wt% of menthol:ibu (3:1), foamed (F) and not foamed (NF).

Although the controlled release of menthol:ibu (3:1) needs optimization, it is still possible to model its diffusion kinetics with the obtained results. The knowledge of the mass transport mechanisms and the kinetics of the drug release are essential for the design of new delivery systems.

From Fick's law of diffusion (*equation 2.10, chapter 2*) an equation can be derived, which models the drug release mechanism, considering that diffusion is the dominating mass transport mechanism and the drug release is diffusion-controlled. Nonetheless, a merely Fickian diffusion is hardly ever the case, as the water uptake of the matrices may also play an important role in the release profile of the active compound. An heuristic equation can be applied in situations of release processes, which fall between the Fickian diffusion and the zero-order release kinetics (i.e, when the drug release rate is independent of time) [104]. This power law reads (eq. 6.1)

$$\frac{M_{t_0}}{M_\infty} = k t^n \tag{6.1}$$

where M_{t_0} is the absolute cumulative amount of drug released at time t_0, M_∞ is the absolute cumulative amount of drug released at infinite time, k is a constant that incorporates structural and geometrical characteristics of the controlled release system, and n is the release exponent, indicative of the mechanism of the drug release, calculated from the slope of the curve [104]. Additionally, from the power law it is also possible to derive the kinetic constant of the system, which is characteristic of properties of the matrices prepared as it incorporates the structural and geometrical characteristics of the device. It is important to notice that this relationship is only valid for the first 60 % of the drug released.

Table 6.5 shows the results obtained for the release of ibuprofen from the SPCL system doped with 10 and 30 wt% of menthol:ibu (3:1), obtained from a linear regression (Figure 6.16) applied to the data presented in Figure 6.11.
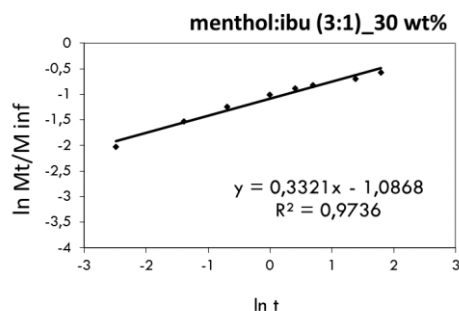
Figure 6.16- Example of a linear regression obtained for the data of the controlled release, and from which the parameters of the power law can be obtained. Data for SPCL doped with 30 wt% of menthol:ibu (3:1)).

Table 6.5- Results obtained for the modelling of the release of ibuprofen from foamed and non-foamed SPCL matrices, doped with 10 and 30 wt% of menthol:ibu (3:1) (NF stands for non-foamed, and F for foamed).

Sample	R^2	n	k
10 wt% NF	0.978	0.387	1.36
10 wt% F	0.969	0.326	1.40
30 wt% NF	0.989	0.281	1.08
30 wt% F	0.973	0.332	1.31

According to equation 6.1, n = 1.0, indicates that the drug release rate is independent of time (zero order kinetics) [104]. When the pure Fickian diffusion is the mechanism that governs the drug release, and in the case of slabs, the exponent n should be 0.5. Values of the diffusional exponent between 0.5 and 1 indicate that the drug release follows an anomalous transport, in which both Fickian diffusion and water uptake play an important role [104].

The power law release exponents calculated from our experiments (<0.5) indicate that the ibuprofen release from the SPCL scaffolds is not only governed by Fickian diffusion, but other diffusion mechanisms may be involved, such as anomalous transport. This behaviour is often called "less Fickian", and has already been observed in some cases of drug release form polymeric matrices [188,189].

In the case of the samples loaded with 30 wt% of THEDES, the foaming effect is more noticeable and the kinetic constant increases from 1 to 1.3 due to the variation of the porosity of the sample.

The porosity and mean pore size of the final porous structure are important parameters, because they influence the controlled release mechanism. This is intimately associated with the SCF foaming process and the foaming parameters, such as temperature, pressure, pressure drop and rate of depressurization, which will ultimately create more or less, and wider or smaller pores in SPCL, hence leading to different release profiles.

6.4. Conclusions

The work presented in this chapter shows one of the possible applications of DES, namely NADES and THEDES, as additives for the processing of natural based polymers by SCF foaming. This is a more sustainable and "green" methodology, which combines the benefits of DES and supercritical fluid technology.

As with ILs, and because NADES can be highly hydrophilic (especially those that contain ChCl), the effect of the water amount present in these solvents is an important parameter that must be controlled. However, for the SCF foaming process, the amount of water present in the NADES does not have a significant effect, interactions established in the polymer-NADES-scCO$_2$ system prevailing.

The presence of NADES in SPCL after doping has an effect on the mechanical properties of the polymer, lowering the Young's Modulus and the elongation at break, which is consistent with the interactions of SPCL and NADES increasing the mobility of the polymeric chains.

From the results obtained and discussed here, it is clear that NADES act as a SCF foaming enhancer for the SPCL polymer blend. In fact, the foaming of undoped SPCL occurs in a non-homogeneous manner, leading to reduced porosity. In the case of NADES composed by choline chloride and sucrose (1:1 molar ratio) the SCF foaming can lead up to a 52 % of porosity in the SPCL matrix. This foaming enhancement is higher than that obtained when doping with [BMIM]Ac, which makes NADES promising candidates for the SCF foaming of SPCL.

From the visual observation of the SCF foaming process, carried out in a view cell under high pressure, it is seen that the pressurization step is accompanied by a colour change of the polymer and some swelling (although not extensive).

In the work here presented, the ability to prepare DES with therapeutic properties (THEDES) and their potential use in SPCL foaming were also studied. The preparation of THEDES composed of ChCl and mandelic acid, and menthol and ibuprofen was achieved. The possibility to obtain previously crystalline or semi-crystalline drugs in the liquid form through formation of a eutectic is very advantageous, since it avoids possible polymorphism problems, and lends itself to applications of THEDES as therapeutic agents for transdermal treatments.

Furthermore, the use of THEDES as foaming enhancers of the SPCL polymeric blend proved successful, adding the advantage of impregnating the SPCL with a therapeutic agent or drug. In this manner, SPCL becomes a porous therapeutic agent carrier, and controlled drug release applications can be envisaged.

The controlled release of ibuprofen from SPCL doped with menthol:ibu (3:1) was tested, showing that although there is still a need for optimization of the drug delivery system, it holds a great potential.

The processing strategy here presented combines renewable and biodegradable materials and methodologies, opening doors for the fabrication of supported materials, whose applications can be modulated according to the eutectic solvent characteristics.

Chapter 7

Conclusions and Future Work

7.1. Conclusions and Future Work

The work presented in this thesis is focused on establishing new and more sustainable processing methodologies for natural based polymers. To that end, it is proposed to combine SCF technology with the use of ILs or DES.

The processing of natural based polymers is challenging and time consuming, and is normally carried out using highly toxic solvents and processes with a high energy input. To overcome these drawbacks, alternative processing methodologies were developed in this thesis. These alternatives are believed to be very relevant as drivers for the utilization of natural based polymers, thereby diminishing today's dependence on petroleum based polymers.

Starch and other aliphatic polyesters were the polymers selected in this work to validate the proposed processing methodologies. They combine key features for the fabrication of "greener" polymers, such as biodegradability, biocompatibility, and the fact that they are renewable and naturally abundant materials. Two different starch-based blends were used and processed through a foaming technique, using $scCO_2$ as a foaming agent.

Initially, the ability to produce porous structures by SCF foaming of a starch-based polymer blend was assessed. The polymer blends studied were composed by starch and poly(lactic acid) (PLA), and differed in the amount of starch: SPLA50 (with 50 wt% of starch) and SPLA70 (with 70 wt% of starch). Since the foaming effect of this blend was not expressive, an imidazolium based ionic liquid – [BMIM]Cl – was added as a foaming enhancer. The doping of SPLA with [BMIM]Cl proved to be effective, and porous structures were obtained with a substantial increase in porosity, as seen in micro-CT results.

The success of the SCF foaming process in the presence of the IL was attributed to the interactions established between starch and the IL, as evidenced by FTIR-ATR and DSC analysis. These interactions compete with interactions between the polymeric chains, which become weaker, leading to an increase in the mobility and flexibility of the SPLA structure, making the foaming process easier. It was also shown that the IL acts as a plasticizer for SPLA. This was also reflected in a lower crystallinity exhibited by SPLA matrices doped with IL.

The apparent sorption and desorption coefficients of $scCO_2$ in the SPLA-IL systems were also determined. For that purpose, sorption experiments were carried out under the same conditions as SCF foaming. It was observed that the foaming effect is highly dependent on the crystallinity of the polymeric blend and on the sorption coefficient. When the crystallinity is lower and IL is present, the apparent sorption coefficient is one order of magnitude higher than the value obtained for undoped samples. Ultimately this results in an enhanced SCF foaming effect.

The work presented in chapter 4 intended to give a more detailed description of materials composed by biopolymer blends and ILs, prepared via SCF foaming. In this case, a different polymer blend was used (SPCL), composed of starch and poly(ε-caprolactone), doped with [BMIM]Cl or with [BMIM]Ac.

The presence of IL proved to be essential to obtain foamed structures with the desired morphological characteristics. The interactions between starch and the IL were one of the reasons for the success of the foaming process, as evidenced by FTIR-ATR. An extensive DSC

analysis was carried out, which confirmed this interaction, since the thermal characteristics attributed to the PCL component do not seem to undergo alterations upon IL doping and SCF foaming.

In addition, DRS experiments were performed to complement the DSC results and also assess the conductivity of the polymer-IL composites prepared. DRS revealed subtle differences in the mobility of the different materials, and confirmed a mobility enhancement of SPCL doped with IL compared to SPCL alone.

These data also showed that the conductivity depends mostly on the IL. SPCL doped with [BMIM]Cl showed conductivity values comparable to those of pure IL, but with an enhanced stability. This can open doors to potential applications of these materials as bio-based, self-supported, polymeric, conductive systems, where SPCL could serve as a carrier for a conductive specie, providing enhanced stability for the IL conductive performance.

As a general conclusion of the first part of this work, it can be said that ILs act as efficient plasticizers and foaming enhancers for SPLA and SPCL, enabling the production of porous materials by SCF foaming. These materials were initially envisaged for biomedical applications, in which case the removal of IL from the material is needed, due to the possible toxicity of the ILs used. This can be performed by solvent exchange methods. On the other hand, these materials can be used as prepared, for electrochemical purposes.

Although ILs are considered by many authors as sustainable, or even "green" solvents, this label is now subject to some controversy. Although in general ILs have negligible vapour pressure, the term green should not be attributed to all ILs. And even though ILs can be recycled, their synthesis is often not sustainable, since it involves the use of a large amount of organic solvents, most of them toxic and harmful to the environment. The manufacturing of ILs is very expensive, which for large applications can be a major drawback. Also, ILs have been developed to serve different purposes and their physicochemical properties can vary widely according to their composition, which is the same for their toxicity and biodegradability. ILs must not be termed "green" solvents just because they are ILs, but rather if they indeed deserve that label.

With the development of the third generation of ILs, exhibiting biodegradability and even biocompatibility, DES began to gain attention, and to replace ILs in applications where ILs used to be the solvents of choice.

In the work presented in chapter 5, DES composed of natural occurring components such as sugars and organic acids, termed NADES, were studied. NADES share many of the characteristics of ILs, but are easier to prepare, biodegradable, in most cases biocompatible, and derive from renewable resources. They can be viable and cheaper alternatives when designing more sustainable processes.

For a better understanding of these solvents and of their potential applications, their characterization in terms of density, viscosity, polarity, conductivity and thermal behaviour was carried out. The NADES presented in this study are composed of ChCl and organic acids and sugars, all primary metabolites.

It was observed that water content had significant effects on the properties of NADES, and for this reason, all the results obtained should be rationalized taking into account the amount of water present.

All the NADES presented in chapter 5 are considered to be glass formers, as seen by DSC and POM results. Some NADES exhibit unusual thermal behaviour, showing events of melt

crystallization and cold crystallization (e.g. ChCl:xylose (3:1)). The presence of ChCl was shown to influence the crystallization events.

The DRS study of the NADES presented in chapter 5 shows that they have conductivities close to those of ILs, thereby unveiling possible applications in the electrochemistry area. Furthermore, in some cases like ChCl:xyl (3:1), ca:suc (1:1) and ca:gluc (1:1), the dependence of the conductivity on temperature could be fitted by the Vogel-Fulcher-Tammann (VFT) equation, and the association of the conductivity mechanism with the phenomenon of dynamic glass transition was established.

A greater amount of knowledge on the properties and characteristics of NADES was the starting point for the rationalization of their potential applications. In this work, the main goal was to replace the use of ILs in the SCF foaming of SPCL.

This work was presented in chapter 6, where several NADES proved to be very successful SCF foaming enhancers. In fact, replacing ILs with NADES has led to porous polymeric structures with enhanced characteristics, namely porosity values up to 52%. In our opinion, the foaming effect is directly related with the interactions established within the polymer-NADES-scCO$_2$, and thus a detailed study of this system should be performed, using high pressure FTIR methodologies and possibly high pressure NMR. One other reason for the SCF foaming enhancement by NADES is that like ILs, NADES can dissolve high amounts of CO$_2$. A more detailed study on the solubility of CO$_2$ in NADES should be carried out, and data on the gas-liquid phase equilibria of NADES-scCO$_2$ systems should be generated. This will allow better understanding of the SCF foaming process using NADES.

The presence of NADES, like in the case of ILs, changes the mechanical properties of SPCL (lower Young's modulus and elongation at break).

The preparation of DES can also be used to transform crystalline compounds into liquids (amorphous materials) through a decrease in melting point, resulting from the interactions that characterize a eutectic system. This can prove a very useful strategy when dealing with therapeutic compounds (e.g. active pharmaceutical ingredients, APIs), which sometimes see their bioactive activity and application diminished by polymorphism.

DES with therapeutic properties – THEDES – and their potential use in SPCL foaming were also studied by combining ChCl with mandelic acid (an antibacterial compound), and menthol (anaesthetic and skin permeation enhancer) with ibuprofen (model non-steroidal, anti-inflammatory drug, NSAID). The THEDES obtained showed differences in thermal behaviour relative to the thermal behaviour of the individual components. The THEDES composed of ChCl and mandelic acid is liquid above 70 °C and the one composed of menthol and ibuprofen is liquid, at least from 0 to 120 °C. This latter THEDES can have potential uses in topical and transdermal applications.

Furthermore, the use of THEDES as foaming enhancers of the polymeric blend SPCL proved successful, leading to polymers s with 40 % porosity and good interconnectivity, adding the advantage of impregnating the SPCL with a therapeutic agent or drug. In this manner, SPCL becomes a porous carrier, and controlled drug release applications can be envisaged. The controlled release behaviour was also studied applying a power law to describe the release kinetics. The results indicate a release mechanism that is not only governed by Fickian diffusion, but other diffusion mechanisms such as anomalous transport.

DES have proven to be versatile solvents with a minimum environmental impact, and the determination of their physicochemical properties will surely be a field in expansion in the

coming years. Like ILs, DES can be prepared with different compositions to meet different applications, which makes them also "tailor-made" solvents.

The processing methodology presented here, combining the use of $scCO_2$ with an IL or DES, has also proved to be efficient for the foaming of natural based polymers. It is a versatile approach, since the preparation of different materials is possible, such as conducting materials and materials for the biomedical field.

The work presented in this thesis joins raw materials, solvents and processing methods that do indeed embody the green chemistry philosophy, putting forward a truly sustainable, versatile process holding great potential.

References

1.   ModernPlastics & Harper, C. A. *Modern Plastics Handbook*. (2000).

2.   Baird, D. G. & Collins, D. I. *Polymer Processing: Principles and Design*. (2014).

3.   American Chemical Society National Historic Chemical Landmarks. Bakelite: The World's First Synthetic Plastic. at <http://www.acs.org/content/acs/en/education/whatischemistry/landmarks/bakelite.html (accessed September 16, 2014).>

4.   Storz, H. & Vorlop, K. Bio-based plastics : status , challenges and trends. *Appl Agric For. Res* **4,** 321–332 (2013).

5.   Jeon, B. *et al.* Microcellular foam processing of biodegradable polymers — review. *Int. J. Precis. Eng. Manuf.* **14,** 679–690 (2013).

6.   Plastic waste. at <http://ec.europa.eu/environment/waste/plastic_waste.htm>

7.   Babu, R. P., O'Connor, K. & Seeram, R. Current progress on bio-based polymers and their future trends. *Prog. Biomater.* **2,** 8 (2013).

8.   Lu, D. R. Starch-based completely biodegradable polymer materials. *eXPRESS Polym. Lett.* **3,** 366–375 (2009).

9.   Mohanty, A. K., Misra, M. & Hinrichsen, G. Biofibres , biodegradable polymers and biocomposites : An overview. *Maromol. Mater. Eng.* **276/277,** 1–24 (2000).

10.   Zhang, Y., Rempel, C. & Liu, Q. Thermoplastic starch processing and characteristics-a review. *Crit. Rev. Food Sci. Nutr.* **54,** 1353–70 (2014).

11.   wt0813c. *Cruiziat, P. and Richter, H. 2006. Essay 4.2: The cohesion–tension theory at work. Plant Physiology, Fifth Edition Online. <http://www.plantphys.net> Accessed 12/09/2014*

12.   Duarte, A. R. C., Silva, S. S., Mano, J. F. & Reis, R. L. Ionic liquids as foaming agents of semi-crystalline natural-based polymers. *Green Chem.* **14,** 1949 (2012).

13.   Xiao, L., Wang, B., Yang, G. & Gauthier, M. in (2006).

14.   Garlotta, D. A Literature Review of Poly (Lactic Acid). *J. Polym. Environ.* **9,** 63–84 (2002).

15.   Dorozhkin, S. V. Calcium orthophosphate-based biocomposites and hybrid biomaterials. *J. Mater. Sci.* **44,** 2343–2387 (2009).

16.   Woodruff, M. A. & Hutmacher, D. W. The return of a forgotten polymer—Polycaprolactone in the 21st century. *Prog. Polym. Sci.* **35,** 1217–1256 (2010).

17. Del Monte, F., Carriazo, D., Serrano, M. C., Gutiérrez, M. C. & Ferrer, M. L. Deep eutectic solvents in polymerizations: a greener alternative to conventional syntheses. *ChemSusChem* **7,** 999–1009 (2014).

18. Anastas, P. T. & Warner, J. C. *Green chemistry: Theory and practice*. (2000).

19. Trost, B. . The atom economy --a search for synthetic efficiency. *Science (80-.).* **254,** 1471–1477 (1991).

20. Sheldon, R. A. Atom efficiency and catalysis in organic synthesis. *Pure Appl. Chem.* **72,** 1233–1246 (2000).

21. Constable, D. J. C., Curzons, A. D. & Cunningham, V. L. Metrics to 'green' chemistry-which are the best? *Green Chem.* **4,** 521–527 (2002).

22. http://www.epa.gov/nrmrl/std/lca/lca.html. at <http://www.epa.gov/nrmrl/std/lca/lca.html>

23. Plechkova, N. V & Seddon, K. R. Applications of ionic liquids in the chemical industry. *Chem. Soc. Rev.* **37,** 123–50 (2008).

24. Earle, M. J. & Seddon, K. R. Ionic liquids . Green solvents for the future. *Pure Appl. Chem.* **72,** 1391–1398 (2000).

25. Rebelo, L. P. N., Canongia Lopes, J. N., Esperança, J. M. S. S. & Filipe, E. On the critical temperature, normal boiling point, and vapor pressure of ionic liquids. *J. Phys. Chem. B* **109,** 6040–3 (2005).

26. Nemoto, F., Kofu, M. & Yamamuro, O. Thermal and Structural Studies of Imidazolium-Based Ionic Liquids with and without Liquid-Crystalline Phases: The Origin of Nanostructure. *J. Phys. Chem. B* **119,** 5028–5034 (2015).

27. Sheldon, R. Catalytic reactions in ionic liquids. *Chem. Commun.* 2399–2407 (2001). doi:10.1039/b107270f

28. Sheldon, R. a., Lau, R. M., Sorgedrager, M. J., van Rantwijk, F. & Seddon, K. R. Biocatalysis in ionic liquids. *Green Chem.* **4,** 147–151 (2002).

29. Habulin, M., Primožič, M. & Knez, Ž. in *Application of Ionic Liquids in Biocatalysis* (2001).

30. Armand, M., Endres, F., MacFarlane, D. R., Ohno, H. & Scrosati, B. Ionic-liquid materials for the electrochemical challenges of the future. *Nat. Mater.* **8,** 621–9 (2009).

31. Vidinha, P. *et al.* Ion jelly: a tailor-made conducting material for smart electrochemical devices. *Chem. Commun.* 5842–4 (2008). doi:10.1039/b811647d

32. Cevasco, G. & Chiappe, C. Are ionic liquids a proper solution to current environmental challenges? *Green Chem.* **16,** 2375 (2014).

33. Winterton, N. Solubilization of polymers by ionic liquids. *J. Mater. Chem.* **16,** 4281 (2006).

34.   Swatloski, R. P., Spear, S. K., Holbrey, J. D. & Rogers, R. D. Dissolution of Cellose with Ionic Liquids. *J. Am. Chem. Soc.* 4974–4975 (2002).

35.   Xu, A., Zhang, Y., Lu, W., Yao, K. & Xu, H. Effect of alkyl chain length in anion on dissolution of cellulose in 1-butyl-3-methylimidazolium carboxylate ionic liquids. *J. Mol. Liq.* **197,** 211–214 (2014).

36.   Lindman, B., Karlström, G. & Stigsson, L. On the mechanism of dissolution of cellulose. *J. Mol. Liq.* **156,** 76–81 (2010).

37.   Barthel, S. & Heinze, T. Acylation and carbanilation of cellulose in ionic liquids. *Green Chem.* **8,** 301 (2006).

38.   Hanke, C. G., Atamas, N. a. & Lynden-Bell, R. M. Solvation of small molecules in imidazolium ionic liquids: a simulation study. *Green Chem.* **4,** 107–111 (2002).

39.   Domínguez de María, P. & Maugeri, Z. Ionic liquids in biotransformations: from proof-of-concept to emerging deep-eutectic-solvents. *Curr. Opin. Chem. Biol.* **15,** 220–5 (2011).

40.   Earle, M. J. *et al.* The distillation and volatility of ionic liquids. *Nature* **439,** 831–4 (2006).

41.   Deetlefs, M. & Seddon, K. R. Assessing the greenness of some typical laboratory ionic liquid preparations. *Green Chem.* **12,** 17 (2010).

42.   Pham, T. P. T., Cho, C.-W. & Yun, Y.-S. Environmental fate and toxicity of ionic liquids: a review. *Water Res.* **44,** 352–72 (2010).

43.   Abbott, A. P., Capper, G., Davies, D. L., Rasheed, R. K. & Tambyrajah, V. Novel solvent properties of choline chloride/urea mixtures. *Chem. Commun. (Camb).* 70–1 (2003). at <http://www.ncbi.nlm.nih.gov/pubmed/12610970>

44.   Zhang, Q., De Oliveira Vigier, K., Royer, S. & Jérôme, F. Deep eutectic solvents: syntheses, properties and applications. *Chem. Soc. Rev.* **41,** 7108–46 (2012).

45.   Stott, P. W., Williams, a C. & Barry, B. W. Transdermal delivery from eutectic systems: enhanced permeation of a model drug, ibuprofen. *J. Control. Release* **50,** 297–308 (1998).

46.   Naser, J., Mjalli, F., Jibril, B., Al-Hatmi, S. & Gano, Z. Potassium Carbonate as a Salt for Deep Eutectic Solvents. *Int. J. Chem. Eng. Appl.* **4,** 114–118 (2013).

47.   Morrison, H. G., Sun, C. C. & Neervannan, S. Characterization of thermal behavior of deep eutectic solvents and their potential as drug solubilization vehicles. *Int. J. Pharm.* **378,** 136–139 (2009).

48.   Dai, Y., van Spronsen, J., Witkamp, G.-J., Verpoorte, R. & Choi, Y. H. Ionic liquids and deep eutectic solvents in natural products research: mixtures of solids as extraction solvents. *J. Nat. Prod.* **76,** 2162–73 (2013).

49. Tang, B., Park, H. E. & Row, K. H. Simultaneous Extraction of Flavonoids from Chamaecyparis obtusa Using Deep Eutectic Solvents as Additives of Conventional Extractions Solvents. *J. Chromatogr. Sci.* **53,** 836–840 (2015).

50. Zdanowicz, M. & Spychaj, T. Ionic liquids as starch plasticizers or solvents. *Polimery* **56,** 861–864 (2011).

51. Gill, I. & Vulfson, E. Enzymic catalysis in heterogeneous eutectic mixtures of substrates. *Trends Biotechnol.* **12,** 118–122 (1994).

52. Lopezfandino, R., Gill, I. & Vulfson, E. Protease-catalyzed synthesis of oligopeptides in heterogeneous substrate mixtures. *Biotechnol. Bioeng.* **43,** 1024–1030 (1994).

53. Clouthier, C. M. & Pelletier, J. N. Expanding the organic toolbox: a guide to integrating biocatalysis in synthesis. *Chem. Soc. Rev.* **41,** 1585–605 (2012).

54. Durand, E., Lecomte, J. & Villeneuve, P. Deep eutectic solvents: Synthesis, application, and focus on lipase-catalyzed reactions. *Eur. J. Lipid Sci. Technol.* **115,** 379–385 (2013).

55. Verevkin, S. P. *et al.* Separation Performance of BioRenewable Deep Eutectic Solvents. *Ind. Eng. Chem. Res.* **54,** 3498–3504 (2015).

56. Gállego, I., Grover, M. a. & Hud, N. V. Folding and Imaging of DNA Nanostructures in Anhydrous and Hydrated Deep-Eutectic Solvents. *Angew. Chemie Int. Ed.* **54,** 6765–6769 (2015).

57. LeSeur, R. & Nkuku, C. A. Electrochemistry in deep eutectic solvents. *Abstr. Pap. Am. Chem. Soc.* **93,** 455–459 (2007).

58. Drylie, E. a *et al.* Ionothermal synthesis of unusual choline-templated cobalt aluminophosphates. *Angew. Chem. Int. Ed. Engl.* **46,** 7839–43 (2007).

59. Haerens, K., Matthijs, E., Chmielarz, A. & Van der Bruggen, B. The use of ionic liquids based on choline chloride for metal deposition: A green alternative? *J. Environ. Manage.* **90,** 3245–3252 (2009).

60. Tuntarawongsa, S. & Phaechamud, T. Polymeric Eutectic Drug Delivery System. *J. Met. Mater. Miner.* **22,** 27–32 (2012).

61. Paiva, A. *et al.* Natural Deep Eutectic Solvents-Solvents for the 21st Century. *Green Chem.* (2014).

62. Dai, Y., van Spronsen, J., Witkamp, G.-J., Verpoorte, R. & Choi, Y. H. Natural deep eutectic solvents as new potential media for green technology. *Anal. Chim. Acta* **766,** 61–68 (2013).

63. Choi, Y. H. *et al.* Are Natural Deep Eutectic Solvents the Missing Link in Understanding Cellular Metabolism and Physiology? *Plant Physiol.* **156,** 1701–1705 (2011).

64. Tang, B. & Row, K. H. Recent developments in deep eutectic solvents in chemical sciences. *Monatshefte für Chemie - Chem. Mon.* **144,** 1427–1454 (2013).

65. Dai, Y., Witkamp, G.-J., Verpoorte, R. & Choi, Y. H. Natural deep eutectic solvents as a new extraction media for phenolic metabolites in Carthamus tinctorius L. *Anal. Chem.* **85,** 6272–8 (2013).

66. Duarte, A. R. C., Mano, J. F. & Reis, R. L. Supercritical fluids in biomedical and tissue engineering applications: a review. *Int. Mater. Rev.* **54,** 214–222 (2009).

67. Knez, Ž., Markočič, E., Novak, Z. & Hrnčič, M. K. Processing Polymeric Biomaterials using Supercritical CO2. *Chemie Ing. Tech.* **83,** 1371–1380 (2011).

68. Reverchon, E. & De Marco, I. Supercritical fluid extraction and fractionation of natural matter. *J. Supercrit. Fluids* **38,** 146–166 (2006).

69. Azevedo, A. B. A. De, Mazzafera, P. & Mohamed, R. S. EXTRACTION OF CAFFEINE , CHLOROGENIC ACIDS AND LIPIDS FROM GREEN COFFEE BEANS USING SUPERCRITICAL CARBON DIOXIDE AND CO-SOLVENTS. *Brazilian J. Chem. Eng.* **25,** 543–552 (2008).

70. Kim, W.-J., Kim, J.-D., Kim, J., Oh, S.-G. & Lee, Y.-W. Selective caffeine removal from green tea using supercritical carbon dioxide extraction. *J. Food Eng.* **89,** 303–309 (2008).

71. Mohamed, R. S. & Mansoori, G. A. The Use of Supercritical Fluid Extraction Technology in Food Processing. *Food Technol.* (2002).

72. Jacobs, L. J. M., Kemmere, M. F. & Keurentjes, J. T. F. Sustainable polymer foaming using high pressure carbon dioxide: a review on fundamentals, processes and applications. *Green Chem.* **10,** 731 (2008).

73. Ning, S. & Leung, S. Mecahnisms of cell nucleation, growth, and coarsening in plastic foaming: Theory, Simulation, and Experiment. (University of Toronto, 2009).

74. Jacobs, L. J. M., Kemmere, M. F. & Keurentjes, J. T. F. Sustainable polymer foaming using high pressure carbon dioxide: a review on fundamentals, processes and applications. *Green Chem.* **10,** 731 (2008).

75. Kazarian, S. G. Polymer Processing with Supercritical Fluids. *Polym. Sci. Ser. C* **42,** 78–101 (2000).

76. Kazarian, S. G. *et al.* Specific Intermolecular Interaction of Carbon Dioxide with Polymers. *J. Am. Chem. Soc.* **118,** 1729–1736 (1996).

77. Knez, Ž., Markočič, E., Novak, Z. & Hrnčič, M. K. Processing Polymeric Biomaterials using Supercritical CO2. *Chemie Ing. Tech.* 1371–1380 (2011). doi:10.1002/cite.201100052

78. Martins, M. *et al.* Enhanced Performance of Supercritical Fluid Foaming of Natural-Based Polymers by Deep Eutectic Solvents. *AIChe Lett. Biomol. Eng. Bioeng. Biochem. Biofuels Food* **60,** 3701–3706 (2014).

79. Reverchon, E. & Cardea, S. Production of controlled polymeric foams by supercritical CO2. *J. Supercrit. Fluids* **40,** 144–152 (2007).

80.   Tomasko, D. . *et al.* A Review of CO2 Applications in the Processing of Polymers. *Ind. Eng. Chem. Res.* **42,** 6431–6456 (2003).

81.   Jacobs, L. J. M., Kemmere, M. F. & Keurentjes, J. T. F. Sustainable polymer foaming using high pressure carbon dioxide: a review on fundamentals, processes and applications. *Green Chem.* **10,** 731–738 (2008).

82.   Duarte, A. R. C., Silva, S. S., Mano, J. F. & Reis, R. L. Ionic liquids as foaming agents of semi-crystalline natural-based polymers. *Green Chem.* **14,** 1949 (2012).

83.   Crank, J. *Diffusio in Polymers*. (Academic Press, 1968).

84.   Jespersen, H. T. Studies of Sorption and Modification of Polymer Films in Supercritical Carbon Dioxide. (University of Copenhagen, 2002).

85.   Duarte, A. R. C. *et al.* Sorption and diffusion of dense carbon dioxide in a biocompatible polymer. *J. Supercrit. Fluids* **38,** 392–398 (2006).

86.   Swapp, S. Scanning Electron Microscopy (SEM). at <http://serc.carleton.edu/research_education/geochemsheets/techniques/SEM.html>

87.   Wickramanayake, S. *et al.* Mechanically robust hollow fiber supported ionic liquid membranes for CO2 separation applications. *J. Memb. Sci.* **470,** 52–59 (2014).

88.   Carlton, R. A. *Pharmaceutical Microscopy*. (Springer New York, 2011). doi:10.1007/978-1-4419-8831-7

89.   Holbrey, J. D. & Seddon, K. R. The phase behaviour of 1-alkyl-3-methylimidazolium tetarfluorobortaes; ionic liquids and ionic liquid crystals. *J. Chem. Soc., Dalt. Trans.,* **13,** 2133–2139 (1999).

90.   Bruttel, P. & Schlink, R. *Water Determination by Karl Fischer Titration*. (2003).

91.   Perkin Elmer. FT-IR Spectroscopy Attenuated Total Reflectance (ATR), Technical Note. (2005).

92.   Jessop, P. G., Jessop, D. a., Fu, D. & Phan, L. Solvatochromic parameters for solvents of interest in green chemistry. *Green Chem.* **14,** 1245 (2012).

93.   Carmichael, A. J. & Seddon, K. R. Polarity study of some 1-alkyl-3-methylimidazolium ambient-temperature ionic liquids with the solvatochromic dye, Nile Red. *J. Phys. Org. Chem.* **13,** 591–595 (2000).

94.   Jessop, P. G., Jessop, D. a., Fu, D. & Phan, L. Solvatochromic parameters for solvents of interest in green chemistry. *Green Chem.* **14,** 1245 (2012).

95.   Pissis, P. in *Electromagnetic Aquametry- Electromagnetic Wave Interaction with Water and Moist Substances* (ed. Kupfer, K.) (Springer New York, 2005).

96.   Kremer, F. & Schönals, A. *Broadband Dielectric Spectroscopy*. (Springer, 2003).

97.   Gill, P., Moghadam, T. T. & Ranjbar, B. Differential Scanning Calorimetry Techniques: Applications in Biology and Nanoscience. *J. Biomol. Tech.* **21,** 167–193 (2010).

98.   Liew, C.-W., Ramesh, S., Ramesh, K. & Arof, a. K. Preparation and characterization of lithium ion conducting ionic liquid-based biodegradable corn starch polymer electrolytes. *J. Solid State Electrochem.* **16,** 1869–1875 (2012).

99.   No Title. at <http://chemwiki.ucdavis.edu/Physical_Chemistry/Thermodynamics/Calorimetry/Differential_Scanning_Calorimetry>

100.   No Title. at <http://mee-inc.com/tensile-testing.html>

101.   No Title. at <http://www.cyberphysics.co.uk/topics/forces/young_modulus.htm>

102.   Malkin, A. Y. & Isayev, A. I. *Rheology: Concepts, Methods, and Applications*. (ChemTec, 2006).

103.   Sojoudi, A. & Saha, S. C. Shear Thinning and Shear Thickening Non- Newtonian Confined Fluid Flow over Rotating Cylinder. *Am. J. Fluid Dyn.* **2,** 117–121 (2013).

104.   Siepmann, J. & Peppas, N. A. Modeling of drug release from delivery systems based on hydroxypropyl methylcellulose (HPMC). *Adv. Drug Deliv. Rev.* **48,** 139–157 (2001).

105.   Chiellini, E. & Solaro, R. Biodegradable Polymeric Materials. *Adv. Mater.* **8,** 305–313 (1996).

106.   Albertsson, A. C. & Karlsson, S. Degradable polymers for the future. *Acta Polym.* **46,** 114–123 (1995).

107.   Jun, C. L. Reactive Blending of Biodegradable Polymers : PLA and Starch. **8,** 33–37 (2000).

108.   Fanovich, M. a. & Jaeger, P. Sorption and diffusion of compressed carbon dioxide in polycaprolactone for the development of porous scaffolds. *Mater. Sci. Eng. C* **32,** 961–968 (2012).

109.   Cooper, A. I. Porous Materials and Supercritical Fluids. *Adv. Mater.* **15,** 1049–1059 (2003).

110.   Davies, O. R. *et al.* Applications of supercritical CO2 in the fabrication of polymer systems for drug delivery and tissue engineering. *Adv. Drug Deliv. Rev.* **60,** 373–87 (2008).

111.   Jacobs, L. J. M., Kemmere, M. F. & Keurentjes, J. T. F. Sustainable polymer foaming using high pressure carbon dioxide: a review on fundamentals, processes and applications. *Green Chem.* **10,** 731 (2008).

112.   Zhu, S. *et al.* Dissolution of cellulose with ionic liquids and its application: a mini-review. *Green Chem.* **8,** 325 (2006).

113. Xie, H., Zhang, S. & Li, S. Chitin and chitosan dissolved in ionic liquids as reversible sorbents of CO2. *Green Chem.* **8,** 630 (2006).

114. Seoud, O. A. El, Koschella, A., Fidale, L. C., Dorn, S. & Heinze, T. Applications of Ionic Liquids in Carbohydrate Chemistry: A Window of Opportunities. *Biomacromolecules* **8,** 2629–2647 (2007).

115. Sankri, A. *et al.* Thermoplastic starch plasticized by an ionic liquid. *Carbohydr. Polym.* **82,** 256–263 (2010).

116. Kazarian, S. G., Vincent, M. F., Bright, F. V, Liotta, C. L. & Eckert, C. A. Specific Intermolecular Interaction of Carbon Dioxide with Polymers. *J. Am. Chem. Soc.* **118,** 1729–1736 (1996).

117. Aubert, J. H. Solubility of carbon dioxide in polymers by the quartz crystal microbalance technique. *J. Supercrit. Fluids* **11,** 163–172 (1998).

118. Cravo, C., Duarte, A. R. C. & Duarte, C. M. M. Solubility of carbon dioxide in a natural biodegradable polymer: Determination of diffusion coefficients. *J. Supercrit. Fluids* **40,** 194–199 (2007).

119. Berens, A. R., Huvard, G. S., Korsmeyer, R. W. & Kunig, F. W. Application of compressed carbon dioxide in the incorporation of additives into polymers. *J. Appl. Polym. Sci.* **46,** 231–242 (1992).

120. Avérous, L. Biodegradable Multiphase Systems Based on Plasticized Starch: A Review. *J. Macromol. SCcience, Part CPolymer Rev.* **44,** 231–274 (2004).

121. Shiflett, M. B., Kasprzak, D. J., Junk, C. P. & Yokozeki, a. Phase behavior of {carbon dioxide+[bmim][Ac]} mixtures. *J. Chem. Thermodyn.* **40,** 25–31 (2008).

122. Mano, J. F., Koniarova, D. & Reis, R. L. Thermal properties of thermoplastic starch/synthetic polymer blends with potential biomedical applicability. *J. Mater. Sci. Mater. Med.* **14,** 127–35 (2003).

123. Fischer, E. W., Sterzel, H. J. & Wegner, G. Investigation of the structure of solution grown crystals of lactide copolymers by means of chemical reactions. *Kolloid.Z. Z. Polym.* **990,** 980–990 (1973).

124. Kang, S. *et al.* A Spectroscopic Analysis of Poly(lactic acid) Structure. *Macromolecules* **34,** 4542–4548 (2001).

125. Jacobsen, S. & Fritz, H. G. Plasticizing polylactide- The Effect of Different Plasticizers on the Mechanical Properties. *Polym. Eng. Sci.* **39,** 1303–1310 (1999).

126. Silva, S. S., Duarte, A. R. C., Carvalho, A. P., Mano, J. F. & Reis, R. L. Green processing of porous chitin structures for biomedical applications combining ionic liquids and supercritical fluid technology. *Acta Biomater.* **7,** 1166–72 (2011).

127. Liao, X., Nawaby, A. V. & Whitfield, P. S. Carbon dioxide-induced crystallization in poly(L-lactic acid) and its effect on foam morphologies. *Polym. Int.* **59,** 1709–1718 (2010).

128. Zavrel, M., Bross, D., Funke, M., Büchs, J. & Spiess, A. C. High-throughput screening for ionic liquids dissolving (ligno-)cellulose. *Bioresour. Technol.* **100,** 2580–7 (2009).

129. Winterton, N. Solubilization of polymers by ionic liquids. *J. Mater. Chem.* **16,** 4281 (2006).

130. Feng, L. & Chen, Z. Research progress on dissolution and functional modi fi cation of cellulose in ionic liquids. *J. Mol. Liq.* **142,** 1–5 (2008).

131. Cao, Y. *et al.* Room temperature ionic liquids (RTILs): A new and versatile platform for cellulose processing and derivatization. *Chem. Eng. J.* **147,** 13–21 (2009).

132. Heinze, T., Schwikal, K. & Barthel, S. Ionic liquids as reaction medium in cellulose functionalization. *Macromol. Biosci.* **5,** 520–5 (2005).

133. Xie, H., King, A., Kilpelainen, I., Granstrom, M. & Argyropoulos, D. S. Thorough Chemical Modification of Wood-Based Lignocellulosic Materials in Ionic Liquids. *Biomacromolecules* **8,** 3740–3748 (2007).

134. Remsing, R. C., Swatloski, R. P., Rogers, R. D. & Moyna, G. Mechanism of cellulose dissolution in the ionic liquid 1-n-butyl-3-methylimidazolium chloride: a 13C and 35/37Cl NMR relaxation study on model systems. *Chem. Commun. (Camb).* 1271–3 (2006). doi:10.1039/b600586c

135. Scott, M. P. *et al.* Application of ionic liquids as plasticizers for poly (methyl methacrylate). *Chem. Commun.* 1370–1371 (2002). doi:10.1039/b204319j.4

136. Scott, M. P., Rahman, M. & Brazel, C. S. Application of ionic liquids as low-volatility plasticizers for PMMA. *Eur. Polym. J.* **39,** 1947–1953 (2003).

137. Chesnokov, S. A., Zakharina, M. Y. U., Shaplov, A. S. & Lozinskaya, E. I. Photopolymerization of Poly (ethylene glycol) Dimethacrylates : The Influence of Ionic Liquids on the Formulation and the Properties of the Resultant Polymer Materials. *J. Polym. Sci. Part A Polym. Chem.* **48,** 2388–2409 (2010).

138. Martins, M., Craveiro, R., Paiva, A., Duarte, A. R. C. & Reis, R. L. Supercritical fluid processing of natural based polymers doped with ionic liquids. *Chem. Eng. J.* **241,** 122–130 (2014).

139. Chiono, V. *et al.* Characterisation of blends between poly(ε-caprolactone) and polysaccharides for tissue engineering applications. *Mater. Sci. Eng. C* **29,** 2174–2187 (2009).

140. Jiang, Q., Yang, C. C. & Li, J. C. Size-Dependent Melting Temperature of Polymers. *Macromol. Theory Simulations* **12,** 57–60 (2003).

141. Kremer, F. & Schönals, A. *Broadband Dielectric Spectroscopy*. (Springer, 2003).

142.   Carvalho, T. *et al.* Understanding the ion jelly conductivity mechanism. *J. Phys. Chem. B* **116,** 2664–76 (2012).

143.   Meiβner, D., Einfeldt, J. & Kwasniewski, A. Contributions to the molecular origin of the dielectric relaxation processes in polysaccharides ± the low temperature range. *J. Non. Cryst. Solids* **275,** 199–209 (2000).

144.   Butler, M. F. & Cameron, R. E. A study of the molecular relaxations in solid starch using dielectric spectroscopy. *Polymer (Guildf).* **41,** 2249–2263 (2000).

145.   Einfeldt, J., Meiβner, D., Kwasniewski, A. & Einfeldt, L. Dielectric spectroscopic analysis of wet and well dried starches in comparison with other polysaccharides. *Polymer (Guildf).* **42,** (2001).

146.   Wang, Y., Rodriguez-Perez, M. a., Reis, R. L. & Mano, J. F. Thermal and Thermomechanical Behaviour of Polycaprolactone and Starch/Polycaprolactone Blends for Biomedical Applications. *Macromol. Mater. Eng.* **290,** 792–801 (2005).

147.   Ramesh, S., Liew, C.-W. & Arof, a. K. Ion conducting corn starch biopolymer electrolytes doped with ionic liquid 1-butyl-3-methylimidazolium hexafluorophosphate. *J. Non. Cryst. Solids* **357,** 3654–3660 (2011).

148.   Hayyan, A., Hashim, M. A., Hayyan, M., Mjalli, F. S. & AlNashef, I. M. A new processing route for cleaner production of biodiesel fuel using a choline chloride based deep eutectic solvent. *J. Clean. Prod.* **65,** 246–251 (2014).

149.   Leuner, C. & Dressman, J. Improving drug solubility for oral delivery using solid dispersions. *Eur. J. Pharm. Biopharm.* **50,** 47–60 (2000).

150.   Abbott, A. P., Boothby, D., Capper, G., Davies, D. L. & Rasheed, R. K. Deep eutectic solvents formed between choline chloride and carboxylic acids: Versatile alternatives to ionic liquids. *J. Am. Chem. Soc.* **126,** 9142–9147 (2004).

151.   Dai, Y., van Spronsen, J., Witkamp, G.-J., Verpoorte, R. & Choi, Y. H. Natural deep eutectic solvents as new potential media for green technology. *Anal. Chim. Acta* **766,** 61–8 (2013).

152.   Florindo, C., Oliveira, F. S., Rebelo, L. P. N., Fernandes, A. M. & Marrucho, I. M. Insights into the Synthesis and Properties of Deep Eutectic Solvents Based on Cholinium Chloride and Carboxylic Acids. *ACS Sustain. Chem. Eng.* **2,** 2416–2425 (2014).

153.   Legrand, V., Descamps, M. & Alba-Simionesco, C. Glass-forming meta-toluidine: A thermal and structural analysis of its crystalline polymorphism and devitrification. *Thermochim. Acta* **307,** 77–83 (1997).

154.   Dudognon, E., Danède, F., Descamps, M. & Correia, N. T. Evidence for a new crystalline phase of racemic ibuprofen. *Pharm. Res.* **25,** 2853–8 (2008).

155.   Menczel, J. D. & Prime, R. B. *Thermal Analysis of Polymers, Fundamentals and Applications*. (Wiley, 2009).

156. Diogo, H. P. & Moura Ramos, J. J. Are Crystallization and Melting the Reverse Transformation of Each Other? *J. Chem. Educ.* **83,** 1389 (2006).

157. Carvalho, T. *et al.* Ion jelly conductive properties using dicyanamide-based ionic liquids. *J. Phys. Chem. B* **118,** 9445–59 (2014).

158. Kremer, F. & Schönals, F. *Broadband Dielectric Spectroscopy*. (Springer Verlag, 2003).

159. Bowlas, C. J., Bruce, D. W. & Seddon, K. R. Liquid-crystalline ionic liquids. *Chem. Commun.* 1625–1626 (1996). doi:Doi 10.1039/Cc9960001625

160. Widegren, J. a., Saurer, E. M., Marsh, K. N. & Magee, J. W. Electrolytic conductivity of four imidazolium-based room-temperature ionic liquids and the effect of a water impurity. *J. Chem. Thermodyn.* **37,** 569–575 (2005).

161. Sangoro, J. R., Iacob, C., Serghei, A., Friedrich, C. & Kremer, F. Universal scaling of charge transport in glass-forming ionic liquids. *Phys. Chem. Chem. Phys.* **11,** 913–916 (2009).

162. Leys, J. *et al.* Temperature dependence of the electrical conductivity of imidazolium ionic liquids. *J. Chem. Phys.* **128,** 064509 (2008).

163. Mano, J. F. & Dionísio, M. *Handbook of Thermal Analysis and Calorimetry*. (Elsevier, 2008).

164. Reichardt, C. Polarity of ionic liquids determined empirically by means of solvatochromic pyridinium N-phenolate betaine dyes. *Green Chem.* **7,** 339 (2005).

165. Kulkarni, P. S. *et al.* Comparison of physicochemical properties of new ionic liquids based on imidazolium, quaternary ammonium, and guanidinium cations. *Chem. Eur. J.* **13,** 8478–8488 (2007).

166. Craveiro, R. *et al.* Starch-based polymer-IL composites formed by compression moulding and supercritical fluid foaming for self-supported conductive material. *Rsc Adv.* **4,** 17161–17170 (2014).

167. Romero, A., Santos, A., Tojo, J. & Rodríguez, A. Toxicity and biodegradability of imidazolium ionic liquids. *J. Hazard. Mater.* **151,** 268–73 (2008).

168. Hayyan, M. *et al.* Are deep eutectic solvents benign or toxic? *Chemosphere* **90,** 2193–5 (2013).

169. Dobler, D., Schmidts, T., Klingenhofer, I. & Runkel, F. Ionic liquids as ingredients in topical drug delivery systems. *Int. J. Pharm.* **441,** 620–627 (2013).

170. Ferraz, R. *et al.* Development of novel ionic liquids based on ampicillin. *Medchemcomm* **3,** 494 (2012).

171. Ferraz, R., Branco, L. C., Prudêncio, C., Noronha, J. P. & Petrovski, Z. Ionic liquids as active pharmaceutical ingredients. *ChemMedChem* **6,** 975–85 (2011).

172. Frizzo, C. P. *et al.* in *Ionic Liquids - New ASpects for the Future* 557–580 (InTech, 1992).

173. Hough, W. L. *et al.* The third evolution of ionic liquids: active pharmaceutical ingredients. *New J. Chem.* **31,** 1429 (2007).

174. Carriazo, D., Serrano, M. C., Gutiérrez, M. C., Ferrer, M. L. & del Monte, F. Deep-eutectic solvents playing multiple roles in the synthesis of polymers and related materials. *Chem. Soc. Rev.* **41,** 4996–5014 (2012).

175. Ruß, C. & König, B. Low melting mixtures in organic synthesis – an alternative to ionic liquids? *Green Chem.* **14,** 2969 (2012).

176. Ferraz, R., Branco, L. C., Prudêncio, C., Noronha, J. P. & Petrovski, Z. Ionic liquids as active pharmaceutical ingredients. *ChemMedChem* **6,** 975–85 (2011).

177. Shamsuri, A. A. & Daik, R. Plasticizing effect of choline chloride/urea eutectic-based ionic liquid on physicochemical properties of agarose films. *Bioresources* **7,** 4760–4775 (2012).

178. Choi, S. Y. *et al.* Dual functional ionic liquids as plasticisers and antimicrobial agents for medical polymers. *Green Chem.* **13,** 1527–1535 (2011).

179. Craveiro, R. *et al.* Starch-based polymer-IL composites formed by compression moulding and supercritical fluid foaming for self-supported conductive material (Accepted). *Rsc Adv.*

180. Martins, M., Craveiro, R., Paiva, A., Duarte, A. R. C. & Reis, R. L. Supercritical fluid processing of natural based polymers doped with ionic liquids. *Chem. Eng. J.* **241,** 122–130 (2014).

181. Tai, H. Y. *et al.* Control of pore size and structure of tissue engineering scaffolds produced by supercritical fluid processing. *Eur Cell Mater* **14,** 64–76 (2007).

182. Duarte, A. R. C., Silva, S. S., Mano, J. F. & Reis, R. L. Ionic liquids as foaming agents of semi-crystalline natural-based polymers. *Green Chem.* **14,** 1949 (2012).

183. Lin, C. M., Leron, R. B., Caparanga, A. R. & Li, M. H. Henry's constant of carbon dioxide-aqueous deep eutectic solvent (choline chloride/ethylene glycol, choline chloride/glycerol, choline chloride/malonic acid) systems. *J. Chem. Thermodyn.* **68,** 216–220 (2014).

184. Zubeir, L., Lacroix, M. & Kroon, M. Low Transition Temperature Mixtures as Innovative and Sustainable CO2 Capture Solvents. *J. Phys. Chem. A* **118,** 14429–14441 (2014).

185. Leron, R. B. & Li, M. H. Solubility of carbon dioxide in a eutectic mixture of choline chloride and glycerol at moderate pressures. *J. Chem. Thermodyn.* **57,** 131–136 (2013).

186. Aubuchon, S. R. Interpretation of the Crystallization Peak of Supercooled Liquids using Tzero(r) DSC. 1–7

187. Corvis, Y., Négrier, P., Massip, S., Leger, J.-M. & Espeau, P. Insights into the crystal structure, polymorphism and thermal behavior of menthol optical isomers and racemates. *Cryst Eng Comm* **14,** 7055 (2012).

188. Petropoulos, J., Sanopoulou, M. & Papadokostaki, K. Beyond Fick: How Best to Deal with non-Fickian Behavior in a Fickian Spirit. *Basic Princ. Diffus. Theory, Exp. Appl.* **11,** 1–2 (2009).

189. Li, S., Shen, Y., Li, W. & Hao, X. A common profile for polymer-based controlled release and its logical interpretation to general release process. *J Pharm Pharm Sci* **9,** 238–244 (2006).